

OLYMPIC DAM EXPANSION

DRAFT ENVIRONMENTAL IMPACT STATEMENT 2009

APPENDIX L

GREENHOUSE GAS AND AIR QUALITY



bhpbilliton

resourcing the future

ISBN 978-0-9806218-0-8 (set)
ISBN 978-0-9806218-4-6 (appendices)

GREENHOUSE GAS AND AIR QUALITY

CONTENTS

L1	Greenhouse gas management	3
L1.1	Introduction	4
	L1.1.1 Overview	4
	L1.1.2 Climate change science	4
L1.2	Climate change regulation and policy	7
	L1.2.1 Overview	7
	L1.2.2 International regulation	7
	L1.2.3 National regulation	7
	L1.2.4 State regulation	8
	L1.2.5 BHP Billiton position	9
	L1.2.6 Olympic Dam expansion position	10
L1.3	Emissions assessment methodology	10
	L1.3.1 Scope	10
	L1.3.2 Boundaries	11
	L1.3.3 Emission factors	11
	L1.3.4 Other emission sources	11
	L1.3.5 Scope 1, 2 and 3 emissions	12
L1.4	Existing environment	13
L1.5	Proposed expansion	17
	L1.5.1 Installed mitigation	17
	L1.5.2 Emissions assessment	17
	L1.5.3 Estimation of emissions	17
	L1.5.4 Expanded operation greenhouse gas emissions in context	21
L1.6	Greenhouse gas mitigation and management	23
	L1.6.1 Overview	23
	L1.6.2 Methodology	23
	L1.6.3 Current and near-future mitigation options	25
	L1.6.4 Demand-side levers	27
	L1.6.5 Carbon reduction options for alternate energy supply	30
L1.7	References	32
L2	Air quality impact assessment	35
L2.1	Introduction	36
	L2.1.1 Overview	36
L2.2	Project description	36
L2.3	Climate and meteorology	36
L2.4	Topography	36
L2.5	Dispersion modelling	37
L2.6	Air quality assessment criteria	37
	L2.6.1 Regulations, standards and guidelines	37
	L2.6.2 Adopted criteria	37
L2.7	Point source emission rates	38
L2.8	Fugitive sources	40
	L2.8.1 Key data and assumptions	40
	L2.8.2 Mitigation effectiveness	41
	L2.8.3 Emissions estimations	42
L2.9	Attachment	45
L2.10	References	46

11 December 2008

David Winterburn
Senior Sustainability Advisor
Olympic Dam Expansion EIS Project

Dear David

Re: Peer review: GHG Strategy document & EIS summary for ODX

Further to BHP Billiton ODX' request, Energetics has reviewed the following documentation (dated 14th November 2008) relating to the EIS for this project:

1. Draft EIS Chapter 13 (Greenhouse gas component).doc
2. Appendix_L1_GHG_RevS.doc

We have also noted revisions made to the wording of the commitments in relation to greenhouse gas targets, advised via email on 3rd December 2008.

Energetics has not reviewed any referenced or related parts of the EIS other than those parts noted above, nor any other contextual information related to the project.

It is our opinion based on the review we have conducted that:

- The methodologies employed to define emissions scope and boundaries, construct the greenhouse gas baseline and develop abatement scenarios that could enable target setting for greenhouse gas emissions reductions to be achieved is clear, logical and appropriate for the scale of project;
- The ODX project team has undertaken a comprehensive review of currently available technologies, and future potential opportunities for reducing reportable greenhouse gas emissions associated with the project, and have a sound understanding of the scale of their commitments and of the financial implications of reaching their targets for reducing emissions;
- The intent of the greenhouse gas strategy (Appendix_L1_GHG_RevS.doc) is reflected in the EIS (Draft EIS Chapter 13 (Greenhouse gas component).doc).

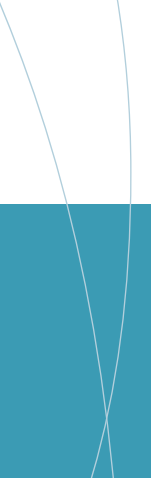
If you have any queries regarding this opinion or in relation to the review carried out, please contact me on 02 9492 9535 / 0408 413 597.

Regards



Patrick Denvir
General Manager Consulting





APPENDIX L1

Greenhouse gas management

L1 GREENHOUSE GAS MANAGEMENT

L1.1 INTRODUCTION

The expanded Olympic Dam operation would consume more energy, particularly in the form of electricity and diesel, which would result in an increase in greenhouse gas emissions necessitating additional greenhouse gas management. The overall approach to greenhouse gas management for the proposed expansion would be to:

- apply a goal of reducing greenhouse gas emissions (reportable under the National Greenhouse and Energy Reporting (Measurement) Determination 2008) to an amount equivalent to at least a 60% reduction (to an amount equal to or less than 40%) of 1990 emissions, by 2050
- constructing an on-site cogeneration power station (250 MW capacity) by recovering waste heat
- sourcing renewable energy (35 MW capacity) via the national electricity market for the seawater desalination plant
- producing an annual 'road map' that quantifies emission reduction opportunities and achievements.

This appendix presents the detail to support the information presented in Chapter 13, Greenhouse Gas and Air Quality, of the Draft EIS, specifically with regards to the emission factors used and potential future mitigation measures. Climate change is discussed in Chapter 8, Meteorological Environment and Climate, providing a context to the assessment of greenhouse gas emissions included in this appendix.

L1.1.1 Overview

Australia's appreciation of climate change is rapidly changing due to the improved quality and understanding of the scientific data, increased community concern, and the introduction of greenhouse gas regulations into the Australian jurisdiction.

Reporting greenhouse gas emissions has historically been voluntary. From July 2008, however, new federal legislation requires mandatory reporting of emissions from Australia's larger emitters. This mandatory reporting is the first step in the process of establishing the national emissions trading scheme, referred to as the Carbon Pollution Reduction Scheme (CPRS). A timetable for the CPRS, released in March 2008, has indicated that emissions trading would commence in 2010.

South Australia has responded to climate change by setting statutory emissions targets. The *Climate Change and Emissions Reduction Act 2007 (SA)* caps state emissions at an amount that is equal to or less than 40% of 1990 levels by 2050 and requires 20% of electricity produced and consumed in South Australia to be generated from renewable sources by 2014.

While the current Olympic Dam operations contribute only a small amount to overall state emissions (approximately 3.5%), the proposed Olympic Dam expansion has the potential to increase greenhouse gas emissions by a significant volume (up to 4.7 million tonnes per annum of CO₂-e). This would increase the Olympic Dam contribution to around 10% of South Australia's projected future greenhouse gas emissions.

The greenhouse gases likely to be emitted as a result of the proposed expansion of Olympic Dam are quantified and qualified within this Appendix. An analysis of existing greenhouse gas emissions and existing and proposed greenhouse gas-related legislation and regulations is undertaken to provide a context for the expanded emissions. Finally, cost curves for greenhouse gas reduction have been developed for the proposed expanded operation, identifying both potential mitigation measures and their potential greenhouse gas reduction benefit, together with the costs associated with their implementation. These are discussed in the context of progress towards the goal of reducing greenhouse gas emissions from the Olympic Dam operation to an amount that is equal to or less than 40% of 1990 levels by 2050.

L1.1.2 Climate change science

Greenhouse gases

Greenhouse gases include gases such as water vapour, carbon dioxide, methane, chlorofluorocarbons (CFCs) and hydrochlorofluorocarbons (HCFCs) that absorb and re-emit infra-red radiation (heat), warming Earth's surface and contributing to climate change. The greenhouse effect is synonymous with climate change and global warming and has recently been defined as 'any change in climate over time, whether due to natural variability or as a result of human activity' (IPCC 2007).

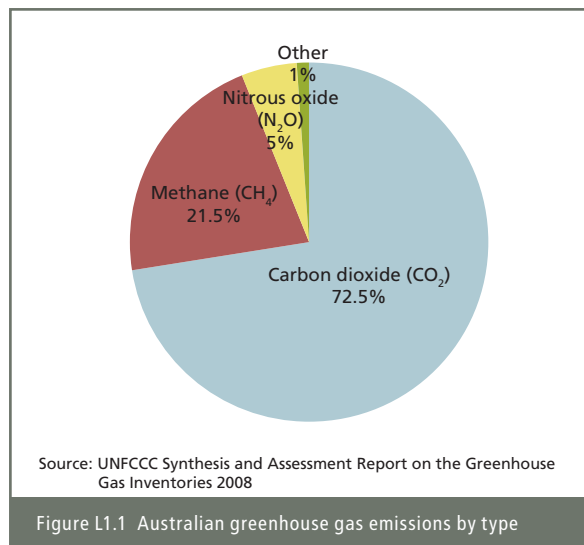
The impact of greenhouse gas emissions on the atmosphere is the combined effect of the radiative properties of the gases (that is, their ability to absorb solar and infra-red radiation) and also the time that it takes for those gases to be removed from the atmosphere by natural processes. In order to compare the relative effects of different gases over a particular time period, Global Warming Potentials (GWP) are used, referenced in units of carbon dioxide equivalents (CO₂-e); carbon dioxide is used as the base reference, and has a GWP of one. There are six major groups of greenhouse gases, as listed in Table L1.1. The table also shows the GWP for each of the gases, calculated over a 100-year time scale. The table indicates, for example, that an emission of 1 kg of methane has the same global warming potential as an emission of 21 kg of carbon dioxide. In this instance, if 1 kg of carbon dioxide was emitted together with 1 kg of methane, then the total emission would be valued at 22 kg of CO₂-e.

Table L1.1 Greenhouse gas categories and indicative global warming potentials¹

Greenhouse gas	Global warming potential range
Carbon dioxide	1
Methane	21
Nitrous oxide	310
Hydrofluorocarbons (HFC)	150–11,700
Hydrofluoroethers (HFE)	100–500
Perfluorocarbons (PFC)	6,500–23,900

¹ Sourced from National Greenhouse Accounts Factors 2008.

The breakdown of Australian greenhouse gas emissions by gas type is provided in Figure L1.1.



Climate change

Scientists have concluded that human-induced increases in greenhouse gas (GHG) emissions are enhancing the natural greenhouse effect. Human activities, especially burning fossil fuels, clearing forests and changing land use, have been the major drivers of global warming and climate change in recent decades (Government of South Australia 2005).

In 2004, the Intergovernmental Panel on Climate Change (IPCC) warned that an increasing body of observation painted a collective picture of a warming planet and climate change. The Working Group II report, *Impacts, Adaptation and Vulnerability* (IPCC 2007a) from the recent Fourth IPCC Assessment Report, indicates that predictions of the severity of climate change in Australia are matched by recent climate data. Table L1.2 lists some of the climate change predictions and warnings of relevance to Australia.

Table L1.2 Climate change predictions and warnings

Warming of the lower atmosphere and upper ocean has occurred. The uptake of anthropogenic carbon by the ocean since 1750 has resulted in a slight increase in acidity, with a decrease in pH by 0.1 units on average. During the 21 st century a further increase in acidity is expected with a reduction in pH of between 0.14 and 0.35 units.
An increase in global average precipitation has been observed in many regions from 1900 to 2005, although it appears highly variable. An increase in the density and duration of droughts has been observed globally and is predicted to continue.
Most of the global warming observed over the past 50 years is attributable to human activity. Several greenhouse gases occur naturally within the environment but increases in atmospheric conditions over the past 250 years can be attributed to human activity.
By the year 2100 it is estimated that global average temperatures may rise 2.4 °C to 6.4 °C and global sea levels may rise 26–59 cm, relative to 1980 levels, if greenhouse gas emissions continue at current levels.
By the year 2100 current predictions estimate that sea levels may rise 18–59 cm, relative to 2000 levels. However, these predictions for Australia are subject to regional modifications which could potentially result in a change in sea level of up to ± 25% of the estimated figure.
By the year 2020 it is estimated that in Australia an increase in temperature ranging between 0.1 °C and 1.3 °C, relative to 1990, is likely to occur within 800 km of the coast. By 2050 an increase ranging between 0.3 °C and 3.4 °C is likely and by 2080 this prediction increases to between 0.4 °C and 6.7 °C.
A decrease in annual rainfall is considered likely across the majority of southern and sub-tropical Australia. Increases in extreme daily rainfall events are also considered likely. The projected change in annual average rainfall for central Australia ranges between ± 5% by 2020, ± 13% by 2050 and ± 27% by 2080. By the year 2030 in parts of South Australia, the intensity of the daily rainfall event (one-in-20 year daily rainfall event) is likely to increase by up to 10%.
Water balance models indicate a likely reduction in both soil moisture and run-off across the majority of Australia. For the period 2021 to 2050 a decline in run-off of 6% to 8% is predicted across the majority of eastern Australia and 14% across south-western Australia. Models of drought occurrence (one-in-10 year soil moisture deficit) predict an increase of up to 20% more droughts likely to occur over the majority of Australia by 2030, and up to 80% more likely by 2070 in south-western Australia.
By the year 2030 water security problems resulting from a continued decrease in precipitation coupled with an increase in evaporation are predicted to intensify in southern and eastern Australia.
By the year 2030 an increase in risk to major infrastructure by exceeding extreme event design criteria is considered very likely to occur in Australia, including: failure of flood plain protection and urban drainage / sewage systems; increased storm and fire damage; and an increase in heatwaves. It is predicted that the increase in heatwaves would contribute to an increase in the number of blackouts and deaths associated with heat.
A decline in species migration resulting from a loss and/or change of habitat is considered likely to occur, although the effect is dependent on the species' ability to adapt to climate change.

Source: Summarised from the Intergovernmental Panel on Climate Change (IPCC) (2007a)

Increased atmospheric concentrations of carbon dioxide (CO₂) and other GHG emissions have been measured. Based on National Oceanic and Atmospheric Administration data, the atmospheric concentration of CO₂ has risen to a 2007 average of 384 parts per million (ppm) (NOAA, 2008). This is a 21% increase in CO₂ from the 1959 average recorded at the Mauna Loa observatory in Hawaii, which provides the longest, continuous, instrumental measurement of CO₂ levels. If GHG and aerosol emissions were held constant at 2005 levels, CO₂ and equivalent gas (CO₂-e) concentrations would rise to 531 ppm by 2100. The predicted temperature increase of this CO₂-e level is 2 °C (Hare & Meinshausen 2004).

The IPCC, United Nations Convention on Biological Diversity, and the Council of the European Union consider a global average surface temperature rise above 2 °C likely to have critical and irreversible climate change effects. To avoid the 2 °C temperature rise, atmospheric concentrations of CO₂-e need to stabilise at 400–450 ppm (Hare & Meinshausen 2004). To achieve this with reasonable certainty, GHG emissions need to be cut by at least 30% of 1990 levels by 2050 (Hare & Meinshausen, 2004). Net greenhouse gas emissions, as reported in the *National Greenhouse Gas Inventory 2006* (Department of Climate Change, 2008), were 4.2% above 1990 levels.

In Australia, between 1910 and 2004, there has been an average maximum temperature increase of 0.6 °C and an average minimum temperature increase of 1.2 °C, which has predominantly occurred since 1950 (IPCC 2007a). The IPCC state with confidence that since 1950 there has been a rise in temperature in Australia between 0.4 °C and 0.7 °C, with an increase in heatwaves and frosts and a decrease in the amount of rainfall in southern and eastern Australia.

A significant degree of climate change across Australia now seems inevitable, and is likely to become increasingly apparent during the latter half of this century (Suppiah et al. 2006). Changes are expected in climate averages and in the magnitude and frequency of climate extremes. Suppiah et al. (2006) and CSIRO (2002) suggest that long-term planning should not be based on the assumption that future climate statistics and resources will be the same as they were over the past century. Climate change will have an impact on water supply, flooding, sea level and storm surges.

Uncertainties

Although the majority perspective of the mainstream science of climate change has been largely accepted, uncertainties with regards to the potential impacts of climate change remain. The three main uncertainties, according to Garnaut (2008) are:

- the relationship between the rate of greenhouse gas emissions and the concentrations of these gases in the atmosphere
- the extent of the warming that results from any specified change in concentrations
- the timing and extent of the impacts from a given degree of warming.

The cumulative nature of these uncertainties means that the range of outcomes, when they are all included, can be considerable. Climate change projections, developed by the CSIRO in 2007, suggest a temperature increase for Australia in 2070 of between 1.0 °C and 2.5 °C (with an average of 1.8 °C) for the low emissions case and between 2.2 °C and 5.0 °C (with an average of 3.4 °C) for the high emissions case.

L1.2 CLIMATE CHANGE REGULATION AND POLICY

L1.2.1 Overview

In the past year the regulatory framework concerning climate change in Australia has changed considerably. The main state, federal and international legislation and policy instruments that form the regulatory framework for climate change in Australia are:

- Kyoto Protocol
- United Nations Framework Convention on Climate Change (UNFCCC), Bali 2007 – Bali Roadmap
- Australian National Greenhouse Strategy
- Greenhouse Challenge and Greenhouse Challenge Plus Schemes
- *Energy Efficiency Opportunities Act 2006* (Cwlth)
- *National Greenhouse and Energy Reporting Act 2007* (Cwlth)
- South Australian Greenhouse Strategy
- *Climate Change and Emissions Reduction Act 2007* (SA)

The impact of these regulatory instruments on the Australian climate change response is discussed below.

L1.2.2 International regulation

Australia ratified the Kyoto Protocol in December 2007. The protocol caps Australian emissions at 108% of 1990 greenhouse gas levels during the first commitment period (2008–2012). Australia was one of three countries – the other two being Norway and Iceland – granted an exemption permitting an increase in its greenhouse gas emission levels over its 1990 base year level. In contrast, other developed countries collectively agreed to reduce their aggregate greenhouse gas emissions by at least 5% from 1990 levels in the first commitment period.

In December 2007 the United Nations Framework Convention on Climate Change (UNFCCC) 2007 Bali Conference developed the agenda or framework for the post-Kyoto negotiations – the Bali Roadmap. The likely cornerstone, agreed at Bali, is that developed countries will take on quantitative commitments, while developing countries are to undertake ‘measurable, reportable and verifiable’ mitigation actions, but not with quantitative, national commitments and emissions trading.

Sectoral approaches to mitigation, incentive mechanisms to reduce tropical deforestation, and a broadened clean development mechanism are expected to expand the reach of a post-2012 framework. New support mechanisms are likely to be created for adaptation, technology development and diffusion, as well as financing and investment. The Bali Roadmap envisages such a plan to be agreed at the 2009 UNFCCC conference in Copenhagen.

L1.2.3 National regulation

National greenhouse strategy

The National Greenhouse Strategy was developed in 1998 as Australia’s response to climate change, providing a strategic framework without specifying state-specific or project-specific targets. The Australian Greenhouse Office was established to coordinate Commonwealth action on climate change matters.

Greenhouse Challenge was initiated as a voluntary program between the Australian Government and industry to abate greenhouse gas emissions and increase energy efficiency. Greenhouse Challenge Plus builds on the success of Greenhouse Challenge integrating Generator Efficiency Standards and the Greenhouse Friendly™ initiative into a single industry program.

The aim of the voluntary Greenhouse Challenge Plus is to:

- reduce greenhouse gas emissions (including promotion of awareness of greenhouse gas abatement opportunities in industry)
- accelerate the uptake of energy efficiency
- integrate greenhouse issues into business decision-making
- provide more consistent reporting of greenhouse gas emissions levels.

BHP Billiton is a current member of Greenhouse Challenge Plus.

Mandatory reporting requirements for sizeable emitters were introduced by the *National Greenhouse and Energy Reporting Act 2007* (NGER Act) from 1 July 2008 (NGER 2008).

The NGER Act has been designed to provide robust data as a foundation for an Australian emissions trading scheme, and to facilitate the reporting of abatement and offsets prior to commencement of emissions trading. A timetable for emissions trading was released in March 2008 stating that a national emissions trading scheme is likely to commence in 2010.

The NGER system will provide company-level information on greenhouse and energy performance to the public, and create a single online entry point for reporting. Reporting is administered by the Department of Climate Change as part of the Prime Minister and Cabinet's portfolio.

The NGER Act requires controlling corporations to register and then report, on a financial year basis, greenhouse gas emissions and energy production and consumption if specified thresholds are exceeded. The first registration deadline is 31 August 2009, and the first reporting deadline is 31 October 2009. A controlling corporation's group will meet the threshold for a year if:

- the total amount of greenhouse gases emitted from the operation of facilities under the operational control of members of the corporation's group is greater than or equal to 125 kilotonnes (kt) of CO₂-e (FY2008), 87.5 kt of CO₂-e (FY2009) and 50 kt of CO₂-e (FY2010)
- the total amount of energy produced from operating the facilities under the operational control of members of the corporation's group is greater than or equal to 500 terrajoules (TJ) (FY2008), 350 TJ (FY2009) and 200 TJ (FY2010)
- the total amount of energy consumed from operating the facilities under the operational control of members of the corporation's group is greater than or equal to 500 TJ (FY2008), 350 TJ (FY2009) and 200 TJ (FY2010); or
- a group member has operational control of a facility and the operation causes the emission of 25 kt of CO₂-e or more, or production or consumption of greater than 100 TJ of energy.

Energy efficiency opportunities

The aim of the *Energy Efficiency Opportunities Act 2006* is to improve the identification and evaluation of energy efficiency opportunities by energy intensive business and, as a result, to encourage the implementation of cost-effective energy efficiency opportunities.

The Act requires a controlling corporation to register and report its energy use once it meets the threshold of 0.5 petajoules of energy per financial year. Registered corporations are required to submit an assessment plan to the Australian Government that sets out their proposal to assess the opportunities for improving their energy efficiency. The first plan must cover a period of five years. Registered corporations must also prepare and make public a report of this assessment, the results, and the response of the corporation.

L1.2.4 State regulation

South Australia

The South Australian Government has developed a South Australian greenhouse strategy for tackling climate change based heavily on the *Climate Change and Greenhouse Emissions Reductions Act 2007*.

The key objectives of the legislation are:

- to reduce greenhouse emission levels by 60% (to an amount that is equal to or less than 40% of 1990 levels) by 2050
- to increase the proportion of renewable electricity generated so that it comprises at least 20% of electricity generated in South Australia by 2014
- to increase the proportion of renewable electricity consumed so that it comprises at least 20% of electricity consumed in South Australia by 2014.

The legislation also aims to promote action within South Australia by developing specific targets for various sectors of the state's economy, and developing policies and programs to reduce greenhouse gas emissions.

BHP Billiton is currently negotiating a Sector Agreement with the South Australian Government, specifically for the Olympic Dam expansion. Sector Agreements are voluntary agreements between the Minister for Sustainability and Climate Change and a business or industry grouping. They may set out the objectives and strategies for greenhouse emission abatement, as well as covering intended research, development and innovation in technologies or industry practices. The Agreement would be entered into on a voluntary basis for the purposes of facilitating strategies to meet targets set under the *Climate Change and Greenhouse Emissions Reductions Act 2007*.

Northern Territory

The *Northern Territory Strategy for Greenhouse Action 2006* (Northern Territory Government 2006) was prepared in line with the goals and principles of the Northern Territory Government's Greenhouse Policy Framework released in 2002. The strategy describes the following objectives:

- provide leadership to the community by demonstrating how the Northern Territory Government is addressing greenhouse gas emissions generated by its own activities
- minimise greenhouse gas emissions by management of savanna burning
- minimise greenhouse gas emissions from agriculture and land use changes and encourage the enhancement of carbon sinks
- minimise greenhouse gas emissions by improving management of transport and urban land use
- minimise greenhouse gas emissions from the supply and use of electricity
- minimise greenhouse gas emissions from industry and waste
- support efforts to increase our understanding of likely climate change and the actions needed to prepare for adaptation to the changing climate.

L1.2.5 BHP Billiton position

In June 2007, BHP Billiton released its Climate Change Position. The position comprises a multifaceted approach to tackling climate change and aims to:

- understand the emissions caused over the full life cycle of BHP Billiton's products
- improve the management of energy and greenhouse gas emissions across BHP Billiton's businesses
- commit US\$300 million over the next five years to support low emissions technology development, internal energy excellence projects and encourage emissions abatement by BHP Billiton employees and BHP Billiton local communities
- use BHP Billiton technical capacity and experience to assist governments and other stakeholders in the design of effective and equitable climate change policies including market-based mechanisms such as emissions trading.

BHP Billiton's action plan for these four targets is reprinted below.

Increase understanding of emissions caused over the life cycle of our products

It is essential that we understand the sources, scope and extent of greenhouse gas emissions associated with our activities:

- We will continue transparent public reporting of our emission profile, including our emissions from production activities, the use of BHP Billiton fossil fuel products by our customers, and the actions we undertake to manage and mitigate emissions.
- We will work with experts to improve our understanding of the full life cycle of our products and strategies for effectively reducing greenhouse gas emissions from their production and use.

Improve management of energy and greenhouse gas emissions from production

Some of our businesses are among the most energy efficient in the world. We build on this leading practice within the BHP Billiton Group, using external standards of excellence, to continually improve energy and greenhouse gas management at our sites. Emissions abatement and energy saving considerations are built into our decision-making processes, through:

- **Business excellence** – Our business excellence systems promote and share leading practice and innovation in energy and operational efficiency to deliver savings in emissions and costs.
- **Group targets** – We have set energy and greenhouse gas emissions intensity reduction targets of 13% and 6% respectively for the Group over the period 2006–2012.
- **Site based plans and targets** – Every site is required to have a greenhouse gas and energy management plan, including targets that are incorporated into their business plans with associated monitoring and reporting.
- **Carbon pricing** – We require carbon pricing sensitivity analysis to be undertaken in capital decisions on assets of US\$100 million or more or those that emit greater than 100,000 tonnes of CO₂-e per annum.
- **Market trading** – We trade emissions reduction instruments as a means of managing our emissions exposure and assisting our customers to manage their exposures.
- **Project-based emissions reductions** – We will continue to pursue external projects and other opportunities that deliver tangible reductions in greenhouse gas emissions and generate credits.

Working collaboratively with customers, communities and employees to reduce emissions and support internal emissions reduction projects

We will commit US\$300 million over the period 2008–2012 to:

- support industry research, development and demonstration of low emissions technologies including collaborative research dedicated to accelerating the commercial uptake of technologies such as carbon capture and geo-sequestration
- provide capital funding for internal energy projects with a greenhouse gas emissions reduction component that might not otherwise be competitive within our normal capital allocation processes
- support the efforts of our employees and our local communities to reduce their emissions.

Progressing climate change policy within our sphere of influence

Policy makers have a particularly important role in encouraging actions by all stakeholders and ensuring a fair distribution of the costs of emissions reduction. BHP Billiton is working with governments and other stakeholders on the development of policies that provide the necessary incentives and tools for effective, equitable abatement, including:

- policies aimed at accelerating the cost-effective reduction of emissions
- support for market-based mechanisms, provided that the measures are efficient, broad-based (geographically and cross-industry sectors) and are progressively introduced.

L1.2.6 Olympic Dam expansion position

The Olympic Dam expansion is implementing the BHP Billiton-wide position goals as part of its Greenhouse Gas and Energy Management Plan. To date a number of studies have been conducted that review the potential greenhouse gas footprint of the proposed expansion and analyse potential mitigation measures. These are summarised in Sections 3, 4 and 5 of this Appendix.

As well as complying with BHP Billiton's Climate Change Position, the company has set additional goals and targets specific to the Olympic Dam expansion in order to minimise the potential impacts of the expanded operation. These are:

- applying a goal of reducing greenhouse gas emissions (reportable under the National Greenhouse and Energy Reporting (Measurement) Determination 2008) to an amount equivalent to at least a 60% reduction (to an amount equal to or less than 40%) of 1990 emissions, by 2050
- constructing an on-site cogeneration power station (250 MW capacity) by recovering waste heat
- sourcing renewable energy (35 MW capacity) via the national electricity market for the seawater desalination plant
- producing an annual 'road map' that quantifies emission reduction opportunities and achievements.

The company will establish specific short-term targets for greenhouse gas emission reduction in its Environmental Management Program (EMP) at Olympic Dam in accordance with the International Standard AS/NZS 14001: 2004 Environmental Management Systems guidelines. BHP Billiton will also develop a detailed Greenhouse Gas and Energy Management Plan for Olympic Dam that will:

- establish modelling to project the likely emissions from the expanded Olympic Dam operation from commencement to 2050
- establish targets and timelines for greenhouse gas reduction
- identify greenhouse gas reduction strategies and projects.

The EMP and Greenhouse Gas and Energy Management Plans will be reviewed annually.

L1.3 EMISSIONS ASSESSMENT METHODOLOGY

L1.3.1 Scope

The potential greenhouse gas footprint of the expanded operation was assessed by incorporating emissions generated from the following sources:

- stationary energy emissions (such as from fuelburning equipment like furnaces)
- transport fuel emissions
- emissions associated with electricity use
- emissions associated with changes to land use (such as land clearing)
- emissions associated with oxidation reactions within the metallurgical process, the rock storage facility (RSF) and the tailings storage facility (TSF).

The scope of the greenhouse gas assessment was the entire expansion as outlined in Chapter 5, Description of the Proposed Expansion. The assessment estimated emissions from electricity purchased through the national electricity market (NEM) as a worst case. The addition of an on-site combined cycle gas turbine (CCGT) power station would reduce the emissions estimated in Section 13.2.5 by using solely natural gas to generate electricity.

L1.3.2 Boundaries

To estimate greenhouse gas emissions for the proposed expansion the following assumptions and limitations were used:

- electricity was assessed as purchased from the NEM
- electricity demand reflected the operation of the 250 MW cogeneration plant and the use of renewable electricity (purchased under contract from the NEM) for the desalination plant (35 MW)
- natural gas was not used to replace other liquid fuels (diesel, fuel oil etc) as an estimation of worst-case emissions
- material transport emissions were limited to transport within Australia.

L1.3.3 Emission factors

Fuel and energy emission sources

The emissions for the existing Olympic Dam operation were calculated by multiplying the volume or mass of a greenhouse gas emitting fuel or process by an emission factor, resulting in a value for the likely amount of CO₂-e emitted. The CO₂-e value accounts for the various greenhouse gases emitted, taking into account their respective GWP and the amount emitted.

The emission factors used in this study were sourced from the National Greenhouse and Energy Reporting (Measurement) Determination 2008 (NGER 2008) or, where NGER factors were not available, the National Greenhouse Accounts Factors (NGAF 2008). NGAF factors were also used in the determination of Scope 2 and 3 emissions.

The electricity emission factor slightly declines over time (i.e. the CO₂-e per MWh of electricity consumed decreases), reflecting the de-carbonisation of the South Australian electricity mix as the proportion of coal used to generate electricity declines and the proportionate use of fuels such as natural gas and renewables increases (ABARE 2006). This is shown in Table L1.3.

Table L1.3 Electricity emission factor over time

Development phase	Emission factor (kg CO ₂ -e per MWh)
Existing	840
Initial development (to 20 Mtpa ¹ ore)	840
Intermediate development (to 40 Mtpa ore)	840
Full capacity of expansion (to 60 Mtpa ore)	803
At closure (Year 40)	734

¹ Mtpa = million tonnes per annum.

The above de-carbonisation of the electricity mix is exclusive of de-carbonisation that may occur as a result of compliance with the *South Australian Climate Change and Emissions Reduction Act 2007* targets, under which the State Government has committed to producing 20% of electricity from renewable sources by 2014.

L1.3.4 Other emission sources

Metallurgical process

CO₂ is emitted from the metallurgical process when flotation tailings containing carbonate minerals is leached with sulphuric acid to extract the copper and uranium. The primary carbonate is siderite (FeCO₃) with the proportion of other carbonates (including dolomite) being relatively small. Siderite displays around 80% solubility during leaching. Emissions from the proposed metallurgical plant were estimated using ore feed geochemical data.

Tailings storage facility

The emission of CO₂ from the tailings storage facility (TSF) occurs as acidic seepage is neutralised by the underlying limestone in the following series of reactions:



The bicarbonate that forms reacts further as follows:



For the purpose of this assessment, a seepage rate from the TSF of 3,200 m³/d, at an acidity of 43 g CaCO₃ eq/L, has been used to estimate potential CO₂ generation. This equates to about 22,230 t of CO₂ per cell per annum while the tailings are actively deposited in the cell. Thereafter the rate of generation would decrease as percolation decreased.

An investigation by John Chapman (SRK 2008) concluded that "Due to the overlying tailings, release of CO₂ to the atmosphere is expected to be inhibited. Rather, the CO₂ would tend to accumulate beneath the TSF cells which would lead to a condition of temporary sequestration. Over time, the CO₂ would, however, dissipate by diffusion from beneath the TSF (possibly combined with transport away as a dissolved constituent) so that the release would tend to lag the generation by many years (decades to centuries)".

For the purpose of developing a GHG inventory, it has been assumed that the CO₂ emissions from tailings are emitted to atmosphere in the year that they are generated.

Rock storage facility

In a process similar to that occurring within the metallurgical plant and TSF, acidic liquor generated within the rock storage facility (RSF) (as a result of reactions between rainfall and reactive mine rock) would react with carbonates in the mine rock, releasing CO₂. The CO₂ would diffuse through the RSF and be emitted to atmosphere. The volume of CO₂ emitted would depend on a number of factors including the volume of rainfall entering the RSF and the reaction kinetics that generate acid and subsequently the potential of the acidic leachate to contact carbonate materials.

Emissions from the RSF would not commence until some time after the RSF began operating, and would continue for at least 100 or 200 years post-closure as the pore water within the RSF percolated through the facility. Emission estimates from the RSF were provided by HLA ENSR and are based on geochemical information from the RSF geochemical studies (see Chapter 12, Groundwater and Appendix K4 and K5 for details).

Land use change

In addition to the above-mentioned sources, land use change associated with land clearing for infrastructure results in one-off greenhouse gas emissions. Emissions from changes to land use were estimated using the National Greenhouse Accounting Toolkit FullCam model. The assumptions used for this assessment were:

- that the disturbed land has not been grazed or used for agriculture previously
- that the area of disturbance was classified as an even mix of Chenopod shrubland and Acacia shrubland
- that the total area of disturbance at Year 40 was 17,270 ha (see Chapter 15, Terrestrial Ecology, for further details of land disturbance)

L1.3.5 Scope 1, 2 and 3 emissions

Emissions are reported in terms of scope, which defines how and where the greenhouse gases are generated within an organisation. Scope 1, 2 and 3 emissions are included in this assessment, and are defined as:

Scope 1

The Federal Government definition for Scope 1 emissions is 'direct emission from sources within the boundary of an organisation' (WBCSD and WRI 2004). An example of Scope 1 is the diesel used to haul ore from the mine up to the metallurgical area, or train haulage if BHP Billiton owns the tracks. For this assessment all Scope 1 emissions have been included.

Scope 2

Scope 2 emissions are 'indirect emissions from the consumption of purchased electricity, steam or heat produced by another organisation' (WBCSD and WRI 2004). This includes emissions from electricity purchased from the National Electricity Market (NEM). All Scope 2 emissions have been assessed. The other rationale for including these emissions is that electricity usage at Olympic Dam is substantial and would have an impact on the South Australian Government's targets under the *Climate Change and Emissions Reductions Act 2007* (SA).

Scope 3

Scope 3 includes all other indirect emissions other than those that are covered by Scope 2, namely all emissions that are the consequence of an organisation's activities but are not from sources owned or controlled by the organisation (excluding indirect emissions from the consumption of purchased electricity, steam or heat produced by another organisation). For example, it includes diesel used to transport copper from Olympic Dam to Adelaide by open road. To give an overall indication of the expanded operation's carbon footprint this assessment includes all Australian transport emissions. There is also a chance that these emissions could be Scope 1 emissions depending on whether or not BHP Billiton owns the transport option (e.g. trucks or rail). The assessment does not include transport outside Australia, transport to the final customer (after port), or embedded emissions in raw materials.

L1.4 EXISTING ENVIRONMENT

Fuel and electricity consumption data for the existing Olympic Dam operation are described in Table L1.4 below.

Table L1.4 Typical fuel and electricity consumption by type

Energy type and units	Volume/mass consumed per annum
On-site diesel (kL)	24,250
Electricity (MWh)	870,000
Explosives – Ammonium nitrate (t)	3,000
Explosives – Emulsion (t)	2,000
LPG (GJ)	780,000
Natural gas (GJ)	0
Fuel oil (kL)	8,000
Soda ash (t)	1,000
Coke (t)	13,000
Electrical switchyard gases ¹ (t)	0.33
Material transport diesel (kL)	1,825

¹ Refers to volumes stored within electrical switchgear expressed in CO₂ equivalent tonnes.

Table L1.5 provides the energy content factors and emissions factors for calculating the expected annual emissions that would be reported under the NGER Act for the existing operation. Table L1.6 details the estimated totals of other greenhouse gas emissions emitted by the existing operation but not covered within the NGER methodology, including indirect and process-related emissions, derived from NGAF and other emissions estimation methodologies.

Table L1.5 Existing operation annual NGER greenhouse gas emissions

Energy type and units	Energy content factor (GJ/unit)	Emission factor (kg CO ₂ -e / GJ)			t CO ₂ -e			
		CO ₂	CH ₄	N ₂ O	Existing operation			
					CO ₂	CH ₄	N ₂ O	SF ₆
Gaseous fuels								
LPG (m ³)	0.0393	51.2	0.1	0.03	39,936	78	23	n.a.
Natural gas (m ³)	0.0393	51.2	0.1	0.03	0	0	0	n.a.
Liquid fuels								
Fuel oil (stationary energy) (kL)	39.7	72.9	0.03	0.2	23,153	10	64	n.a.
Diesel (transport) (kL)	38.6	69.2	0.2	0.5	69,449	201	502	n.a.
Industrial processes – mineral products								
Soda ash use (t)	0.415 ¹	n.a.	n.a.	n.a.	415	n.a.	n.a.	n.a.
Industrial processes – metal industry								
Carbon reductant – coke (t)	30	90	0.02	0.2	35,100	7.8	78	n.a.
Industrial processes – gas insulated switchgear and circuit breakers								
Sulphur hexafluoride (SF ₆) (t)	0.005 ²	n.a.	n.a.	n.a.	n.a.	n.a.	n.a.	12
Scope 2 emissions								
Purchase of electricity from network (kWh)	0.84 ³	n.a.	n.a.	n.a.	730,800	n.a.	n.a.	n.a.
Sub-totals					898,853	296	667	12
Total							899,828	

¹ measured in t of CO₂-e per tonne of soda ash used² refers to leakage rate relative to total installed volume (in CO₂-e tonnes)³ electricity emission factor measured in kg CO₂-e per kWh

Table L1.6 Existing operation annual greenhouse gas emissions from non-NGER sources

Source	Energy content factor (GJ/unit)	Emission factor (kg CO ₂ -e / GJ)		Source	Existing operation	
		t CO ₂ -e			Scope 1	Scope 3
		Scope 1	Scope 3			
Process emissions						
Metallurgical process emissions	n.a.	See note 1	n.a.	BHPB	68,940	n.a.
TSF	n.a.	See note 2	n.a.	SRK	22,230	n.a.
Liquid fuels						
On-site diesel (kL)	38.6	n.a.	5.3	NGAF	n.a.	5,319
Fuel oil (kL)	39.7	n.a.	5.3	NGAF	n.a.	1,683
Material transport diesel (kL)	38.6	n.a.	74.8	NGAF	n.a.	5,269
Gaseous fuels						
LPG (t)	25.5	n.a.	5.3	NGAF	n.a.	4,134
Natural gas (m ³)	0.0393	n.a.	18.6	NGAF	n.a.	0
Purchased electricity						
Electricity (kWh)	n.a.	n.a.	0.14	NGAF	n.a.	121,800
Explosives						
ANFO (t)	n.a.	0.17 ³	n.a.	NGAF	510	n.a.
Emulsion (t)	n.a.	0.17 ³	n.a.	NGAF	340	n.a.
Industrial processes – metal industry						
Carbon reductant – coke (t)	30	n.a.	20.7	NGAF	n.a.	8,073
Sub-totals					92,020	146,279

¹ where CO₂-e equals tonnes per annum of ore throughput x the proportion of siderite x the siderite dissolution factor x molecular mass of CO₂ / molecular mass FeCO₃, and:

Siderite dissolution 80%

Siderite proportion (25-year average) 2.5%

Ratio of molecular masses 0.383

² estimate provided by SRK based on tailings geochemical data

³ Units are tonne of CO₂-e per tonne of explosive

Table L1.7 summarises the estimated total greenhouse gas emissions for the existing operation by scope.

Table L1.7 Existing total annual greenhouse gas emissions by scope (all sources)

Scope	Existing operation (t CO ₂ -e)
Scope 1	261,048
Scope 2	730,800
Scope 3	146,279
Total	1,138,127

Total greenhouse gas emissions from the existing Olympic Dam operation are around 1.14 Mtpa of CO₂-e per annum, with an NGER-reportable component of around 0.9 Mtpa of CO₂-e. Figures L1.2 and L1.3 show the annual greenhouse gas emissions (all sources) for the existing operation by source and scope, respectively.

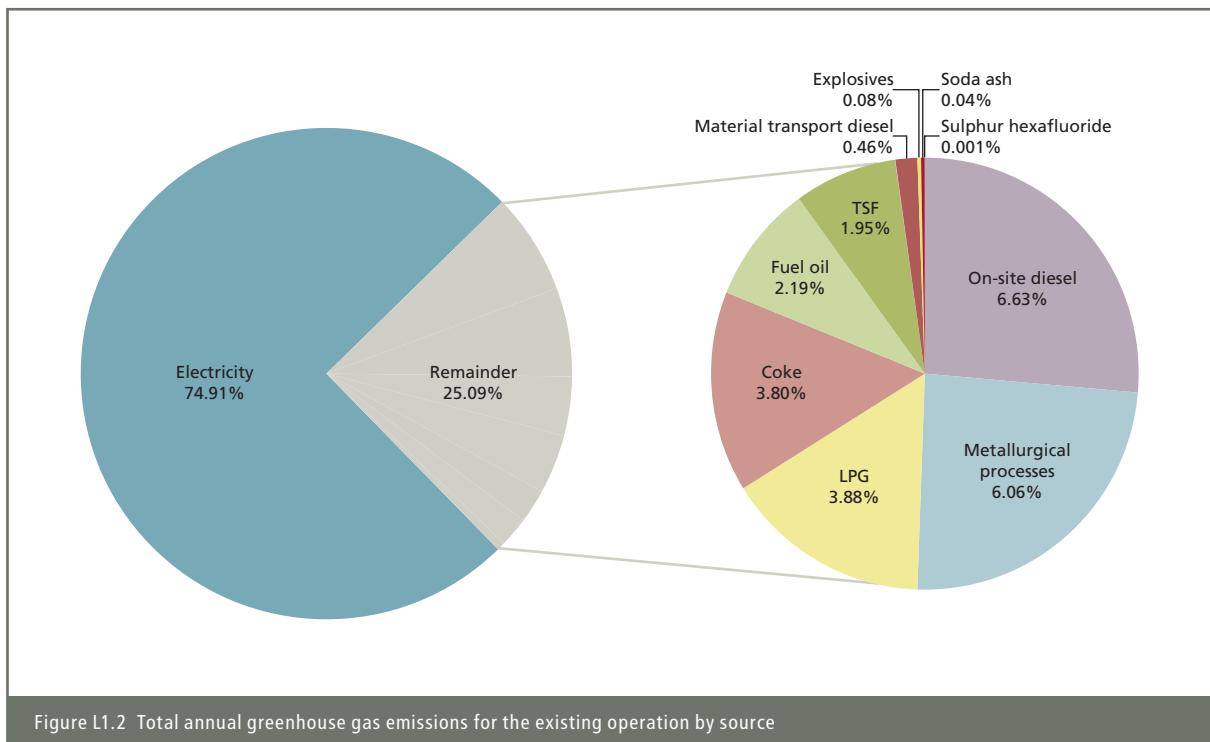


Figure L1.2 Total annual greenhouse gas emissions for the existing operation by source

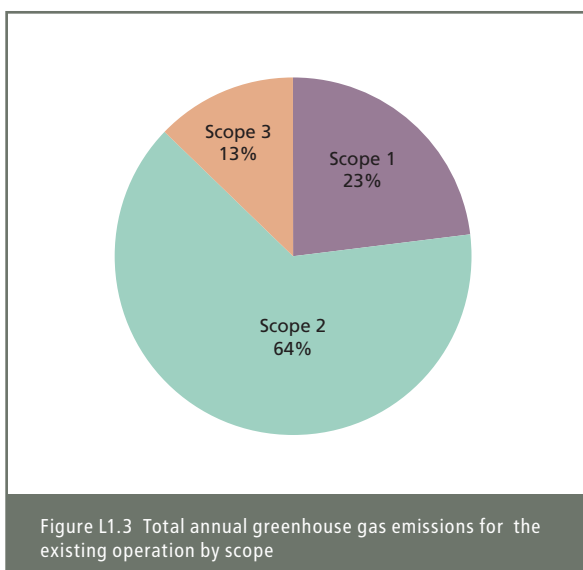


Figure L1.3 Total annual greenhouse gas emissions for the existing operation by scope

L1.5 PROPOSED EXPANSION

L1.5.1 Installed mitigation

The proposed expanded operation would reduce its fossil fuel electricity demand through committing to two mitigation strategies:

- installing 250 MW of cogenerated electricity capacity
- using renewable electricity (sourced from the NEM) to meet the electricity demand (35 MW) for the proposed coastal desalination plant.

These are detailed below.

Cogeneration

Overview

Four sulphur-burning acid plants of around 3,500 tonnes per day sulphuric acid producing capacity would be constructed to supply acid to the new hydrometallurgical plant. Significant waste heat is generated during the exothermic sulphur burning process. This would be captured and used to operate a steam turbine to produce electricity.

The capacity of the cogeneration plant would vary depending on the number and throughput of the acid plants, which would vary where the capacity of the acid plants was being ramped up to match the throughput of material in the hydrometallurgical plant. The cogeneration plant would have a capacity of around 250 MW, reducing the proposed electricity demand for the expansion to around 400 MW.

Design

The output of the cogeneration plant would be stepped up from 11 kV to 132 kV and connected to the new metallurgical plant substation for distribution around the operation. The output from the cogeneration plant would reduce the draw in power from the main intake substation, reducing the demand on the NEM.

Renewable electricity

A commitment to use renewable electricity to power the coastal desalination plant has been made. This would most likely be in the form of purchased wind energy contracted through the NEM.

L1.5.2 Emissions assessment

Fuel and energy data

Annual fuel and electricity consumption data for the various development phases of the expanded operation (exclusive of existing operation) are described in Table L1.8.

Table L1.8 Fuel and electricity annual consumption for the proposed expansion

Energy type and units	Volume / mass consumed			
	Initial development to 20 Mtpa	Intermediate development to 40 Mtpa	Full operating capacity of 60 Mtpa	At closure (Year 40)
On-site diesel (kL)	330,000	367,000	454,000	454,000
Electricity (MWh)	1,465,000	2,050,000	2,573,000	2,573,000
Explosives – ANFO (t)	110,000	110,000	110,000	110,000
Explosives – Emulsion (t)	4,500	4,500	4,500	4,500
LPG (GJ)	0	816,000	816,000	816,000
Natural gas (GJ)	0	0	0	0
Fuel oil (kL)	0	14,000	14,000	14,000
Soda ash (t)	0	6,700	6,700	6,700
Coke (t)	0	18,300	18,300	18,300
Electrical switchgear gases ¹ (t)	4,800	9,700	14,500	14,500
Material transport diesel (kL)	16,000	27,000	36,500	36,500

¹ Refers to volumes stored within the electrical switchgear expressed in CO₂-e tonnes.

L1.5.3 Estimation of emissions

Annual emissions

Table L1.9 provides the energy content factors and emissions factors for calculating the expected annual emissions that would be reported under the NGER Act for the proposed expansion (exclusive of the existing operation). Table L1.10 details the estimated totals of other greenhouse gas emissions expected to be emitted by the proposed operation but not covered within the NGER methodology, including indirect and process-related emissions, derived from NGAF and other emissions estimation methodologies.

Table L1.9 Expanded operation annual NGER greenhouse gas emissions

Energy type and units	Energy content factor (GJ/unit)	Emission factor (kg CO ₂ -e / GJ)			t CO ₂ -e																
						Initial development to 20 Mtpa				Intermediate development to 40 Mtpa				Full operating capacity of 60 Mtpa				At closure (year 40)			
		CO ₂	CH ₄	N ₂ O		CO ₂	CH ₄	N ₂ O	SF ₆	CO ₂	CH ₄	N ₂ O	SF ₆	CO ₂	CH ₄	N ₂ O	SF ₆	CO ₂	CH ₄	N ₂ O	SF ₆
Gaseous fuels																					
LPG (m ³)	0.0393	51.2	0.1	0.03	0	0	0	n.a.	41,779	81.6	24.48	n.a.	41,779	82	24	n.a.	41,779	82	24	n.a.	
Natural gas (m ³)	0.0393	51.2	0.1	0.03	0	0	0	n.a.	0	0	0	n.a.	0	0	0	n.a.	0	0	0	n.a.	
Liquid fuels																					
Fuel oil (stationary energy) (kL)	39.7	72.9	0.03	0.2	0	0	0	n.a.	40,518	17	111	n.a.	40,518	17	111	n.a.	40,518	17	111	n.a.	
Diesel (transport) (kL)	38.6	69.2	0.2	0.5	881,470	2,548	6,369	n.a.	980,301	2,833	7,083	n.a.	1,076,461	3,111	7,778	n.a.	1,076,461	3,111	7,778	n.a.	
Industrial processes - mineral products																					
Soda ash use (t)	0.415 ¹	n.a.	n.a.	n.a.	0	n.a.	n.a.	n.a.	2,781	n.a.	n.a.	n.a.	2,781	n.a.	n.a.	n.a.	2,781	n.a.	n.a.	n.a.	
Industrial processes - metal industry																					
Carbon reductant - coke (t)	30	90	0.02	0.2	0	0	0	n.a.	49,410	11	110	n.a.	49,410	11	110	n.a.	49,410	11	110	n.a.	
Industrial processes - gas insulated switchgear and circuit breakers																					
Sulphur hexafluoride (SF ₆) (t)	0.005 ²	n.a.	n.a.	n.a.	n.a.	n.a.	n.a.	24	n.a.	n.a.	n.a.	49	n.a.	n.a.	n.a.	73	n.a.	n.a.	n.a.	73	
Scope 2 emissions																					
Purchase of electricity from network (kWh)	see below ³	n.a.	n.a.	n.a.	1,230,600	n.a.	n.a.	n.a.	1,722,000	n.a.	n.a.	n.a.	2,066,119	n.a.	n.a.	n.a.	1,888,582	n.a.	n.a.	n.a.	
					Sub-total	2,112,070	2,548	6,369	24	2,836,789	2,942	7,329	49	3,277,068	3,220,414	8,023.34	73	3,099,530.88	3,220	8,023	73
									Total					Total				Total			Total
									2,121,010					2,847,108				3,288,384			3,110,847

¹ measured in t of CO₂-e per tonne of soda ash used

² refers to leakage rate relative to total installed volume (in CO₂-e tonnes)

³ electricity emission factor changes with time as per the following:

Initial	0.84 kg CO ₂ -e per kWh
Intermediate	0.84 kg CO ₂ -e per kWh
Full capacity	0.803 kg CO ₂ -e per kWh
Year 40	0.734 kg CO ₂ -e per kWh

Table L1.10 Expanded operation annual greenhouse gas emissions from non-NGER sources

Source	Energy content factor (GJ/unit)	Emission factor (kg CO ₂ -e / GJ)		Source	Initial development (to 20 Mtpa)		Intermediate development (to 40 Mtpa)		Full capacity of expansion (to 60 Mtpa)		At Year 40 (60 Mtpa)	
		Scope 1	Scope 3		t CO ₂ -e		t CO ₂ -e		t CO ₂ -e		t CO ₂ -e	
					Scope 1	Scope 3	Scope 1	Scope 3	Scope 1	Scope 3	Scope 1	Scope 3
Process emissions												
Tails leach	n.a.	See note 1	n.a.	BHPB	153,200	n.a.	306,400	n.a.	459,600	n.a.	459,600	n.a.
RSF	n.a.	See note 2	n.a.	HLA	0	n.a.	0	n.a.	160,000	n.a.	160,000	n.a.
TSF	n.a.	See note 3	n.a.	SRK	66,700	n.a.	133,400	n.a.	200,080	n.a.	200,080	n.a.
Liquid fuels												
On-site diesel (kL)	38.6	n.a.	5.3	NGAF	n.a.	67,511	n.a.	75,081	n.a.	82,446	n.a.	82,446
Fuel oil (kL)	39.7	n.a.	5.3	NGAF	n.a.	0	n.a.	2,946	n.a.	2,946	n.a.	2,946
Material transport diesel (kL)	38.6	n.a.	74.8	NGAF	n.a.	46,196	n.a.	77,957	n.a.	105,386	n.a.	105,386
Gaseous fuels												
LPG (t)	25.5	n.a.	5.3	NGAF	n.a.	0	n.a.	4,325	n.a.	4,325	n.a.	4,325
Natural gas (m3)	0.0393	n.a.	18.6	NGAF	n.a.	0	n.a.	0	n.a.	0	n.a.	0
Purchased electricity												
Electricity (kWh)	n.a.	n.a.	0.14	NGAF	n.a.	205,100	n.a.	287,000	n.a.	360,220	n.a.	360,220
Explosives												
ANFO (t)	n.a.	0.17 ⁴	n.a.	NGAF	18,700	n.a.	18,700	n.a.	18,700	n.a.	18,700	n.a.
Emulsion (t)	n.a.	0.17 ⁴	n.a.	NGAF	765	n.a.	765	n.a.	765	n.a.	765	n.a.
Industrial processes - metal industry												
Carbon reductant - coke (t)	30	n.a.	20.7	NGAF	n.a.	0	n.a.	11,364	n.a.	11,364	n.a.	11,364
Sub-total					239,365	318,808	459,265	458,672	839,145	566,686	839,145	566,686

¹ where CO₂-e equals tonnes per annum of ore throughput x the proportion of siderite x the siderite dissolution factor x molecular mass of CO₂ / molecular mass FeCO₃, and

Siderite dissolution 80%

Siderite proportion (25-year average) 2.5%

Ratio of molecular masses 0.383

² estimated based on work undertaken by BHPB by HLA ENSR and geochemical studies (see Appendix K of the EIS) and based on reactions commencing 6 years after initial development

³ estimate provided by SRK

⁴ Units are tonne of CO₂-e per tonne of explosive

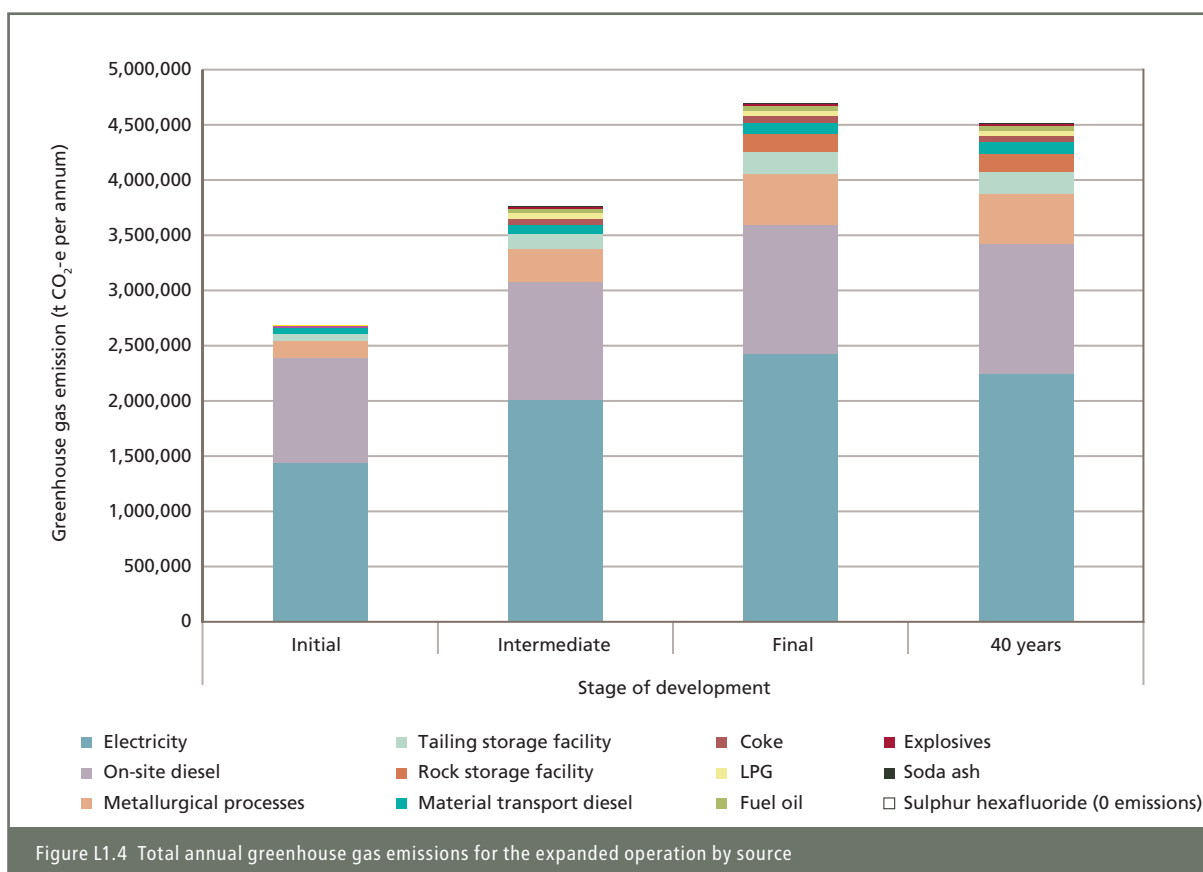
Table L1.11 summarises the estimated total annual greenhouse gas emissions for the proposed expansion by scope.

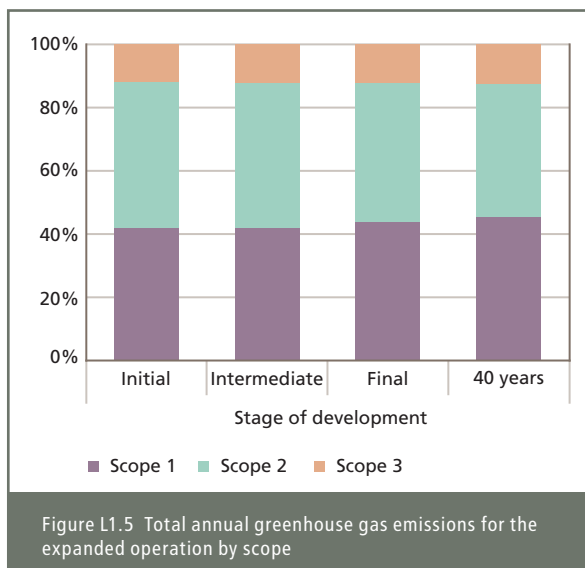
Table L1.11 Estimated total annual greenhouse gas emissions by scope (all sources)

Scope	GHG emission (t CO ₂ -e per annum)			
	Initial development to 20 Mtpa	Intermediate development to 40 Mtpa	Full operating capacity of 60 Mtpa	At closure (Year 40)
Scope 1	1,129,775	1,584,373	2,061,410	2,061,410
Scope 2	1,230,600	1,722,000	2,066,119	1,888,582
Scope 3	318,808	458,672	566,686	566,686
Total	2,679,183	3,765,045	4,694,215	4,516,678

Predicted total annual greenhouse emissions from the proposed expansion would peak at approximately 4.7 Mtpa of CO₂-e, with an NGER-reportable component of around 3.3 Mtpa of CO₂-e.

The breakdown of emission source varies with each phase of development, however Scope 2 emissions (being off-site electricity production) account for approximately 42–46% of all greenhouse gas emissions for the proposed expansion. Scope 1 emissions (largely on-site diesel consumption and on-site process-related CO₂ emissions) comprise between 42–46% with Scope 3 emissions being the balance (see Figures L1.4 and L1.5).





The proposed expansion would result in an increase in the proportion of Scope 1 emissions compared with the existing operation as a result of the significant increase in diesel (required by the new open pit mining fleet) and the positive influence of using cogenerated electricity. The proportion of Scope 3 emissions also increases as a result of the increased transport volumes and distances associated with transporting sulphur from Outer Harbor to Olympic Dam and copper concentrate containing uranium to the Port of Darwin for export.

Land use change

In addition to the above-mentioned sources, land use change associated with land clearing for infrastructure associated with the expansion would result in one-off greenhouse gas emissions totalling approximately 0.92 Mt of CO₂-e over the life of the expansion, comprising:

- 330,000 t of CO₂-e associated with carbon loss from vegetation clearing
- 260,000 t of CO₂-e associated with carbon loss from removal of debris
- 330,000 t of CO₂-e associated with carbon loss from soil

In addressing vegetation clearance, significant environmental benefit (SEB) offsets would be used to comply with the *SA Native Vegetation Act 1991*. BHP Billiton would offset land disturbance by setting aside approximately 126,650 ha of arid land for conservation, including de-stocking (see Chapter 15, Terrestrial Ecology).

L1.5.4 Expanded operation greenhouse gas emissions in context

Over the next five decades, Australian and global greenhouse gas emissions are predicted to rise from the current 506 Mtpa and 36,200 Mtpa. No specific emission projections for South Australia exist, however assuming the proportion of South Australia's greenhouse gas emissions (relative to Australia) remains constant (at around 7.5%), South Australian greenhouse gas emissions can be inferred. This is described in Table L1.12.

Table L1.12 Projected Australian and global greenhouse gas emissions in Mtpa of CO₂-e (excluding land use change)

Source	2010	2020	2030	2040	2050
South Australia ¹	41.2	47.8	52.1	56.4	60.5
Australia	549	638	695	752	806
Global	42,300	53,800	63,600	75,800	89,600

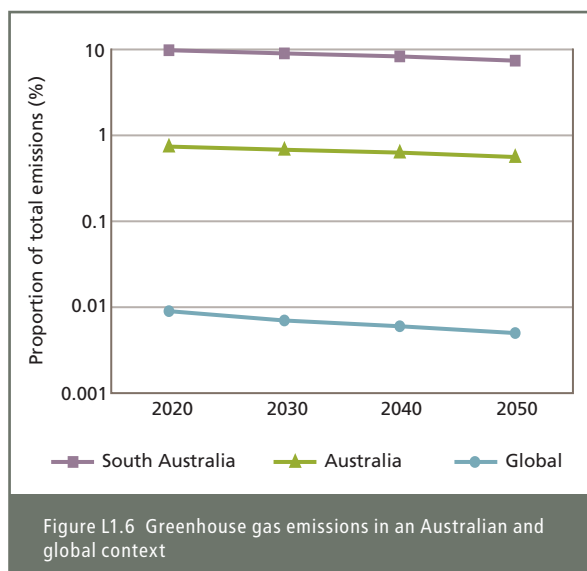
Source: ABARE 2007

¹South Australian data inferred from Department of Climate Change 2008.

The additional greenhouse gas emissions associated with the proposed expansion would constitute only a relatively small proportion of overall state, national and international emissions as described in Table L1.13 below and shown in Figure L1.6.

Table L1.13 Proposed expansion emissions represented as a proportion (in per cent) of projected state, national and international emissions (excluding land use change)

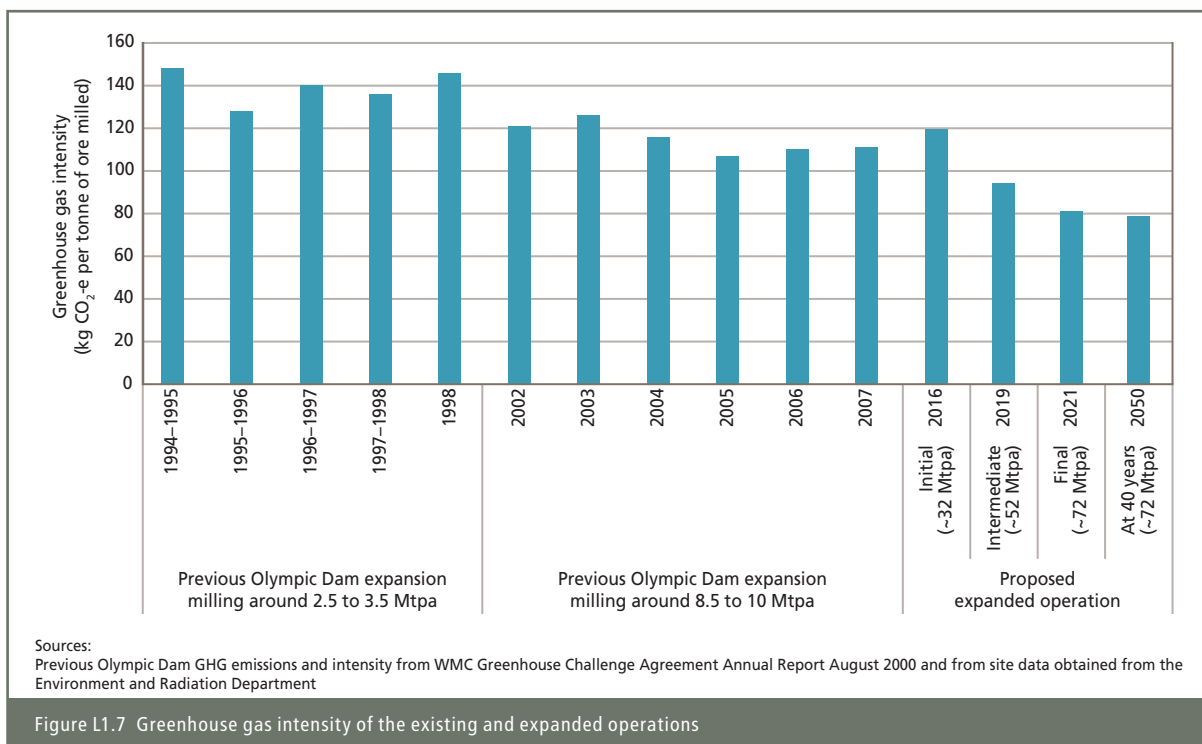
Source	2010	2020	2030	2040	2050
South Australia	0	9.8	9.0	8.3	7.4
Australia	0	0.74	0.68	0.63	0.56
Global	0	0.009	0.007	0.006	0.005



On the basis of the data presented in Table L1.13, the residual impacts of greenhouse gas emissions have been categorised as moderate.

For the purpose of providing context to global emissions, the abatement potential of the uranium oxide produced at Olympic Dam has been estimated. At full operating capacity, the expanded operation would produce up to 19,000 tpa of uranium oxide, which when used in nuclear power plants by customer countries would produce about 756,000 GWh of electricity. If, for example, this was used to substitute electricity supplied by typical fuel mixes in Australia, China and the United States of America, it would reduce direct greenhouse gas emissions by 615 Mtpa, 687 Mtpa and 438 Mtpa of carbon dioxide equivalents, respectively. This compares to Australia's total 2006 carbon emissions of 575 Mt of carbon dioxide equivalents.

The greenhouse gas intensity (emissions of CO₂-e per tonne of ore milled) of Olympic Dam has decreased since the commencement of operations, reflecting increased efficiencies associated with previous optimisations and expansions. The proposed expansion would result in an initial increase in the greenhouse gas intensity to around 119 kg of CO₂-e per tonne of ore milled, from the current 105 kg of CO₂-e per tonne of ore milled, as a result of the ramp-up in mining and the energy usage associated with the movement of overburden during the initial development phases. This would decrease as the development progressed, with greenhouse gas intensity reducing to around 79 kg of CO₂-e per tonne of ore milled (see Figure L1.7) as the ore extraction rate increased and the mine rock extraction rate decreased.



L1.6 GREENHOUSE GAS MITIGATION AND MANAGEMENT

L1.6.1 Overview

Earlier sections of this appendix detailed the overall carbon footprint of the existing Olympic Dam operation and the proposed Olympic Dam expansion. If no further measures, beyond those detailed in Section L5.1, were taken to mitigate greenhouse gases, it is estimated that the proposed expansion would emit approximately 4.7 Mtpa of CO₂-e per annum at full operating capacity, in addition to the 1.1 Mtpa of CO₂-e associated with the existing Olympic Dam operation.

As detailed in Section L2.6, BHP Billiton is committed to a goal of achieving significant emissions reductions over the life of the proposed expansion as detailed in Chapter 5, Description of the Proposed Expansion, of the Draft Environmental Impact Statement. The following sections detail potential mitigation options that are presently being investigated with a view to understanding their potential to cost-effectively reduce the proposed expansion's carbon footprint. As technologies are constantly evolving, and new and innovative mitigation and management measures are developed, this list will also develop and mature. Overall progress to the goal outlined above, including the establishment of interim targets, trajectories, updated descriptions of technologies being investigated, and the current state of investigations, would be detailed in the Greenhouse Gas and Energy Management Plan and site EMP documentation, to be reviewed annually.

L1.6.2 Methodology

Carbon reduction cost curves

To understand the path to achieving the goal, BHP Billiton has undertaken modelling using McKinsey & Company's Australian carbon reduction methodology (2008). The carbon reduction cost curves featured below show that significant greenhouse gas reduction is possible with current and near-future technologies. Figures L1.8 to L1.11 detail one potential pathway to achieving reductions in emissions from project inception to the year 2050. To arrive at these conclusions, the cost and carbon reduction potential of specific projects have been analysed using a three-step process:

- (1) A project baseline was established, as detailed in the earlier sections of this appendix.
- (2) A range of emission-reduction opportunities was identified through project workshops and fact-based estimates were made of the costs and potential abatement volume presented by each opportunity. A range of assumptions was made, including power capacity forecasts, expected learning curves, and initial generation costs.
- (3) These costs and volumes were combined to form the Olympic Dam expansion carbon reduction cost curves.

In interpreting the carbon reduction cost curves, the following should be noted:

- The project baseline (horizontal axis) represents the total carbon emissions if no effort beyond that detailed in Section L5.1 were made to address climate change. The baseline includes all projected Scope 1 and Scope 2 emissions and some Scope 3 emissions for the expansion project (see Section L5 of this appendix).
- The vertical axis represents the cost of carbon reduction. The carbon reduction measures are divided into initiatives that could reduce the demand for energy (demand-side levers) and those that reduce the carbon dioxide emissions in the supply of energy (supply-side levers). All carbon reduction measures are ordered from lowest to highest cost. The measures that have a negative cost are the most cost-effective opportunities to implement.

Offsets

The implementation of demand and supply-side greenhouse gas mitigation measures alone would not achieve the 2050 goal as described previously. Fixed greenhouse gas emissions not related to the demand and supply of energy, such as those from land use change, the metallurgical plant and the RSF and TSF, would require offsets or permits. Options for offsetting these emissions would be investigated under the Greenhouse Gas and Energy Management Plan for the proposed expansion.

Key choices

All carbon reduction opportunities have been assessed through a cost-benefit analysis and trade-offs are then made between mutually exclusive opportunities, interdependent options, timing, modularity and practicality.

Mutually exclusive opportunities

Mutually exclusive opportunities are opportunities that cannot be implemented at the same time. For example, if trolley assist is implemented with haulage trucks, LNG trucks become a safety concern. The approach to choosing between the options is to select the lowest cost, highest abatement option.

Interdependence between opportunities

This involves opportunities that rely on another opportunity or enabling technology to be executed. For example, if a CCGT were built on-site, there would be a gas pipeline built, and this would enable liquid fuel replacement with natural gas and the use of LNG trucks. The approach taken in this case is to combine interdependent ideas.

Timing

Timing may limit when carbon reduction opportunities can occur. For example, the in-pit crushing and conveying options rely on the formation of a pit at a certain depth before such systems can be installed. Options with timing constraints are only brought into the model when the timing is realistic.

Modularity

Modularity is the ability for carbon reduction opportunities to be sized to need. Some plants are only available economically in certain sized blocks. For example, on-site CCGT requires a sizing of 550 MW to be economic. For this reason, the modelling only considered modules of minimum or maximum efficient scale.

Cost-benefit analysis methodology

To determine the exact cost of each measure, capital expenditure, operating expenditure and carbon reduction figures for each option were all inputs into the cost-benefit analysis calculations to produce a net present cost and a carbon reduction volume. Values for future energy prices, captured in both fuel usage and carbon values, and annual escalations were predicted and applied in the analysis.

The carbon reduction cost curve allows the total cost of a greenhouse gas reduction measure and the carbon footprint of each measure to be compared directly. As such, the measures with the most effective trade-off between cost and greenhouse gas reduction have been identified.

L1.6.3 Current and near-future mitigation options

Overview

Potential greenhouse gas reduction projects are divided into those that reduce energy demand, and those that provide a cleaner energy supply. Demand-side projects used in the modelling for the expanded Olympic Dam operation were:

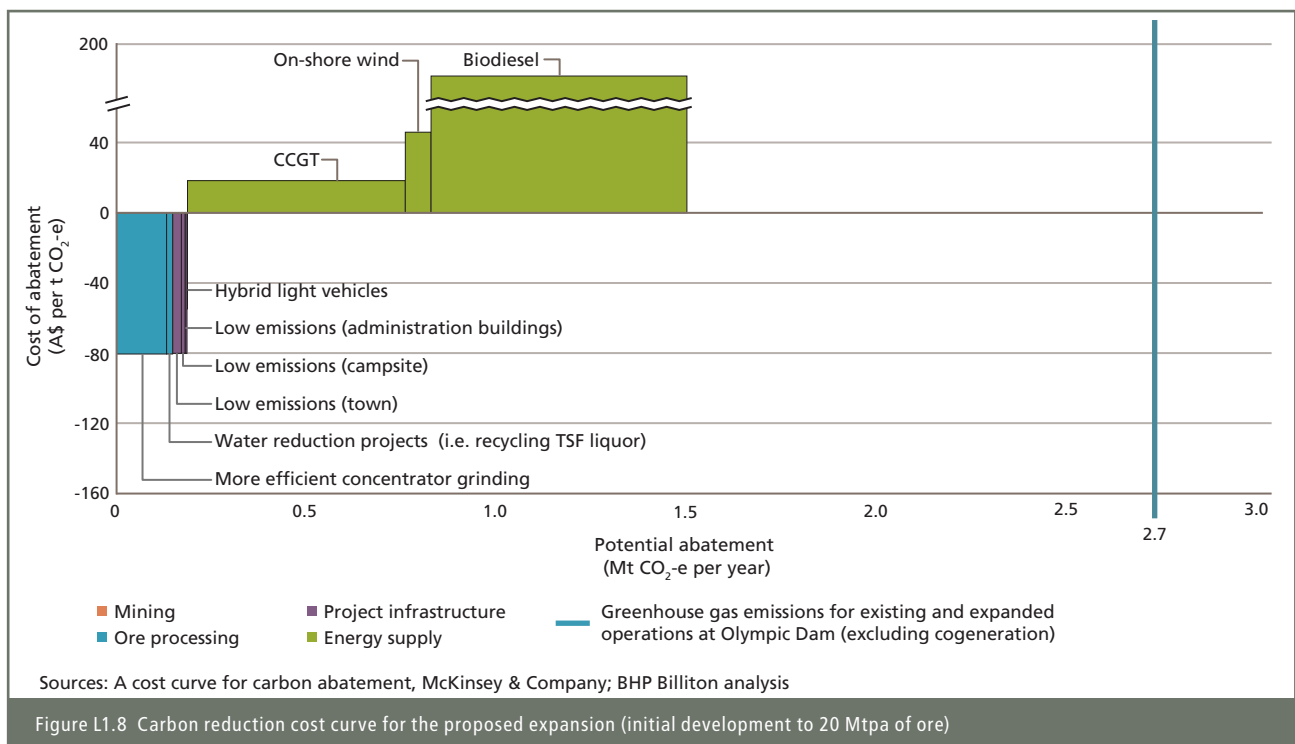
- use of waste engine oil in blasting
- in-pit ore crushing and conveying to the surface
- conveying mine rock to the surface
- trolley assist haulage
- alternative power/fuel supply for haul trucks (LNG)
- hybrid light vehicles
- more efficient crushing/grinding
- reduced water usage through increased recycling of TSF liquor
- low-intensity leaching
- energy efficient design for town, construction camp and administration buildings.

Supply-side projects identified during the modelling were:

- on-site CCGT
- off-site CCGT
- on-shore wind power
- geothermal power
- concentrated solar thermal power (with waste heat recovery plant)
- concentrated solar thermal power (stand-alone)
- solar photovoltaic power
- biodiesel
- coal carbon capture and storage (CCS)
- biomass power.

The carbon reduction cost curves for these demand and supply-side levers are presented as Figures L1.8 to L1.11.

A description of the lever, and the current status of investigations into the options, is detailed further in the following sections, as provided by BHP Billiton.



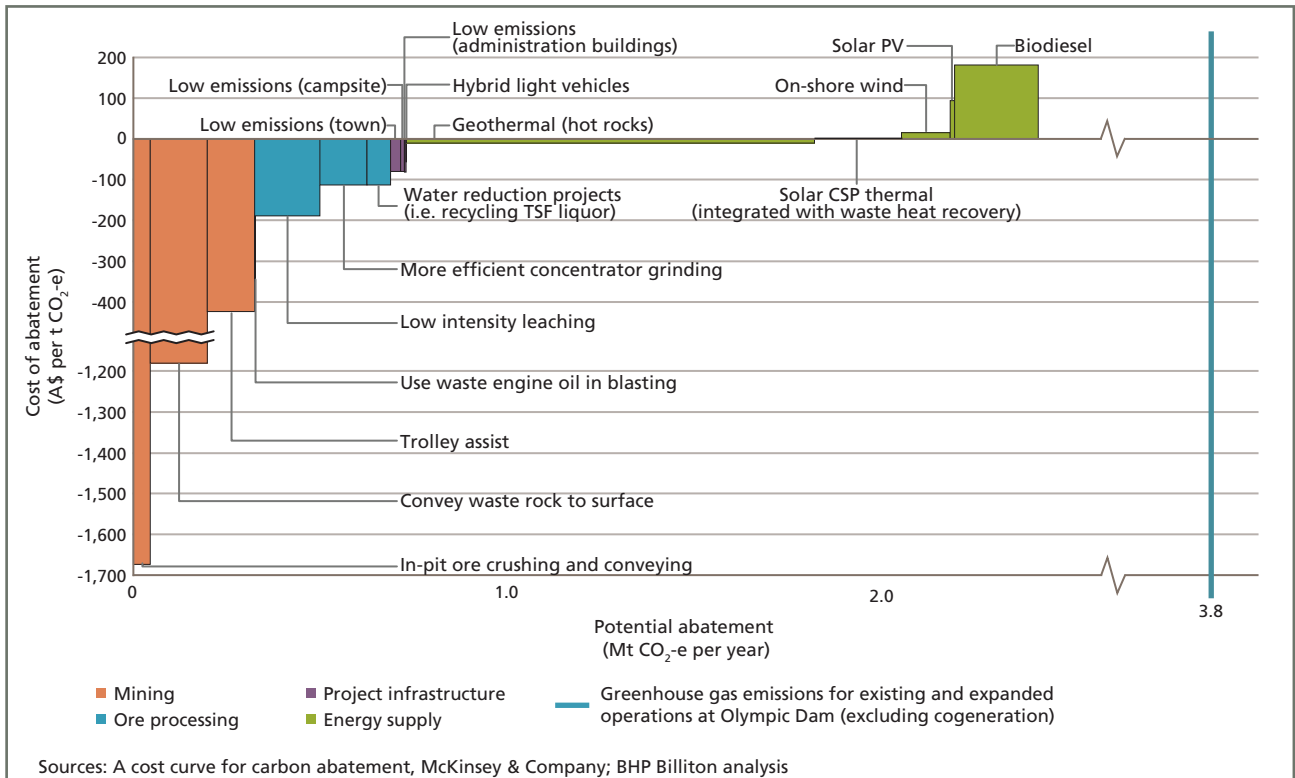


Figure L1.9 Carbon reduction cost curve for the proposed expansion (intermediate development to 40 Mtpa of ore)

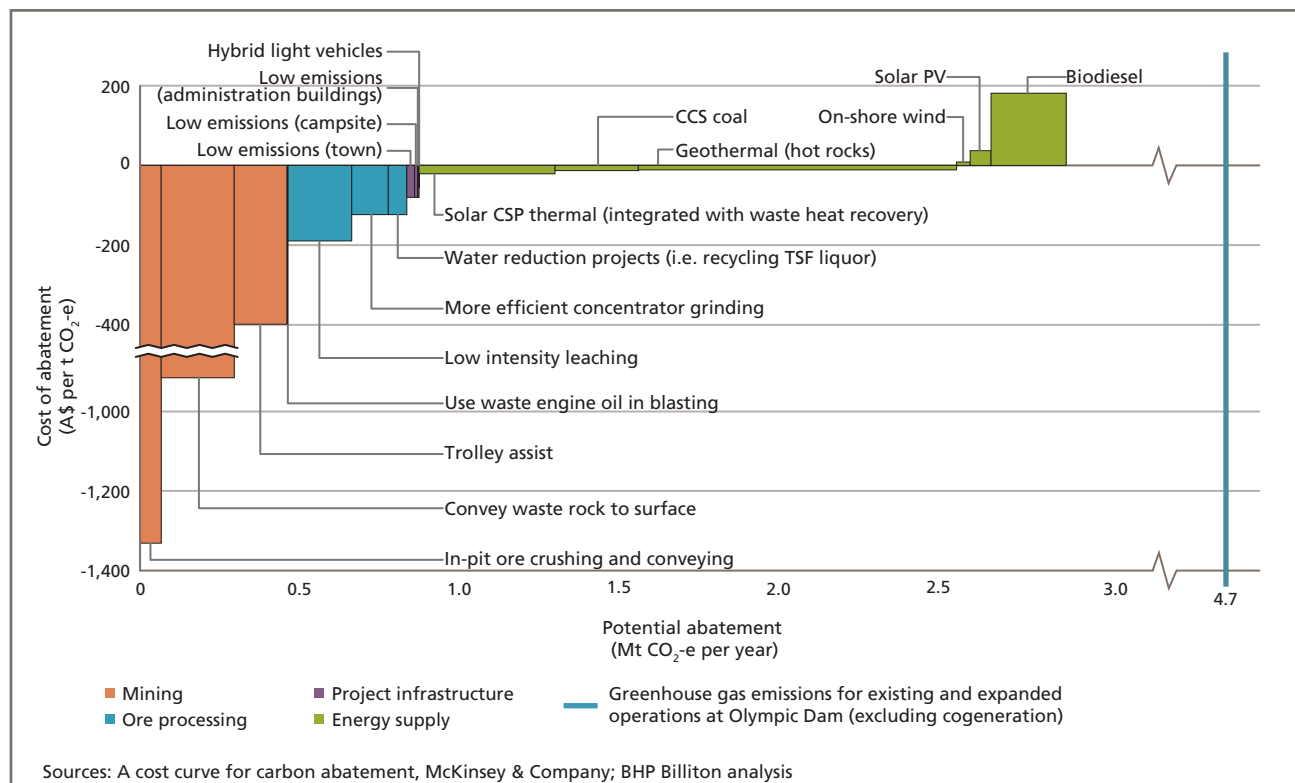


Figure L1.10 Carbon reduction cost curve for the proposed expansion (full capacity of the proposed expansion to 60 Mtpa of ore)

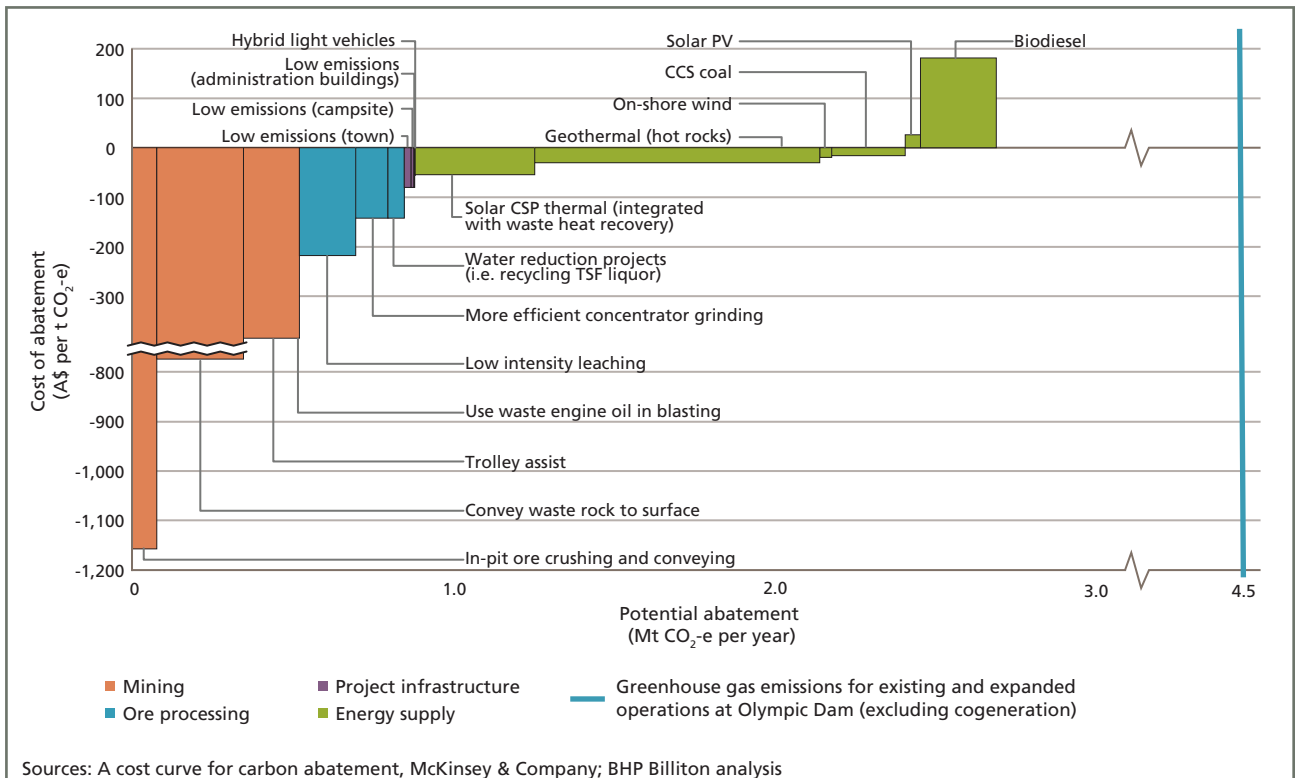


Figure L1.11 Carbon reduction cost curve for the proposed expansion (Year 2050 at 60 Mtpa of ore)

L1.6.4 Demand-side levers

Use waste engine oil in blasting

Description

Ammonium nitrate and fuel oil (ANFO) is the major blasting agent used in mining world-wide as it is safe to transport and handle, relatively inexpensive and easily made, and delivers a good energy conversion. It is a blend of ammonium nitrate and fuel oil (usually diesel), in a ratio of about 94:6. Waste lubrication oils from engines and other sources can be used to replace large proportions of the diesel component and therefore lower diesel usage and the emission of greenhouse gas.

Each blast would still generate similar volumes of CO₂. The greenhouse gas emissions savings would result from reusing a waste product that would otherwise require processing or disposal. Consequently the consumption of diesel for blasting would be reduced.

Study and status

Although a formal study has not been undertaken for the Olympic Dam expansion, other mining operations in Australia have used waste oil as part of the ANFO mix. These sites have regularly achieved a 75% replacement of diesel with waste oil with no detrimental effects on the blast results. A 75% replacement for Olympic Dam could result in direct savings of about 3 ML/annum of diesel, and could remove the need to dispose of the waste oil in other ways. The use of waste engine oil in blasting would be considered further in detailed design.

Alternative power supply for haul trucks (LNG)

Description

This option would convert diesel powered haul trucks to liquid natural gas (LNG) power which would allow for substitution of 90% of diesel consumption. This option would require an LNG conversion facility to be built on-site.

Study and status

BHP Billiton Nickel West has conducted a study into replacing diesel with LNG in haul trucks. Although the technology has not been proven in engines above 600 kW, it is technically feasible; however a development time of three to five years is required. BHP Billiton would continue to review the technology until it has been proven in larger engines.

In-pit ore crushing and conveying to surface

Description

In-pit ore crushing involves shifting the pit-rim ore crusher to the pit floor, substituting haulage via truck with an electrically powered conveyor.

Study and status

An investigation by BHP Billiton for the proposed expansion has recently been completed on the viability of using in-pit crushers and conveyors for primary crushing and transport of ore to the pit rim. The economic viability of in-pit crushing and conveying is reduced in the early phases of the pit life, becoming more favourable as the pit becomes deeper. Due to the relatively attractive cost benefit over the longer term, and the opportunity to reduce haulage truck numbers, crushing and conveying of ore will be further evaluated during detailed design.

In-pit mine rock conveying to surface

Description

This system would convey mine rock to the pit surface and on to the RSF, substituting the need for haulage via truck. It would consist of an electric rope shovel to load easily friable or appropriately blasted overburden material into a mobile sizer unit that would deliver material via a series of conveyors to the out-of-pit spreading system, which would selectively place material in the RSF.

Study and status

Initial investigations by BHP Billiton have considered the use of a fully mobile in-pit crushing and conveying system for the removal of the upper benches of overburden. The economic viability of in-pit crushing and conveying is improved as the pit becomes deeper, and the investigation found that the potential reduction in long-term ongoing operating costs generated by fully mobile in-pit crushing and conveying systems makes further investigation of this technology necessary. The opportunity to significantly reduce the number of haul trucks required is another key driver. This would be further studied during detailed design.

More efficient grinding in the concentrator

Description

High-pressure grinding rolls are currently used in some operations, and are reported to use less water and electricity than conventional grinding operations. Similarly, the use of fine grinders for the regrinding of oversize material, that would otherwise be recycled back to the grinding mills, has the potential to reduce electricity consumption. The microwaving of ore has the potential to reduce electricity required for grinding through softening the ore, making it easier to grind.

Study and status

High-pressure grinding rolls and the use of fine grinders are currently being assessed for their applicability on the Olympic Dam ore for the expanded operation. The microwaving of ore has only been demonstrated on a small scale, and any implementation would be over 20 years away. BHP Billiton is not currently studying this option.

Reduction in water consumption through recycling TSF liquor

Description

The proposed expansion would significantly increase the volumes of fresh water required, necessitating the use of desalination technologies. Consequently, potential opportunities to reduce water usage and reuse waste water are being identified. Reclaiming and recycling liquor from the TSF has been identified as offering a potential opportunity to decrease water consumption, thereby saving energy.

Study and status

BHP Billiton is currently assessing the feasibility of reusing TSF liquor on-site. The opportunity may exist to alter the tailings strategy to generate additional recycle liquor for return to the metallurgical plant without compromising TSF integrity. This would reduce fresh water demand to the site. Significant challenges and uncertainties exist with the reuse of TSF liquor within the metallurgical plant, including the effects of liquor composition, acidity and impurities. To date, BHP Billiton has completed technology and industry benchmarking, has examined alternative processes and TSF strategies and completed some metallurgical test work. A pilot plant study will be established in the near future to investigate impacts on a larger scale.

Low-intensity leaching

Description

Low-intensity leaching involves changing the flotation tails leach process conditions. The leach temperature is decreased from 70 °C to between 60 °C and 65 °C. The acid tenor during leach is reduced from 10–12 g/L to 5 g/l. This change in leach conditions increases the time needed for leaching and increases the use of oxidant. The combination of these parameters results in a reduction in acid consumption of approximately 30%. Reducing sulphuric acid consumption reduces the emissions associated with the transport of sulphur.

Study and status

BHP Billiton has completed initial investigations into alternative metallurgical processes. This investigation suggested that low-intensity leach options become attractive when the acid reduction is greater than 25% over the conventional leaching process. This is due to the trade-off between the high acid saving and the cost of the additional oxidant that is required for low-intensity leaching.

Identification of an alternative and cheaper oxidant to replace sodium chlorate would make the low-intensity leach a more attractive option. An alternative oxidant pilot plant trial is currently being commissioned at Olympic Dam.

Trolley Assist

Description

Trolley assist involves building overhead 'trolley' lines for powering dielectric haul trucks up the pit slope.

Study and status

BHP Billiton has completed initial investigations into utilising this technology for the proposed expansion. The key finding was that there may be significant value in optimising ramps for trolley assist. However, trolley assist was found not to be a viable option prior to 2021 for Olympic Dam because:

- a suitable truck stock is not currently available
- the limited pit depth reduces the advantages in speed that can be obtained through trolley assisted trucks versus conventional diesel mechanical trucks.

An analysis of cumulative savings from trolley assist indicated that implementing trolley assist after 2021 starts to deliver significant value through:

- increased speed on grade (24.7%)
- reduced fuel burn on grade (68.7%)
- improved engine life (6.6%).

The ability of the trolley-equipped truck to connect to a trolley or to use a trolley line is a major driver of value and a risk of realising that value. Trolley assist reduces the number of trucks (and associated capital).

Incorporation of trolley assist into the mine plan after the first replacement of fleet trucks would be investigated during detailed design. The mine design would be optimised and reviewed for possible inclusion of trolley assist after this time.

Energy efficient design for Roxby Downs township, Hiltaba Village and on-site administration buildings

Description

Incorporating energy efficiency into the design of new buildings at Olympic Dam would reduce energy consumption.

Study and status

BHP Billiton has undertaken a sustainability assessment of the Hiltaba Village design. Issues that have arisen as opportunities for reducing energy consumption are:

- layout of the site
- building materials and the design of the individual units
- incorporating natural ventilation into the design
- insulation
- double glazing of windows
- lighting
- heating and cooling
- hot water heating.

BHP Billiton is currently assessing all energy reduction alternatives for potential incorporation into this design. Further study will determine the most suitable opportunities for inclusion in the final building specifications.

BHP Billiton is also seeking registrations of interest for the construction of major housing and rental accommodation, and long distance commute accommodation associated with the expansion. BHP Billiton has requested that the design of new housing be undertaken with the principles of sustainability as the primary focus and states that design should utilise an understanding of shading and thermal mass into buildings to minimise energy use; provide wide eaves; and provide a suite of housing design options from which people can choose a home most suited to their needs and the location.

The permanently occupied Hiltaba Village accommodation would be designed to:

- take account of extremes in temperatures
- be efficient in energy and water use
- be oriented to maximum/minimum sun position
- incorporate recycling initiatives.

BHP Billiton is also assessing ways to reduce energy use in existing buildings through initiatives such as:

- installing solar hot water in existing buildings
- installing timers on air conditioners
- replacing shower heads with low flow types
- replacing incandescent lamps with compact fluorescent lamps
- shutting off unused portions of the dining rooms and kitchens at the villages.

Hybrid or LNG light vehicles

Description

Emissions reductions may be achieved through converting the fleet of light vehicles (e.g. LandCruisers) and some heavy vehicles (such as buses) from pure diesel power to hybrid engines.

Study and status

BHP Billiton are considering the purchase of energy efficient vehicles for its fleet of light vehicles.

L1.6.5 Carbon reduction options for alternate energy supply

Combined cycle gas turbines

Description

Combined cycle gas turbine (CCGT) electrical generation, whether built on-site at Olympic Dam or off-site with the power transmitted to Olympic Dam via the grid, could significantly reduce carbon emissions compared with sourcing electricity from co-fired power generation. A CCGT plant uses gas turbines to generate electricity, then recovers the energy from the hot exhaust and converts it to steam to drive steam turbines for further electrical generation. The combination of the two cycles makes CCGT a highly efficient plant.

Study and status

BHP Billiton is currently negotiating with potential suppliers for the design and construction of a CCGT plant.

On-shore wind

Description

By international standards, South Australia has a high proportion of wind generation. The operating, committed, and announced plants combined would give a capacity of 2,000 MW for South Australia (ESPIC 2008).

Study and status

BHP Billiton is investigating the use of wind power as part of its energy supply for the combined operation. The desalination plant would be powered through the use of renewable energy contracted through the NEM; wind generation may become the source of this power.

Geothermal

Description

Geothermal power is not currently commercially proven at the scale required for the expansion. However, as there are a number of geothermal resources close to Olympic Dam, this form of electrical generation has significant potential to meet the proposed expansion electricity demand in the longer term. The power produces minimal emissions and its generation is baseload.

Study and status

BHP Billiton will continue to explore possible future opportunities with geothermal providers.

Concentrated solar thermal plant

Description

BHP Billiton has undertaken a study to determine whether concentrated solar power (CSP) would be viable for the energy needs of the expansion. The most commercially advanced CSP technology is the parabolic trough, which has had 30 years of commercial exposure.

Study and status

BHP Billiton has developed partnerships with potential CSP plant developers to investigate a range of CSP solutions ranging between 50 MW and 150 MW, with and without storage. These studies are also investigating the integration of a CSP plant with the proposed cogeneration plant.

Solar photovoltaic and building integrated PV

Description

BHP Billiton would look to use solar photovoltaic (PV) and building integrated PV (BIPV) technology on buildings throughout the expansion, including the buildings at the airport and permanently occupied dwellings within Hiltaba Village.

Study and status

Limited investigations have been undertaken by BHP Billiton to identify suitable sites for the use of both BIPV and solar PV cells. Investigations into optimising the position of buildings so they can best incorporate this technology are currently being undertaken.

Solar hot water

Description

BHP Billiton would install solar hot water in the permanent accommodation units, laundries and central buildings in Hiltaba Village.

Study and status

The further use of solar hot water systems in new residences within the expanded Roxby Downs in addition to Hiltaba Village is currently being investigated.

Biodiesel

Description

Biodiesel is a clean burning alternative fuel, produced from domestic, renewable resources. Biodiesel contains no petroleum, but can be blended at any level with petroleum diesel to create a biodiesel blend. It can be used in compression-ignition (diesel) engines with little or no modifications. Biodiesel is made from renewable resources and has lower emissions compared to petroleum diesel.

Study and status

BHP Billiton has commissioned a study into biodiesel to provide a summary of the current Australian biodiesel industry, its sustainable use of feedstocks, and to determine whether biodiesel is a practical option for the Olympic Dam expansion. In general, the proposed Caterpillar engine technology proposed for Olympic Dam is well suited to the use of biodiesel. The engines planned would be able to handle a 5% to 30% biodiesel blend. The report concluded that biodiesel is likely to be a technically viable option to deliver significant reductions in carbon intensity for the expansion, however the security and sustainability of supply require further investigations, to be undertaken during detailed design.

BHP Billiton is continuing to study this option for possible use in the proposed expansion and has developed some principles in regard to biodiesel use. These principles state that:

- biodiesel production must neither interfere with food production nor compete with food crops for available land or water supplies
- biodiesel must not be derived from plants that are grown in ecologically sensitive areas where native vegetation was cleared
- growing biodiesel crops must not present a risk of causing damage as an invasive species to threaten valued environmental, agricultural or social resources
- a life cycle assessment of the fuel should demonstrate a positive greenhouse gas emissions reduction in comparison to an equivalent amount of fossil fuel it is replacing.

Carbon capture and storage

Description

Carbon capture and storage (CCS) captures the CO₂ that would otherwise be emitted from traditional coal-fired power stations and sequesters it into, typically, underground storage rather than emitting it to the atmosphere.

Study and status

Coal generation with CCS is not currently commercially proven, although pilot trials in Germany commenced in early 2008. This form of electrical generation has significant potential for the Olympic Dam expansion.

Nuclear energy

Description

Nuclear power is currently not permitted in Australia so this option has not been studied for the Olympic Dam expansion.

L1.7 REFERENCES

Australian Bureau of Agricultural and Resource Economics 2006, *Australian Energy, National and State Projections to 2029-30*, ABARE, Canberra, viewed 4 September 2008, <http://www.abare.gov.au/publications_html/energy/energy_06/nrg_projections06.pdf>.

Australian Bureau of Agricultural and Resource Economics 2007, *Technology: Towards a Low Emissions Future*, ABARE Research Report 07.16, ABARE, September 2007, Canberra.

Australian Greenhouse Office 2007, *National Greenhouse Gas Inventory 2005*, Department of the Environment and Water Resources, Canberra, viewed 4 September 2008, <<http://www.climatechange.gov.au/inventory/2005/pubs/inventory2005.pdf>>.

BHP Billiton 2008, *Climate Change Position*, BHP Billiton, Melbourne, viewed 14 November 2008, <<http://www.bhpbilliton.com/bbContentRepository/docs/climateChangePosition.pdf>>.

Bureau of Meteorology 2008, *Trend in Mean Temperature 1910–2007*, Australian Bureau of Meteorology, Canberra, viewed 4 September 2008, <http://www.bom.gov.au/cgi-bin/silo/reg/cli_chg/trendmaps.cgi?variable=tmean®ion=aus&season=0112&period=1900>.

Commonwealth Scientific and Industrial Research Organisation & Bureau of Meteorology 2007, *Climate Change in Australia – Observed Changes and Predictions*, CSIRO & Australian Bureau of Meteorology, Canberra, viewed 4 September 2008, <http://www.climatechangeinaustralia.com.au/documents/resources/Summary_brochure.pdf>.

Commonwealth Scientific and Industrial Research Organisation 2002, *Climate Change and Australia's Coastal Communities*, CSIRO Atmospheric Research, Aspendale, Victoria, 13 November 2008, <<http://www.cmar.csiro.au/e-print/open/CoastalBroch2002.pdf>>.

Department of Climate Change 2008, *National Greenhouse Accounts (NGA) Factors*, Department of Climate Change, Canberra, viewed 4 September 2008, <<http://www.climatechange.gov.au/workbook/pubs/workbook-feb2008.pdf>>.

Department of Climate Change 2008, *State and Territory Greenhouse Gas Inventories*, Department of Climate Change, Canberra, viewed 4 September 2008, <<http://www.climatechange.gov.au/inventory/stateinv/index.html>>.

Department of Climate Change 2007, *National Greenhouse and Energy Reporting System*, Department of Climate Change, Canberra, viewed 4 September 2008, <<http://www.climatechange.gov.au/reporting/publications/pubs/fs-nger.pdf>>.

Department of Premier and Cabinet, *Tackling Climate Change: South Australia's Greenhouse Strategy*, Department of Premier and Cabinet, Adelaide, viewed 15 October 2008, <http://www.climatechange.sa.gov.au/PDFs/final_tackling_climate_change_strategy_may_2007/tackling_climate_change_strategy.pdf>.

Department of Premier and Cabinet 2008, *Greenhouse Gases, Sustainability and Climate Change Division*, Department of Premier and Cabinet, Adelaide, viewed 4 September 2008, <http://www.climatechange.sa.gov.au/greenhouse/greenhouse_1_1.htm>.

Electricity Supply Industry Planning Council 2008, *Annual Planning Report*, ESIPC, Adelaide, viewed 4 September 2008, <http://www.esipc.sa.gov.au/webdata/resources/files/2008_APR_Final_for_Web.pdf>.

Environment Protection Agency (EPA) Northern Territory, 2006, *The Northern Territory Strategy for Greenhouse Action*, EPA Northern Territory and Department of Natural Resources, Environment and the Arts, Northern Territory Government, Palmerston, Northern Territory.

Garnaut, R 2008, *Garnaut Climate Change Review: Report to the Commonwealth, State and Territory Governments of Australia*, Canberra, viewed 15 October 2008, <<http://www.garnautreview.org.au/index.htm>>.

Intergovernmental Panel on Climate Change 2001, *Radiative Forcing of Climate Change*, Chapter 6 of the IPCC Third Assessment Report Climate Change, IPCC, SWITZERLAND.

Intergovernmental Panel on Climate Change 2007a, *Summary for Policy Makers – Impacts, Adaptation and Vulnerability, Contribution of Working Group II to the Fourth Assessment Report of the Intergovernmental Panel on Climate Change*, IPCC, SWITZERLAND, viewed 4 September 2008, <<http://www.ipcc.ch/ipccreports/ar4-wg2.htm>>.

Intergovernmental Panel on Climate Change 2007b, *Changes in Atmospheric Constituents and in Radiative Forcing, Climate Change 2007: The Physical Science Basis, Contribution of Working Group I to the Fourth Assessment Report of the Intergovernmental Panel on Climate Change*, IPCC, SWITZERLAND, viewed 4 September 2008, <http://ipcc-wg1.ucar.edu/wg1/Report/AR4WG1_Print_Ch02.pdf>.

McKinsey & Company 2008, *An Australian Cost Curve for Greenhouse Gas Reduction*, McKinsey & Company, Melbourne.

National Oceanic and Atmospheric Administration 2006, *Trends in Atmospheric Carbon Dioxide – Mauna Loa*, Carbon Cycle Greenhouse Gases Group, Global Monitoring Division, Earth System Research Laboratory, US Department of Commerce, Washington DC, viewed 4 September 2008, <<http://www.esrl.noaa.gov/gmd/ccgg/trends>>.

Suppiah, R, Preston, B, Whetton, P, McInnes, K, Jones, R, Macadam, I, Bathols, J & Kirono, D 2006, *Climate change under enhanced greenhouse conditions in South Australia*, CSIRO, Melbourne, viewed 4 September 2008, <http://www.climatechange.sa.gov.au/uploads/pdf/SA_CMAR_report_High_resolution.pdf>.

United Nations Environment Programme – Technology and Economic Assessment Panel 2005, *Montreal Protocol On Substances that Deplete the Ozone Layer, May 2005 Report of the Task Force on Foam End-of-Life Issues*, Nairobi, Kenya, viewed 4 September 2008, <http://www.unep.org/Ozone/Teap/Reports/TEAP_Reports/TEAP-May-2005-Vo2-Forms-End-of-Life.pdf>.

World Business Council for Sustainable Development & World Resources Institute 2004, *Greenhouse Gas Protocol: A Corporate Accounting and Reporting Standard*, WBCSD, Switzerland, & WRI, Washington DC, viewed 4 September 2008, <<http://www.ghgprotocol.org/files/ghg-protocorevised.pdf>>.



Suite 2B 14 Glen Street,
Eastwood, NSW 2122
Phone 61-2-9874-8644
Fax 61-2-9874-8904
E-mail : Nigel.Holmes@holmair.com.au
ACN 003-741-035
ABN 79-003-741-035

27 January 2009

David Winterburn
Olympic Dam EIS Project
GPO Box 11052
Adelaide SA 5001

Dear David,

Review of Air Quality Assessment for Olympic Dam EIS

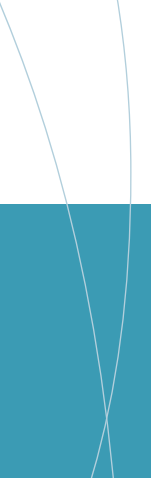
As requested, I have reviewed a number of draft documents dealing with the expected air quality effects of the proposed Olympic Dam expansion. I have provided comments on these in earlier communications. For this final review I have focussed on the methods used to estimate fugitive emissions of dust, the approach used to model the dispersion of emissions and on the results of the modelling.

I confirm that the methods used to estimate emissions are appropriate and consistent with those used to assess other similar proposals. The estimated total annual PM₁₀ emission for the year simulated in the Environmental Impact Statement was 10,141,033 kg. This was associated with the handling of 410 Mtpa of ore and waste. This ratio of PM₁₀ emission to the total mass of material handled is similar to that which I have estimated for other large open cut mines. Further, I have compared the predicted concentrations of PM₁₀ and the way in which these decrease with distance from the mine. The decrease with distance is consistent with the rate I would expect from other projects I have worked on. On this basis I conclude that the air quality assessment is based on realistic forecasts of the likely PM₁₀ concentrations due to emissions from the mine.

Yours faithfully,
Holmes Air Sciences

A handwritten signature in black ink that reads "N.E. Holmes." The signature is written in a cursive, slightly slanted style.

Nigel Holmes PhD
Atmospheric Physicist



APPENDIX L2

Air quality impact assessment

L2 AIR QUALITY IMPACT ASSESSMENT

L2.1 INTRODUCTION

L2.1.1 Overview

BHP Billiton is proposing to expand the Olympic Dam copper and uranium mining operation in far north South Australia. Arup/ENSR have been contracted to develop the Draft Environmental Impact Statement (EIS) associated with the proposed development, an element of which is a study detailing the potential impacts of such an expansion on the local and regional air quality.

An air quality study has been undertaken by Arup/ENSR, with additional input and review by Holmes Air Sciences (Sydney, NSW), Pacific Air and Environment (Brisbane, Qld) and CSIRO Department of Marine and Atmospheric Research (Melbourne, Vic). This study was based on an assessment of existing regional air quality, including topographic and meteorological information, and the development of dispersion models for the estimation of pollutant ground level concentrations associated with the expanded operation.

This appendix presents the raw information and studies utilised as inputs to the air quality modelling. Results and discussion of potential mitigation options are presented in Chapter 13, Greenhouse Gas and Air Quality of the Draft EIS.

L2.2 PROJECT DESCRIPTION

The configuration of the expanded operation is discussed in detail in Chapter 5, Description of the Proposed Expansion. The most significant developments with regard to air quality are:

- the development of an open pit mine
- the construction of an additional concentrator and hydrometallurgical plant
- the modification of the existing feed preparation and smelter to handle greater volumes of copper concentrate
- the construction and operation of an on-site natural gas-fired power station.

L2.3 CLIMATE AND METEOROLOGY

Local climate and meteorology is detailed in Chapter 8, Meteorological Environment and Climate. The variables that most influence the dispersion of pollutants are wind speed and direction, atmospheric stability and mixing height.

L2.4 TOPOGRAPHY

The topography around the existing Olympic Dam operations is discussed in Chapter 10 (Topography and Soils). Figure 10.1 illustrates the topography of Olympic Dam in a regional context.

Building wake effects have not been considered in the development of the air quality model as the height and location of stacks is considered to be unlikely to influence the modelling results.

The existing regional topography would change over time; a result of the development of the open-pit mine, the rock storage facility (RSF) and the tailings storage facility (TSF). The RSF and TSF topography were incorporated into the air quality model, however the Calpuff (and indeed most) local air quality models do not have sufficient capacity to model complex terrain, i.e. terrain with slopes of greater than around 30 to 40 degrees. This limits the potential for the modelling of the open pit mine as a terrain feature.

An alternative approach was used, that being to represent the open pit as an area source, and develop specific open pit retention figures for the proposed operation. The Commonwealth Government provides, through the National Pollutant Inventory (NPI) Emission Estimation Technique Manuals (Mining V2.3), default figures for pit retention, being 0% retention for gases and PM_{2.5}, 5% retention for PM₁₀ and 50% retention for TSP, where PM_{2.5} and PM₁₀ refer to the maximum size (in micron) of the individual dust particles. A review of available literature suggests that these figures have been developed using research at Australian coal mines in the Hunter Valley region, which are typically at depths of about 100 to 300 metres, and not necessarily applicable to an open pit of between 400 and 1,200 m.

Computational fluid dynamics (CFD) modelling of the proposed open pit was undertaken for both the Year 5 pit (at about 400 m deep), and Year 40 pit (about 1,200 m deep) to determine the likely proportion of material retained within the pit by size fraction. This model used the emissions inventory developed for the proposed expanded operation (see Section L1.8). The report detailing the CFD modelling study is included as Attachment A to this Appendix.

L2.5 DISPERSION MODELLING

The objective of pollutant dispersion modelling is to estimate the likely concentration of pollutants at ground level as a result of the expansion of the mining and processing facilities, and to quantify the extent of the change from the existing operations to the expanded case.

The Calpuff 'puff' dispersion model was chosen because it was considered that it better represented the complex terrain associated with the RSF, and because it negates one of the primary limitations of plume based models, that being the so-called "causality problem". This occurs because plume models predict ground level concentrations on an hourly time step and assume that the emission is instantaneously transported from the source to the edge of the model domain in each hour. In practice, the emission would only travel a distance equal to the wind speed in m/s x 3,600 seconds in one hour (e.g. for a 0.2 m/s wind the distance would be 720 m). This would mean that the use of a plume model may have resulted in an over-estimation of ground level concentrations at far-field receptors.

A list of the modelled species is presented in the following section.

L2.6 AIR QUALITY ASSESSMENT CRITERIA

An investigation of the relevant state, national and international guidelines, regulations and standards was undertaken to determine suitable criteria to be used for assessing the predicted pollutant-emission performance of the expanded operation.

L2.6.1 Regulations, standards and guidelines

Regulations, standards and guidelines can be grouped into those applicable to point source emissions and those related to pollutant ground level concentrations. Point source emission limits are detailed in the South Australian *Environment Protection (Air Quality) Policy 1994* and are summarised in Chapter 13, Greenhouse Gas and Air Quality.

The derivation of ground level concentration criteria was described in Chapter 13, Greenhouse Gas and Air Quality. Performance criteria for airborne emissions have been established by State and Commonwealth governments. The criteria are determined at the source of emission through the South Australian *Environment Protection (Air Quality) Policy 1994* and at the receiver through the ambient air quality goals outlined in the *Air quality impact assessment using design ground level pollutant concentrations guideline, 2006* and the National Environment Protection Council's (NEPC's) *National Environment Protection (Ambient Air Quality) Measure, 2003*. The assessment also considers the rescinded National Health and Medical Research Council (NHMRC) *Goals for maximum permissible levels of pollutants in ambient air, 1996*.

L2.6.2 Adopted criteria

The assessment criteria for the proposed expansion have been based on the lower of the ground level concentrations for the major averaging periods as shown in Table L2.1.

Table L2.1 Adopted ambient air quality criteria

Pollutant	Averaging period	Goals ($\mu\text{g}/\text{m}^3$)			Allowable exceedances (days per year)
		SA EPA	NEPC	NHMRC	
TSP	Annual	–	–	90	Nil
PM ₁₀	24 hour	–	50	–	5
	Annual	–	30	–	Nil.
PM _{2.5}	24 hour	–	25	–	n.a.
	Annual	–	8	–	n.a.
Sulphur dioxide	1 hour	450	570	570	1
	24 hour	–	228	–	1
	Annual	–	57	60	Nil
Nitrogen dioxide	1 hour	158	240	320	1
	Annual	–	60	–	Nil
Carbon monoxide	1 hour	29	–	–	Nil
	8 hour	–	10,000	10,000	1
Lead	Annual	–	0.5	1.5	Nil
Fluoride	24 hour	2.9	–	–	Nil
Carbon disulphide	3 minute	130	–	–	Nil

L2.7 POINT SOURCE EMISSION RATES

Emission rates for the selected pollutants were developed utilising data from the existing operation together with preliminary design data for the proposed expanded plant. These are detailed in Chapter 13, Greenhouse Gas and Air Quality, with the exception of radon, which is detailed in Appendix S, Uranium and Radiation.

A description of the point source emissions associated with the expanded plant follows in Table L2.2, and the estimated emission rates are listed in Table L2.3. As described in the following section, the expanded processing operation would be designed for all point source emissions to comply with the requirements of the *Environment Protection (Air Quality) Policy, 1994*.

Table L2.2 Proposed point emission sources and indicative operating data

Stack	Flow rate (Nm ³ /hr)	Height (m AGL)	Velocity (m/s)	Inner diameter (m)	Temp (°C)	Notes
Main smelter stack	635,000	90	24	3.8	55	Addition of new anode furnace (60,000 Nm ³ /hr) and taphole and launder ventilation (100,000 Nm ³ /hr) gases.
Acid plant tails gas stack	100,000	90	6.5	2.9	70	Remains unchanged.
Smelter #1 shaft furnace stack	45,000	40	15.5	1.3	38	Remains unchanged.
Calciner A stack	2,500	29	9	0.5	45	Remains unchanged.
Calciner B stack	3,000	29	9	0.5	85	Remains unchanged.
Slimes treatment roaster stack	30,000	20	23	0.75	60	Flow rates and concentration do not change, although utilisation is increased.
Slimes treatment NO _x stack	6,000	20	14.5	0.4	35	Flow rates and concentration do not change, although utilisation is increased.
Concentrate dryer stack	40,000	22	18	1.2	30	An additional larger dryer, or two smaller dryers, are added, doubling flow rates. Concentrations remain the same.
New acid plant tails gas stack	260,000	50	17	2.9	70	Additional acid plant built to handle additional flash furnace off-gas. Would have a higher flow rate than the existing acid plant, although would operate to the same efficiencies.
New sulphur-burning acid plant stack 1	516,000	50	13	4.6	70	Sulphur burning acid plants constructed adjacent to greenfields processing plant. Would be larger than existing acid plant, and operate to the same efficiencies. There would be two exhaust flues in a common stack.
New sulphur-burning acid plant stack 2	516,000	50	13	4.6	70	
New calciner stack	3,000	30	10	0.5	85	Similar to existing calciner B.

Table L2.3 Indicative average point source emission rates for the expanded operation (mg/Nm³)

Stack	SO ₂	NO _x	CO	Pb	HF
Main smelter stack	150	50	1.6	1	0.05
Acid plant tails gas stack	1,050	75	3.6	0	0.05
Smelter #1 shaft furnace stack	2	20	14.4	8	0.1
Calciner A stack	0	0	1.5	0	0
Calciner B stack	0	0	1.2	0	0
Slimes treatment roaster stack	0	700	0	0.005	0
Slimes treatment NO _x stack	0	170	0	0.005	0
Concentrate dryer stack	1	35	0	0.05	0.5
New acid plant tails gas stack	1,050	75	3.6	0	0.05
New sulphur-burning acid plant stack 1	1,050	75	3.6	0	0.05
New sulphur-burning acid plant stack 2	1,050	75	3.6	0	0.05
New calciner stack	0	0	1.2	0	0

Emissions of carbon disulphide are expected to increase in proportion to the volume of sodium ethyl xanthate used within the new flotation facilities, with the average emission rate from the new facility estimated to be 0.07 g/s (National Pollutant Inventory 1999).

Gas-fired power station

The proposed gas-fired power station would be constructed to the south of the expanded metallurgical plant. Details of the likely stack configuration are presented in Table L2.4.

Table L2.4 Indicative emission point source operating data

Stack information	Values	Comments
Stack height	35 m	
Stack diameter	6.2 m	
Stack temperature	500 °C	Open cycle
Stack temperature	105 °C	Combined cycle
Stack velocity	20 m/s	
Stack flow rate	1,550 KNm ³ /hr	Per stack
Number of stacks	4	

Emissions from the gas-fired power station have been calculated using the NPI Emission Estimation Technique Manual for Fossil Fuel Electric Power Generation (NPI 2005) and estimates of the likely natural gas consumption. Table L2.5 shows the likely annualised emissions from the proposed power station.

Table L2.5 Indicative average emission rates for the proposed 600 MW gas-fired power station

Substance	Annual emission (kg/year)	Estimated emission concentration (mg/Nm ³)
Carbon monoxide	1,155,000	22
Oxides of nitrogen (expressed as nitrogen dioxide, NO ₂)	2,520,000	46
PM ₁₀	92,400	2
Polychlorinated dioxin and furans	0.0003	0
Polycyclic aromatic hydrocarbons	31.4	0
Sulphur dioxide	246	0
TVOCs	30,030	0.6

L2.8 FUGITIVE SOURCES

The majority of the smaller process vessels, including the tailings leach and concentrate leach tanks, would be covered to prevent fugitive emissions. Larger tanks, however, including the counter-current decantation (CCD) tanks and associated clarifiers, and the flotation cells, would not be covered, resulting in the possibility that these would emit some fugitive aerosols.

Additionally, process ponds, including the pregnant liquor solution (PLS) and electrolyte ponds, would not be covered. Emissions from these ponds are expected to be no more significant than from the existing uncovered ponds.

The most significant component of fugitive emissions is the particulate emissions associated with the development and operation of the open pit, stockpile and rock storage facility. The principal sources of particulate emission are listed below:

- drilling
- blasting
- bulldozers and graders
- crushing
- shovels loading haul trucks
- trucks operating on haul roads
- unloading of materials at stockpiles/dumps
- road maintenance activities
- wind erosion of active surfaces.

Details of emission factors used, resultant emission rates and associated assumptions are detailed in the following sections.

L2.8.1 Key data and assumptions

The following tables (Tables L2.6 to L2. 9) detail the key data and assumptions used in the development of the particulate emissions inventory.

Table L2.6 Estimated mining physical data

Mining physicals	Value	Units	Notes
Ore movement rate	60	Mtpa	
Mine rock movement rate	350	Mtpa	
Total material movement rate	410	Mtpa	
Number of blast holes drilled	335	holes per day	
Area of blast	25,000	m ²	
Number of blasts	1	per day	
Number of bulldozers in pit	12		
Number of bulldozers on run-of-mine (ROM)	1		
Number of bulldozers on RSF	12		
Empty weight of haul trucks	260	t	Based on use of CAT 797F Ultra-class haul truck
Gross weight of haul trucks	620	t	Based on use of CAT 797F Ultra-class haul truck
Average speed of haul trucks (uphill + loaded)	13.4	km/h	Based on use of CAT 797F Ultra-class haul truck
Average speed of haul trucks (downhill + empty)	35	km/h	Based on use of CAT 797F Ultra-class haul truck
Average speed of haul trucks (level + loaded)	48	km/h	Based on use of CAT 797F Ultra-class haul truck
Average speed of haul trucks (level + empty)	51	km/h	Based on use of CAT 797F Ultra-class haul truck
Average haul road traffic per hour	121	trucks per hour	
Number of graders	6		
Average speed of graders	5	km/h	
Average width of haul roads	40	m	
Total length of haul roads	12.3	km	
Surface area of ROM stockpile	7	ha	
Active area of RSF	110	ha	
Surface area of in-pit rock stockpile	0.5	ha	

Table L2.7 Estimated haulage distances for the expanded operation at year 25

Distances	Trip	Value	Units
Waste rock haulage	In-pit to pit edge	9.3	km
	Pit edge to RSF	2	km
	RSF to in-pit	11.3	km
Ore haulage	In-pit to pit edge	9.3	km
	Pit edge to ROM	1	km
	ROM to in-pit	10.3	km

Table L2.8 Recorded meteorological data as required for the emission estimation equations

Meteorological data	Value	Units	Notes
Average wind speed	2.5	m/s	Based on recorded met data
Percentage of time when wind speed exceeds 5.4 m/s	11.1	%	Based on recorded met data
Average hourly evaporation rate	0.34	mm/h	Based on recorded met data

Table L2.9 Estimated mine rock and ore properties

Mine rock and ore properties	Value	Units	Notes
Average silt content of haul roads	8.3	%	AP42 Chapter 13.2.2, Table 13.2.2-1 'Stone quarrying and processing' factor
Average moisture content of haul roads	0.2	%	
Average ore density	3	t/m ³	From BHP Billiton blast modelling
Average mine rock density	2.6	t/m ³	From BHP Billiton blast modelling
Average silt content of ore	0.6	%	From BHP Billiton blast modelling
Average silt content of mine rock	0.5	%	From BHP Billiton blast modelling

L2.8.2 Mitigation effectiveness

Mitigation factors were applied to the emission estimation equations where such measures had been committed to and could be applied. These are detailed in Table L2.10.

Table L2.10 Estimated mitigation measure effectiveness

Mitigation effectiveness	Value	Units	Notes
Dust suppression on haul roads	83.5	%	Control Factor derived from the equation of Cowherd (1988) which is $C = 100 - (0.8 \cdot p \cdot d \cdot t) / I$ where p is the average annual evaporation rate (mm/h), d is the hourly road traffic volume, t is the time between water applications and I is the intensity of the application in litres per m ² , using an application rate of 2 litres per m ² /hour and no chemical suppressants
In-pit dust retention (TSP)	47.5	%	From in-pit dust retention CFD modelling study (for a 40-year pit under average wind conditions). See Attachment A
In-pit dust retention (PM ₁₀)	2.9	%	From PAE in-pit dust retention CFD modelling study (for a 40-year pit under average wind conditions). See Attachment A
Vehicle speed factor	actual vehicle speed divided by 24	n.a.	From AP-42 (1998) for haul vehicles travelling at less than 24 km/h. Referenced in the SKM Report "Improvement of NPI Fugitive Particulate Matter Emission Estimation Techniques"

L2.8.3 Emissions estimations

The emissions inventory is presented in the following in Tables L2.11 to L2.24, separated into the mining activity.

Table L2.11 Estimated emissions as a result of blast hole drilling

Size fraction	Emission factor equation	Emission factor reference	Mitigated emission rate (kg/hour)	Notes
TSP	0.59 kg/hole	TSP emission factors sourced from NPI publication EET for Mining v2.3, Dec 2001 (Appendix A1.1.8)	4.32	Incorporates a pit-retention factor
PM ₁₀	0.31 kg/hole	PM ₁₀ emission factors sourced from NPI publication EET for Mining v2.3, Dec 2001 (Appendix A1.1.8)	2.27	
PM _{2.5}	None provided	n.a.	n.a.	

Table L2.12 Estimated emissions as a result of blasting

Size fraction	Emission factor equation	Emission factor reference	Mitigated emission rate (kg/hour)	Notes
TSP	$E = 0.00022 A^{1.5}$	TSP/PM ₁₀ emission factors sourced from AP42 Section 11.9 (Western Surface Coal Mining) Table 11.92	457	Units are kg/blast. Blasting occurs only once per day
PM ₁₀	52% of TSP	TSP/PM ₁₀ emission factors sourced from NPI publication EET for Mining v2.3, Dec 2001 (Appendix A1.1.9)	237	
PM _{2.5}	None provided	n.a.	n.a.	

Table L2.13 Estimated emissions as a result of bulldozers operating on the in-pit stockpile

Size fraction	Emission factor equation	Emission factor reference	Mitigated emission rate (kg/hour)	Notes
TSP	$E = \frac{2.6(S^{1.2})}{M^{1.3}}$	TSP/PM ₁₀ /PM _{2.5} emission factors from 'overburden' section of AP42 Chapter 11.9, Table 11.9-2	58	Incorporates a pit-retention factor, but no wetting of stockpile active areas
PM ₁₀	$E = 0.75 \frac{0.45(S^{1.5})}{M^{1.4}}$	TSP/PM ₁₀ /PM _{2.5} emission factors from 'overburden' section of AP42 Chapter 11.9, Table 11.9-2	17.4	
PM _{2.5}	$E = 0.105 \frac{2.6(S^{1.2})}{M^{1.3}}$	TSP/PM ₁₀ /PM _{2.5} emission factors from 'overburden' section of AP42 Chapter 11.9, Table 11.9-2	6.1	

Table L2.14 Estimated emissions as a result of bulldozers operating on the ROM stockpile

Size fraction	Emission factor equation	Emission factor reference	Mitigated emission rate (kg/hour)	Notes
TSP	$E = \frac{2.6(S^{1.2})}{M^{1.3}}$	TSP/PM ₁₀ /PM _{2.5} Emission Factors from 'overburden' section of AP42 Chapter 11.9, Table 11.9-2	11.4	No pit retention and no wetting of stockpile active areas
PM ₁₀	$E = 0.75 \frac{0.45(S^{1.5})}{M^{1.4}}$	TSP/PM ₁₀ /PM _{2.5} emission factors from 'overburden' section of AP42 Chapter 11.9, Table 11.9-2	1.49	
PM _{2.5}	$E = 0.105 \frac{2.6(S^{1.2})}{M^{1.3}}$	TSP/PM ₁₀ /PM _{2.5} emission factors from 'overburden' section of AP42 Chapter 11.9, Table 11.9-2	1.20	

Table L2.15 Estimated emissions as a result of bulldozers operating on the RSF

Size fraction	Emission factor equation	Emission factor reference	Mitigated emission rate (kg/hour)	Notes
TSP	$E = \frac{2.6(S^{1.2})}{M^{1.3}}$	TSP/PM ₁₀ /PM _{2.5} emission factors from 'overburden' section of AP42 Chapter 11.9, Table 11.9-2.	110	No pit retention and no wetting of stockpile active areas
PM ₁₀	$E = 0.75 \frac{0.45(S^{1.5})}{M^{1.4}}$	TSP/PM ₁₀ /PM _{2.5} emission factors from 'overburden' section of AP42 Chapter 11.9, Table 11.9-2	13.6	
PM _{2.5}	$E = 0.105 \frac{2.6(S^{1.2})}{M^{1.3}}$	TSP/PM ₁₀ /PM _{2.5} emission factors from 'overburden' section of AP42 Chapter 11.9, Table 11.9-2	11.6	

Table L2.16 Estimated emissions as a result of ROM ore crushing

Size fraction	Emission factor equation	Emission factor reference	Mitigated emission rate (kg/hour)	Notes
TSP	0.2 kg/t	TSP/PM ₁₀ emission factors sourced from NPI publication EET for Mining v2.3, Dec 2001 (Table 2)	457	Assumes ore crushing only, and no dust mitigation fitted to crushers
PM ₁₀	0.02 kg/t	TSP/PM ₁₀ emission factors sourced from NPI publication EET for Mining v2.3, Dec 2001 (Table 2)	46	
PM _{2.5}	None provided	n.a.	n.a.	

Table L2.17 Estimated emissions as a result of excavators and shovels loading haul trucks

Size fraction	Emission factor equation	Emission factor reference	Mitigated emission rate (kg/hour)	Notes
TSP	$E = 0.025 \text{ kg/t}$	TSP/PM ₁₀ emission factors sourced from NPI publication EET for Mining v2.3, Dec 2001 (Table 1)	599	Pit retention factor incorporated, but no wetting of stockpile active areas
PM ₁₀	$E = 0.012 \text{ kg/t}$	TSP/PM ₁₀ emission factors sourced from NPI publication EET for Mining v2.3, Dec 2001 (Table 1)	532	
PM _{2.5}	1.9% of TSP	TSP/PM ₁₀ /PM _{2.5} emission factors from 'truck loading' section of AP42 Chapter 11.9, Table 11.9-2	11.4	

Table L2.18 Estimated emissions as a result of the movement of haul trucks on unpaved roads

Size fraction	Emission factor equation	Emission factor reference	Mitigated emission rate (kg/hour)	Notes
TSP	Uncontrolled haul road emission factor of 4.0 kg/VKT for TSP, 1.0 kg/VKT for PM ₁₀ and 0.5 kg/VKT for PM _{2.5} , with a vehicle speed factor (actual speed divided by 24) applied to laden haul trucks going uphill, and a dust suppression factor (83.5% reduction in dust) added to all haul roads)	Uncontrolled factor from Holmes Air Sciences (pers. comm. 2006). Speed factor from AP-42 (1998) for haul vehicles travelling at less than 24 km/h. Referenced in the SKM Report 'Improvement of NPI Fugitive Particulate Matter Emission Estimation Techniques'	217	Laden mine rock haul trucks operating on haul roads (in-pit to pit edge)
PM ₁₀			100	
PM _{2.5}			51.6	
TSP			159	Laden mine rock haul trucks operating on haul roads (pit edge to RSF)
PM ₁₀			39.8	
PM _{2.5}			19.9	
TSP			388	Unladen mine rock haul trucks operating on haul roads (RSF to in-pit)
PM ₁₀			180	
PM _{2.5}			112	
TSP			11.4	Laden ore haul trucks operating on haul roads (in-pit to pit edge)
PM ₁₀			5.28	
PM _{2.5}			2.72	
TSP			4.19	Laden ore haul trucks operating on haul roads (pit edge to ROM)
PM ₁₀			1.05	
PM _{2.5}			0.52	
TSP			20.4	Unladen ore haul trucks operating on haul roads (ROM to in-pit)
PM ₁₀			9.4	
PM _{2.5}			5.39	

Table L2.19 Estimated emissions as a result of unloading ore and mine rock at stockpiles

Size fraction	Emission factor equation	Emission factor reference	Mitigated emission rate (kg/hour)	Notes
TSP	0.012 kg/t	TSP/PM ₁₀ emission factors sourced from NPI publication EET for Mining v2.3, Dec 2001 (Appendix A1.1.6)	548	
PM ₁₀	0.0043 kg/t	TSP/PM ₁₀ emission factors sourced from NPI publication EET for Mining v2.3, Dec 2001 (Appendix A1.1.6)	196	
PM _{2.5}	None provided	n.a.	n.a.	

Table L2.20 Estimated emissions as a result of haul road maintenance

Size fraction	Emission factor equation	Emission factor reference	Mitigated emission rate (kg/hour)	Notes
TSP	$E = \frac{0.0034(S^{2.5})}{VKT}$	TSP/PM ₁₀ emission factors sourced from NPI publication EET for Mining v2.3, Dec 2001 (Appendix A1.1.12)	0.00	Assumes dust mitigation on haul roads
PM ₁₀	$E = \frac{0.0034(S^{2.0})}{VKT}$	TSP/PM ₁₀ emission factors sourced from NPI publication EET for Mining v2.3, Dec 2001 (Appendix A1.1.12)	0.00	
PM _{2.5}	None provided	n.a.	n.a.	

Table L2.21 Estimated emissions as a result of wind erosion of the in-pit rock reserve

Size fraction	Emission factor equation	Emission factor reference	Mitigated emission rate (kg/hour)	Notes
TSP	$E = 1.9 \left(\frac{S}{1.5}\right)^{365} \left(\frac{365-p}{235}\right) \left(\frac{f}{15}\right)$	TSP emission factor from 'active storage pile' section of AP42 Chapter 11.9, Table 11.9-2	0.01	Pit retention factor incorporated, but no wetting of stockpile active areas
PM ₁₀	50% of TSP	PM ₁₀ emission factors sourced from NPI publication EET for Mining v2.3, Dec 2001 (Appendix A1.1.15)	0.00	
PM _{2.5}	None provided	n.a.	n.a.	

Table L2.22 Estimated emissions as a result of wind erosion of the ROM stockpile

Size fraction	Emission factor equation	Emission factor reference	Mitigated emission rate (kg/hour)	Notes
TSP	$E = 1.9 \left(\frac{S}{1.5} \right)^{365} \left(\frac{365-p}{235} \right) \left(\frac{f}{15} \right)$	TSP emission factor from 'active storage pile' section of AP42 Chapter 11.9, Table 11.9-2	0.24	No pit retention and no wetting of stockpile active areas
PM ₁₀	50% of TSP	PM ₁₀ emission factors sourced from NPI publication EET for Mining v2.3, Dec 2001 (Appendix A1.1.15)	0.12	
PM _{2.5}	None provided	n.a.	n.a.	

Table L2.23 Estimated emissions as a result of wind erosion of the RSF

Size fraction	Emission factor equation	Emission factor reference	Mitigated emission rate (kg/hour)	Notes
TSP	$E = 1.9 \left(\frac{S}{1.5} \right)^{365} \left(\frac{365-p}{235} \right) \left(\frac{f}{15} \right)$	TSP emission factor from 'active storage pile' section of AP42 Chapter 11.9, Table 11.9-2	3.11	Assumes that the RSF dumping areas remain active for one week following dumping
PM ₁₀	50% of TSP	PM ₁₀ emission factors sourced from NPI publication EET for Mining v2.3, Dec 2001 (Appendix A1.1.15)	1.56	
PM _{2.5}	None provided	n.a.	n.a.	

Table L2.24 Estimated emissions as a result of wind erosion of the haul roads

Size fraction	Emission factor equation	Emission factor reference	Mitigated emission rate (kg/hour)	Notes
TSP	$E = 1.9 \left(\frac{S}{1.5} \right)^{365} \left(\frac{365-p}{235} \right) \left(\frac{f}{15} \right)$	TSP emission factor from 'active storage pile' section of AP42 Chapter 11.9, Table 11.9-2	3.81	Assumes dust mitigation on haul roads
PM ₁₀	50% of TSP	PM ₁₀ emission factors sourced from NPI publication EET for Mining v2.3, Dec 2001 (Appendix A1.1.15)	1.91	
PM _{2.5}	None provided	n.a.	n.a.	

L2.9 ATTACHMENT

The following document is attached to this appendix:

- Pacific Air and Environment, *Olympic Dam EIS In-Pit Flow and Retention Study – Final Report*, 2008.

L2.10 REFERENCES

Cowherd, C., Muleski, G.E., Kinsey, J.S., *Control of open fugitive dust sources*, Midwest Research Institute, September 1988, Kansas City, United States of America.

National Environment Protection Council 2003, *National Environment Protection (Ambient Air Quality) Measure*.

National Health and Medical Research Council 1996, *Ambient Air Quality Goals Recommended by the National Health and Medical Research Council*, May 1996, NHMRC, Canberra.

National Pollutant Inventory 1999, *Emission Estimation Technique Manual for Copper Concentrating, Smelter and Refining*, NPI, DEWHA, Canberra.

National Pollutant Inventory 2001, *Emission Estimation Technique Manual for mining Version 2.3*, NPI, DEWHA, Canberra.

National Pollutant Inventory 2005, *Emission Estimation Technique Manual for Fossil Fuel Electric Power Generation Version 2.4*, NPI, DEWHA, Canberra.

Sinclair Knight Merz 2005, *Improvement of NPI Fugitive Particulate Matter Emission Estimation Techniques*, May 2005, Perth.

South Australian Environment Protection Authority 2006, *EPA Guideline: Air quality impact assessment using design ground level pollutant concentrations (DLGCs)*, January 2006, Adelaide.

U.S Environmental Protection Agency 1995, *Compilation of Air Pollutant Emission Factors AP-42, Fifth Edition, Volume 1 – Stationary Point and Area Sources*, January 1995, North Carolina, United States of America.

DRAFT REPORT

Final Report:

**OLYMPIC DAM EIS IN-PIT FLOW
AND RETENTION STUDY**

ARUP HLA Olympic Dam EIS Project

20 March 2008 Job No 2265



PROJECT TITLE: Preliminary Report: Olympic Dam EIS In-Pit Flow and Retention Study

JOB NUMBER: 2265

PREPARED FOR: David Winterburn
ARUP HLA Olympic Dam EIS Project

STATUS: Final

DATE OF RELEASE: 20 March 2008

PREPARED BY: J Taylor

APPROVED FOR RELEASE BY: R. Ormerod

DISCLAIMER & COPYRIGHT: This report is to be read subject to the disclaimer and copyright statement located at www.pae.net.au
© Pacific Air & Environment Pty Ltd 2007
ABN 23 887 350 026

Pacific Air & Environment Pty Ltd ABN 23 887 350 026

BRISBANE:

Level 1, La Melba, 59 Melbourne Street South Brisbane Qld 4101
PO Box 3306 South Brisbane Qld 4101
Ph: +61 7 3004 6400
Fax: +61 7 3844 5858

SYDNEY:

3 Spring Street Sydney NSW 2000
PO Box 4216 Sydney NSW 2001
Ph: +61 2 8249 4464
Fax: +61 2 8249 4001

Email: enquiries@pae.net.au

Website: www.pae.net.au

ES1 EXECUTIVE SUMMARY

Computational Fluid Dynamics (CFD) modelling software AVL SWIFT Version 8.41 has been used to assess the flow and dust behaviour within the proposed expansion of the Olympic Dam open pit mining facility during Year 40 of the project operation. The objective of the study was to investigate deposition, and thus retention, of particulate released through in-pit activities.

The simulations were performed with the open pit as the only infrastructure element. The pit was approximately 3 km by 3 km and over 900m deep at Year 40.

The methodology employed a two-phase fluid approach where particulate was represented as a second phase of fluid comprising discrete 'bubbles' of defined radius and density within the continuous primary fluid phase (air). The study of only a single discrete particle size was possible per simulation.

North wind, neutral stability, $U_{10m} = 5$ m/s meteorological conditions were used as a base case for the Year 40 open pit configuration, with simulations covering a range of discrete particles sizes. Perturbations to the base case meteorological condition included an additional four wind directions and variations to atmospheric stability and wind speed for a limited number of discrete particle sizes.

The aspect ratio of the southern section of the pit is such that vortex or recirculating structures that form are in the order of the size of the pit, with the in-pit surface flow typically passing through the pit and out in one, or at most a couple of, circulations.

As a result of the typically similar flow patterns within the pit, the dust, particularly that emitted toward the base of the pit, was generally only in contact with the wall as it travels up one side of the pit. The dust was then observed to either pass back over the pit as it rejoins the external flow, often at an elevated level, or directly out of the pit in the cases where flow passes more directly through the pit. There did not appear to be any regions of significant dust build-up.

Atmospheric stability and thermal influences within the pit were not observed to significantly alter the main flow structure, although they did affect near surface temperatures, particularly in the very base of the pit. During hot daytime periods of high solar insolation, surface temperatures at the base of the pit were predicted to be of the order 20 to 30°C and possibly more, above ambient surface level temperatures.

The dry deposition flux was predicted using a deposition velocity approach as typically used in air quality dispersion models. Particle size and wind speed were found to be the two primary factors that influenced the deposition and thus pit retention rate. As would be expected, higher pit retention was predicted for larger particles and lower wind speeds. The flow within the pit was responsive to winds at an elevation of 100 m or more and thus variations in atmospheric stability did not significantly influence deposition and pit retention rates. Wind direction was also found not to significantly influence pit retention rates.

Cumulative pit retention for standard particle size fractions of PM2.5, PM10 and TSP was calculated for the base case meteorology from the estimated particle size

distribution of dust emissions and the predicted discrete particle size retention rates. Estimates for wind speeds of $U_{10m} = 2$ and 10 m/s were also possible, with results summarised in Table 1.

Table 1: Summary of predicted pit retention rates for PM2.5, PM10 and TSP particle fractions for neutral stability, north wind, $U_{10m} = 2, 5$ and 10 m/s.

	2 m/s	5 m/s	10 m/s
YEAR	40	40	40
PM2.5	0.93%	0.48%	0.26%
PM10	2.9%	1.5%	0.81%
TSP	47.5%	38.0%	27.9%

Predicted particle fraction retention rates were found to be lower than those recommended in the National Pollutant Inventory (NPI). The NPI recommends 50% retention for TSP and 5% retention for PM10. The predicted retention rates at the lower wind speed of $U_{10m} = 2$ m/s were highest, with particularly the TSP fraction estimate closest to the NPI value. At higher wind speeds, the predicted retention rates were a factor of 2 or more less than the NPI recommended values. The retention rate estimates given by this study are believed to be conservative, particularly in relation to the diffusive deposition component. Further investigation of the diffusive deposition predictions and the significance of deposition onto the emission sources (roads and excavation regions) is recommended. Improved characterisation of the particle size distributions of the various in-pit dust emission sources is also recommended.

TABLE OF CONTENTS

1	INTRODUCTION	1
1.1	Objectives	1
1.2	Scenario Examined	2
2	PARTICULATE MATTER AND MINE OPERATIONS	3
2.1	Particle Size	3
2.2	Mining Dust	4
2.2.1	Mining Dust Dispersion Models	4
3	SITE AND PIT CONFIGURATIONS	7
4	IN-PIT PARTICULATE EMISSIONS	9
5	MODEL CONFIGURATION	10
5.1	The CFD Model	10
5.2	Representation of Particulate	10
5.3	CFD Domain Configuration	11
5.3.1	Open Pit Domains	12
5.3.2	Domain Grid	13
5.3.3	General Domain Boundary Conditions	15
5.3.4	Dust Emissions	15
5.4	Atmospheric Flow Initialisation	16
6	MODEL FLOW BEHAVIOUR	20
6.1	Upwind Flow Characteristics	20
6.1.1	North Wind, $U_{10m} = 5$ m/s	20
6.1.2	North Wind, Stable, $U_{10m} = 1.5$ m/s	30
6.1.3	North Wind, Unstable, $U_{10m} = 3$ m/s	39
6.1.4	East Wind, $U_{10m} = 5$ m/s	49
6.1.5	South Wind, $U_{10m} = 5$ m/s	52
6.1.6	45! Wind, $U_{10m} = 5$ m/s	55
6.1.7	135! Wind, $U_{10m} = 5$ m/s	58
7	DUST DEPOSITION AND PIT RETENTION	62
7.1	Dry Deposition Calculation	62
7.1.1	Gravitational Settling Velocity	62
7.1.2	Diffusive Deposition Velocity	64
7.1.3	Deposition CFD Application	64
7.2	Discrete Particle Size Deposition and Retention	65
7.3	Cumulative Pit Retention	69
7.4	Deposition and Retention Summary	72
8	CONCLUSIONS	74
9	REFERENCES	77

LIST OF FIGURES

Figure 3.1: Aerial view of the proposed pit configuration looking from the south.....	8
Figure 5.2 Schematic of the CFD model domain for the proposed pit configuration (dimensions in metres).....	13
Figure 5.2: Open pit configuration CFD domain grid section.....	14
Figure 5.3: Section through the open pit detailing the configuration of the computational grid within the pit.	14
Figure 5.8: Plan of the model pit configuration detailing the excavation and road dust emission locations.	16
Figure 5.9: Initial atmospheric flow velocity profiles.	18
Figure 5.10: Initial atmospheric temperature profiles.	19
Figure 6.64: Streamlines of flow through the pit for the base case neutral boundary layer with $U_{10m} = 5$ m/s.	21
Figure 6.65: Streamlines of flow through the pit for the base case neutral boundary layer with $U_{10m} = 5$ m/s with velocity magnitude contours on a section near the downwind end of the pit ($Y = -1100$).....	22
Figure 6.66: Velocity magnitude in the surface cell within and around the pit for the base case neutral boundary layer with $U_{10m} = 5$ m/s.	23
Figure 6.67: Velocity magnitude profiles through the centre of the pit for the base case neutral boundary layer with $U_{10m} = 5$ m/s.....	24
Figure 6.68: Turbulence intensity profiles through the centre of the pit for the base case neutral boundary layer with $U_{10m} = 5$ m/s.....	25
Figure 6.69: Longitudinal velocity profiles through the centre of the pit for the base case neutral boundary layer with $U_{10m} = 5$ m/s.....	25
Figure 6.70: Lateral velocity profiles through the centre of the pit for the base case neutral boundary layer with $U_{10m} = 5$ m/s.	26
Figure 6.71: Vertical velocity profiles through the centre of the pit for the base case neutral boundary layer with $U_{10m} = 5$ m/s.....	26
Figure 6.72: Iso-surface of Phase II volume fraction (dust concentration) ($1e-9$) within the pit for the base case neutral boundary layer with $U_{10m} = 5$ m/s, $10 \mu\text{m}$ particles.....	28
Figure 6.73: Iso-surface of Phase II volume fraction (dust concentration) ($1e-9$) within the pit and flow streamline for the base case neutral boundary layer with $U_{10m} = 5$ m/s, $10 \mu\text{m}$ particles.....	28
Figure 6.74: Iso-surface of Phase II volume fraction (dust concentration) ($7e-10$) within the pit for the base case neutral boundary layer with $U_{10m} = 5$ m/s, $10 \mu\text{m}$ particles.....	29
Figure 6.75: Pit surface and ground level Phase II volume fraction (dust concentrations) for the pit base case neutral boundary layer with $U_{10m} = 5$ m/s, $10 \mu\text{m}$ particles.....	29
Figure 6.76: Streamlines of flow through the pit for stable atmospheric boundary layer flow with $U_{10m} = 1.5$ m/s.....	31
Figure 6.77: Streamlines of flow through the pit for stable atmospheric boundary layer flow, $U_{10m} = 1.5$ m/s, and velocity magnitude contours on a section near the downwind end of the pit ($Y = -1100$).	31
Figure 6.78: Velocity magnitude in the surface cell within and around the pit for stable atmospheric boundary layer flow, $U_{10m} = 1.5$ m/s.	32
Figure 6.79: Velocity magnitude profiles through the centre of the pit for stable atmospheric boundary layer flow, $U_{10m} = 1.5$ m/s.	32
Figure 6.80: Turbulence intensity profiles through the centre of the pit for stable atmospheric boundary layer flow, $U_{10m} = 1.5$ m/s.	33

Figure 6.81: Longitudinal velocity profiles through the centre of the pit for stable atmospheric boundary layer flow, $U_{10m} = 1.5$ m/s.	33
Figure 6.82: Lateral velocity profiles through the centre of the pit for stable atmospheric boundary layer flow, $U_{10m} = 1.5$ m/s.....	34
Figure 6.83: Vertical velocity profiles through the centre of the pit for stable atmospheric boundary layer flow, $U_{10m} = 1.5$ m/s.....	34
Figure 6.84: Temperature profiles through the centre of the pit for stable atmospheric boundary layer flow, $U_{10m} = 1.5$ m/s.....	35
Figure 6.85: Streamlines of flow through the pit for stable atmospheric boundary layer flow, $U_{10m} = 1.5$ m/s, colour contours of flow temperature on a section near the downwind end of the pit ($Y = -1100$).....	36
Figure 6.86: Iso-surface of Phase II volume fraction (dust concentration) ($1.5e-9$) and streamlines in the pit for stable atmospheric boundary layer flow, $U_{10m} = 1.5$ m/s, $10 \mu\text{m}$ particles.	37
Figure 6.87: Iso-surface of Phase II volume fraction (dust concentration) ($1e-9$) in the pit for stable atmospheric boundary layer flow, $U_{10m} = 1.5$ m/s, $10 \mu\text{m}$ particles.	37
Figure 6.88: Iso-surface of Phase II volume fraction (dust concentration) ($7e-10$) and streamlines in the pit for stable atmospheric boundary layer flow, $U_{10m} = 1.5$ m/s, $10 \mu\text{m}$ particles.	38
Figure 6.89: Pit surface and ground level Phase II volume fraction (dust concentration) pit for stable atmospheric boundary layer flow, $U_{10m} = 1.5$ m/s, $10 \mu\text{m}$ particles.	38
Figure 6.90: Streamlines of flow through the pit for unstable atmospheric boundary layer flow, $U_{10m} = 3$ m/s.	40
Figure 6.91: Streamlines of flow through the pit for unstable atmospheric boundary layer flow, $U_{10m} = 3$ m/s and velocity magnitude contours on a section near the downwind end of the pit ($Y = -1100$).....	40
Figure 6.92: Velocity magnitude in the surface cell within and around the pit for unstable atmospheric boundary layer flow, $U_{10m} = 3$ m/s.....	41
Figure 6.93: Velocity magnitude profiles through the centre of the pit for unstable atmospheric boundary layer flow, $U_{10m} = 3$ m/s.....	41
Figure 6.94: Turbulence intensity profiles through the centre of the pit for unstable atmospheric boundary layer flow, $U_{10m} = 3$ m/s.....	42
Figure 6.95: Longitudinal velocity profiles through the centre of the pit for unstable atmospheric boundary layer flow, $U_{10m} = 3$ m/s.....	42
Figure 6.96: Lateral velocity profiles through the centre of the pit for unstable atmospheric boundary layer flow, $U_{10m} = 3$ m/s.	43
Figure 6.97: Vertical velocity profiles through the centre of the pit for unstable atmospheric boundary layer flow, $U_{10m} = 3$ m/s.....	43
Figure 6.98: Temperature profiles through the centre of the pit for unstable atmospheric boundary layer flow, $U_{10m} = 3$ m/s.	44
Figure 6.99: Streamlines of flow through the pit for unstable atmospheric boundary layer flow, $U_{10m} = 3$ m/s, colour contours of temperature on a section near the downwind end of the pit ($Y = -1100$).....	45
Figure 6.100: Streamlines of flow through the pit for unstable atmospheric boundary layer flow, $U_{10m} = 3$ m/s, colour contours of temperature on a section near the downwind end of the pit ($Y=0$).	46
Figure 6.101: Ground surface temperature contours for the unstable atmospheric boundary layer flow, north winds, $U_{10m} = 3$ m/s.....	46
Figure 6.102: Iso-surface of Phase II volume fraction (dust concentration) ($1.5e-9$) in the pit for unstable atmospheric boundary layer flow, $U_{10m} = 3$ m/s, $10 \mu\text{m}$ particles.	47

Figure 6.103: Iso-surface of Phase II volume fraction (dust concentration) (1.5e-9) in the pit for unstable atmospheric boundary layer flow, $U_{10m} = 3$ m/s, 10 μ m particles.	48
Figure 6.104: Iso-surface of Phase II volume fraction (dust concentration) (2e-9) and streamlines in the pit for unstable atmospheric boundary layer flow, $U_{10m} = 3$ m/s, 10 μ m particles.	48
Figure 6.105: Pit surface and ground level Phase II volume fraction (dust concentration) for unstable atmospheric boundary layer flow, $U_{10m} = 3$ m/s, 10 μ m particles.	49
Figure 6.106: Streamlines of flow through the pit for easterly winds, neutral boundary layer, $U_{10m} = 5$ m/s.	50
Figure 6.107: Iso-surface of Phase II volume fraction (dust concentration) (7.5e-10) and streamlines in the pit for easterly winds, neutral boundary layer, $U_{10m} = 5$ m/s, 10 μ m particles.	50
Figure 6.108: Iso-surface of Phase II volume fraction (dust concentration) (5e-10) and streamlines in the pit for easterly winds, neutral boundary layer, $U_{10m} = 5$ m/s, 10 μ m particles.	51
Figure 6.109: Pit surface and ground level Phase II volume fraction (dust concentration) for easterly winds, neutral boundary layer, $U_{10m} = 5$ m/s, 10 μ m particles.	51
Figure 6.110: Streamlines of flow through the pit for southerly winds, neutral boundary layer, $U_{10m} = 5$ m/s.	53
Figure 6.111: Iso-surface of Phase II volume fraction (dust concentration) (1e-9) and streamlines in the pit for southerly winds, neutral boundary layer, $U_{10m} = 5$ m/s, 10 μ m particles.	53
Figure 6.112: Iso-surface of Phase II volume fraction (dust concentration) (5e-10) and streamlines in the pit for southerly winds, neutral boundary layer, $U_{10m} = 5$ m/s, 10 μ m particles.	54
Figure 6.113: Pit surface and ground level Phase II volume fraction (dust concentration) for southerly winds, neutral boundary layer, $U_{10m} = 5$ m/s, 10 μ m particles.	54
Figure 6.114: Streamlines of flow through the pit for northeast winds, neutral boundary layer, $U_{10m} = 5$ m/s.	55
Figure 6.115: Streamlines of flow through the pit for northeast winds, neutral boundary layer, $U_{10m} = 5$ m/s.	56
Figure 6.116: Iso-surface of Phase II volume fraction (dust concentration) (1e-9) and streamlines in the pit for northeast winds, neutral boundary layer, $U_{10m} = 5$ m/s, 30 μ m particles.	56
Figure 6.117: Iso-surface of Phase II volume fraction (dust concentration) (2e-9) and streamlines in the pit for northeast winds, neutral boundary layer, $U_{10m} = 5$ m/s, 30 μ m particles.	57
Figure 6.118: Pit surface and ground level Phase II volume fraction (dust concentration) for northeast winds, neutral boundary layer, $U_{10m} = 5$ m/s, 30 μ m particles.	57
Figure 6.119: Pit surface and ground level Phase II volume fraction (dust concentration) for northeast winds, neutral boundary layer, $U_{10m} = 5$ m/s, 30 μ m particles.	58
Figure 6.120: Streamlines of flow through the pit for southeast winds, neutral boundary layer, $U_{10m} = 5$ m/s.	59
Figure 6.121: Streamlines of flow through the pit for southeast winds, neutral boundary layer, $U_{10m} = 5$ m/s.	59
Figure 6.122: Iso-surface of Phase II volume fraction (dust concentration) (1e-9) and streamlines in the pit for southeast winds, neutral boundary	

layer, $U_{10m} = 5$ m/s, 30 μm particles.....	60
Figure 6.123: Iso-surface of Phase II volume fraction (dust concentration) (2e-9) and streamlines in the pit for southeast winds, neutral boundary layer, $U_{10m} = 5$ m/s, 30 μm particles.....	60
Figure 6.124: Pit surface and ground level Phase II volume fraction (dust concentration) for southeast winds, neutral boundary layer, $U_{10m} = 5$ m/s, 30 μm particles.....	61
Figure 6.125: Pit surface and ground level Phase II volume fraction (dust concentration) for southeast winds, neutral boundary layer, $U_{10m} = 5$ m/s, 30 μm particles.....	61
Figure 7.1: Comparison of gravitational settling velocity derived from the CFD multiphase simulation over flat terrain with the parameterisations of the atmospheric dispersion model CALPUFF and ADMS over a particle size range from 2.5 μm to 100 μm	63
Figure 7.8: Predicted pit retention variation with discrete particle size for the pit with the base case neutral boundary layer, north winds, $U_{10m} = 5$ m/s.	66
Figure 7.9: Predicted pit retention variation with atmospheric stability for the pit under northerly winds.	67
Figure 7.10: Predicted pit retention variation with wind direction with the base case neutral boundary layer, $U_{10m} = 5$ m/s.....	68
Figure 7.11: Predicted pit retention variation with wind speed under neutral boundary layer northerly winds.	69
Figure 7.14: Normalised mass distribution and estimated pit retention as a function of particle size for the pit north wind, base case neutral boundary layer for $U_{10m} = 5$ m/s.	70
Figure 7.15: Normalised mass distribution and estimated pit retention as a function of particle size for neutral boundary layer, north wind for $U_{10m} = 2, 5$ and 10 m/s. Note: $U_{10m} = 2$ and 10 m/s results are estimated by a constant factor from the $U_{10m} = 5$ m/s retention distribution.....	72

LIST OF TABLES

Table 4.1: Summary of estimated dust emissions for the Year 24 pit operations as used for the Year 40 dust behaviour simulations.....	9
Table 5.1: Summary of wind speeds and temperature profiles of the ambient flow for the simulation configurations.....	18
Table 7.4: Estimated geometric mean and standard deviation for dust emissions.	69
Table 7.5: Summary of estimated pit retention rates for PM2.5, PM10 and TSP particle fractions for the pit dust emissions, with base case neutral boundary layer, north wind, $U_{10m} = 5$ m/s simulated atmospheric conditions.....	71
Table 7.6: Summary of estimated pit retention rates for PM2.5, PM10 and TSP particle fractions with neutral boundary layer, north wind, $U_{10m} = 2, 5$ and 10 m/s simulated atmospheric conditions.	72
Table 8.1: Summary of predicted pit retention rates for PM2.5, PM10 and TSP particle fractions for neutral stability, north wind with $U_{10m} = 2, 5$ and 10 m/s.	76

1 INTRODUCTION

BHP Billiton proposes to expand the existing Olympic Dam mine and processing plant located approximately 570 km NNW of Adelaide, South Australia. Mining and processing of copper, uranium, gold and silver is proposed for an expanded Special Mining Lease. An Arup/HLA consortium was commissioned by BHP Billiton to prepare an Environmental Impact Statement (EIS) for the expansion.

In order to meet the Federal and State Terms of Reference (EIS Guidelines) document, Pacific Air & Environment (PAE) was appointed by the ARUP HLA Olympic Dam EIS Project Team to assess the impact of the proposed expansion of the Olympic Dam mine, processing plant and associated infrastructure on the local climate and to investigate the microclimate within the pit.

The expansion of the Olympic Dam mine is likely to contain the following significant infrastructure elements:

- Waste Rock Dump - The Waste Rock Dump (WRD) will be a rectangular structure of approximately 9.2 km by 4.6 km. The structure height is expected to graduate from ground level at Year Zero of the expanded operation, rising to 100 m at Year 40, prior to reaching a maximum height of 160 m at Year 70.
- Open pit - The proposed open pit will be 2.8 km by 2.8 km by 915 m deep after 40 years.
- Tailings Retention System - The Tailings Retention System (TRS) will be constructed in a sequence of cells, each approximately 2 km by 2 km, with the first grouping of four cells being constructed from ground level to a final height of 50 m over the first 25 years of the operation. An additional set of four cells will be constructed from Year 25 to Year 50, also to a final height of 50 m.

1.1 Objectives

The specific aims of this study, as outlined in the Study Brief (ARUP HLA, 2006), are to:

- Determine the microclimate within the proposed open pit mine having regard to air circulation (refresh) rates and temperature profiles and distribution at Year 40;
- Investigate in-pit retention factors for Total Suspended Particulate (TSP), PM10 and PM2.5 dust fractions, for comparison against the quoted National Pollutant Inventory (NPI) Emission Estimation Technique (EET) Mining Manual (v2.3) values of 50% retention for TSP and 5% retention for PM10.
- Provide a detailed report detailing data and methodologies used, results and conclusions.

Other factors of interest from the investigation include in-pit temperatures under typical summertime meteorological conditions and potential for the development of high pollutant concentrations within the pit due to poor air circulation and low refresh rates.

1.2 Scenario Examined

Owing to the project deadline and the computationally intensive nature of the models employed, only a limited study could be performed. Hence, the study considered the open pit configuration at Year 40 only, for a limited range of meteorological conditions and particle sizes as detailed below:

- One wind direction:
 - Neutral stability, higher/typical wind speed ($U_{10m} = 5$ m/s), up to five discrete particle sizes;
 - Unstable (convective) conditions, summer daytime, dry, light winds ($U_{10m} = 2-3$ m/s), up to two particle sizes;
 - Stable nocturnal inversion, low wind speed ($U_{10m} = 1.5$ m/s), up to two particle sizes; and
 - Neutral stability, additional higher and lower wind speed, up to two particle sizes.
- Up to four additional wind directions:
 - Neutral stability, higher/typical wind speed ($U_{10m} = 5$ m/s), up to two discrete particle sizes;

Each simulation included sufficient “spin-up” of the model to establish a ‘stationary’ flow or circulation within the pit prior to establishment of the specific scenario conditions. The modelling approach and size of the pit also limited the modelling to considering one particle size per simulation only, and assuming no particle-particle interaction, generally a reasonable assumption when dust concentrations are low. The time constraints also restricted our ability to perform detailed investigations into issues associated with domain size, grid configuration and time step in relation to their potential influence on model solutions.

2 PARTICULATE MATTER AND MINE OPERATIONS

Particulate matter (or PM) is the technical term for “dust” or particles in the air we breathe. PM exists naturally in the atmosphere, with contributions from pollens and sea-salt spray being two main natural sources, although human activity is generally the major contributor. Vehicle exhaust, power stations and industrial processes are often significant sources in urban areas, however, mining, farming and smoke from residential heating or bushfires can often have significant local and more regional impacts.

Health and amenity impacts can be associated with PM exposure, with the risk dependent upon factors such as the general health of the person, exposure levels and the chemical composition of the PM, as well as exposure to other associated pollutants.

2.1 Particle Size

Particulate emissions from both natural and manmade sources do not consist of particles of any one size. Typically particles emitted to the air are of a number of different shapes (spherical, irregular, flake, fibre for instance), densities and sizes. Defining a size for a spherical particle is relatively easy, with the particle diameter being a simple characteristic descriptor. However, for more typical non-spherical particles the diameter is not a unique characteristic descriptor. Additionally, particles of similar shape may have different chemical compositions and thus densities, introducing further confusion into the definition of a particle size.

In the field of air pollution a standard particle size definition that relates directly to the behaviour of the particle in a fluid (air) has generally been accepted. This definition is termed the **aerodynamic diameter** and is defined as the diameter of a spherical particle having a density of 1 gm/cm³ (1000 kg/m³) that has the same inertial properties in the gas as the particle of interest. The particle shape and density affects the motion of a particle through a fluid due to the aerodynamic drag force caused by the difference in velocity of the particle and the surrounding fluid. Inertial sampling devices typically used for particle sizing, such as a cascade impactor, use the variation in particle behaviour with aerodynamic diameter to characterise the particles.

The aerodynamic diameter is used for the definition of particle size in this study. The aerodynamic of a particle of known size (> 0.5 µm) and density can be approximated using Equation 2-1:

$$d_{pa} = d_{ps} \sqrt{\rho_p} \quad \text{Equation 2-1}$$

Where,

$$\begin{aligned} d_{pa} &= \text{particle aerodynamic diameter;} \\ d_{ps} &= \text{Stokes particle diameter;} \text{ and} \\ \rho_p &= \text{particle density.} \end{aligned}$$

2.2 Mining Dust

Mining operations have historically generated substantial quantities of airborne respirable dust, and even with improved suppression techniques continue to do so into the present day. The vast majority of dust generated from mining operations consists of coarse particles (4 to 10 μm) and particles larger than 10 μm . Activities such as the mechanic disturbance of rock and soil materials through blasting, bulldozing, shovelling or other methods of excavation and vehicle movements on dirt roads are responsible for the majority of larger particle dust generation. Particles can also be generated through wind erosion over bare ground or stockpiles.

Larger particles can have amenity and health impacts, however, finer particles are generally considered more problematic in relation to health impacts. Respirable dust is commonly defined as particles of size fraction 4 μm or less. Inhalation of such dust has led to the development of lung diseases such as coal worker's pneumoconiosis (CWP) and silicosis in thousands of mine workers. The US National Institute for Occupational Safety and Health (NIOSH) reports approximately 17,500 deaths for the period 1990 to 1999. Fine particles account for only about 5% of the particle mass emitted during the mining process with the majority of these from vehicle and mobile equipment exhausts.

Research into developing new and improved understanding of dust behavior and control is ongoing, particularly in relation to reducing mine-worker exposure to respirable dust. Computer modelling is one tool that can be used to investigate dust generation and dispersion. Modelling is a process whereby a system is created to simulate a real-life situation. This can be the development of a smaller scale physical representation of the main elements of the real-life situation, as typically used in wind tunnel modelling; or development of a virtual or computer model through mathematical representation of the main physical processes. Computer modelling is generally the most cost effective and versatile method of analysing a real-life situation and has become increasingly prevalent in solving problems related to physical processes. More sophisticated computer modelling typically involves a substantial degree of research and development where-by trial and error methods are applied to the model and tested with the actual physical process to optimise or perfect the model. Computer modelling of dust behavior from mine sources can help identify potential hazard areas and evaluate suppression strategies.

2.2.1 Mining Dust Dispersion Models

NIOSH has recently published an Information Circular on significant dust dispersion models for mining operations (IC 9478, Reed 2005). The report discusses various modelling techniques from simple box and Gaussian models to more complex Eulerian and Lagrangian numerical approaches, considering their application to modelling dust dispersion and deposition in primarily underground, but also surface mines.

A number of studies investigating deposition in underground coalmine airways are discussed, including Courtney et al. (1982), Courtney et al. (1986), Bhaskar (1987), Bhaskar and Ramani (1989), and Xu and Bhaskar (1995) who built on the earlier work Bhaskar was involved in. The later studies (Xu and Bhaskar, 1995) found the deposition velocity of coal dust in an underground airway consisted of two main components: gravitational settling and diffusion or turbulent deposition.

Their work concluded turbulent deposition was dominant for fine particles. However, the deposition rate was independent of particle size and airflow or velocity, and thus gravitational settling was more dominant for larger particles. Particle properties and air velocity were found to influence the gravitational settling rate.

Work performed explicitly on deposition in underground mines has not solved the airflow within the mine, but used a mean airway velocity to characterise the airflow. A number of studies have used computational fluid dynamics (CFD) to characterise the airflow in mine entries, however, these have generally only considered characterisation of the airflow (Wala et al., 2001). Srinivasa et al. (1993) considered dust dispersion by initially calculating the airflow and then calculating the dust behaviour within the airflow.

Regulatory models, particularly the Industrial Source Complex model (ISC3), have had the greatest impact on the surface mining industry, primarily as a result of a requirement to use a regulatory approved model to assess air quality. However, such models are based on mean, typically surface, flow parameters, and do not resolve flow within a pit. The affect of re-circulating flow behaviour on both concentration enhancement and particle deposition would not be captured with such a model, requiring some form of parameterisation of the emission character and rate, with the later generally based on a pit retention estimate.

Reed (2005) reports a number of models created to predict pit retention including described by (Winges) Equation 2-2 based on the pit depth, H , vertical diffusivity, K_z , and the particle deposition velocity, v_d , where ε is the mass fraction of dust that escapes the pit (Cole and Fabrick, 1984).

$$\varepsilon = 1 / \left[1 + \left(\frac{v_d}{K_z} \right) H \right] \quad \text{Equation 2-2}$$

Fabrick also created an open pit retention model based upon wind velocity at the top of the pit (Equation 2-3) (Reed, 2005).

$$\varepsilon = 1 - v_d \left[\frac{C}{u} \left(\frac{1}{2} + \ln \frac{w}{4} \right) \right] \quad \text{Equation 2-3}$$

where u is the wind velocity at the top of the pit, C is a dimensionless constant equal to 7 and w is the pit width. Reed reports both models agree well with a study by Shearer (unreferenced) which states that approximately one-third of the emissions from mining activities escape the pit.

In relation to more complex modelling approaches, Reed (2005) discusses a study for the EPA (US) by TRC Environmental Consultants (1995). The TRC study reports on the use of finite-element analysis in a model created by Herwehe in 1984, and another finite-element model (FEM). Such models solve a simplified form of the Navier-Stokes equation for fluid flow to predict particle dispersion, and as such essentially use CFD concepts. It is reported the model of Herwehe is restricted to pit angles less than 35° from the horizontal and is not suitable for stable conditions.

Grainger and Meroney (1993) reported on physical modelling (wind tunnel) of stably stratified flow in an open cut coal mine. Investigating the stagnant accumulation of combustion exhausts, their work used an inverted modelling technique in which stratification is developed along a false roof of the wind tunnel working section, with the open pit extending above the roof. Heating was applied to the pit surface as a surrogate to the cooling a correctly orientated pit may experience. It was concluded that flow penetration within the pit depended upon the approach flow stability (parameterised by the Froude number) and the strength of the inversion within the pit. Passive pollutant dispersion was investigated; with concentrations found to be a strong function of the approach flow Froude number, source location and the duration of the release.

Yong Shi et al. (2000) reported on the use of a high-resolution, non-hydrostatic, three-dimensional planetary boundary-layer (PBL) model to study the planetary boundary layer evolution in a large (2 km by 2 km by > 100 m deep) open cut mine. The results indicated that re-circulation was a major feature of the flow, with the topography and meteorological conditions having a major influence. They concluded thermal and mechanical forcing play different but important roles in the evolution process of the PBL.

While a number of models have considered the atmospheric flow and dispersion in open-pit mines, there appears to be little, if any, detailed simulation of deposition and in-pit-retention of particulate matter. The current study appears to be the first attempt of a detailed numerical simulation of the three-dimensional flow behaviour and corresponding fugitive emission dust transport and deposition within a large open-pit mine.

3 SITE AND PIT CONFIGURATIONS

Olympic Dam is located in central South Australia approximately 10 km north of Roxby Downs in a region of arid climate with hot, dry summers and mild winters. The region immediately around the proposed development is generally flat, with the main surface features being sand dune ridges aligned generally east-west and in the order of 6 to 10 m in height. Further details of the climate and site are discussed in D'Abreton (2006).

BHP Billiton proposes to expand the existing mining operation through the development of a new and more extensive pit to the east of the current infrastructure. It is proposed that the new pit will expand in size over a 70-year period, with the Waste Rock Dump (WRD) and Tailings Retention System (TRS) developing simultaneously with the pit growth. The current study concentrates on the Year 40 pit configuration.

The pit retention study does not consider the influence of the simultaneous expansion of the WRD or TRS, with terrain immediately surrounding the pit considered flat for both pit configurations simulated. Time and computing restraints prohibited the inclusion of surrounding infrastructure within the model domain. More detail of the individual pit configuration is provided below.

By the end of 40 years of operation it is proposed the pit will have expanded significantly in width and less so in length to be relatively symmetrical in shape and close to circular, with a diameter of approximately 3.0 km. The pit will also have expanded significantly in depth with the base now over 900 m below the surface, with a number of smaller platforms toward the bottom as opposed to a single base. The wall angles will still be in the order of 50° to 60° to the horizontal, broken by the roads spiralling down to the base. In reality, the walls would be terraced, however such detail is too fine for inclusion in a practical representation of these very large pits. It is anticipated most excavation activity will take place in the lower sections of the pit around the Year 40 stage. A 3-dimensional rendered aerial perspective of the pit configuration is presented in Figure 3.1.

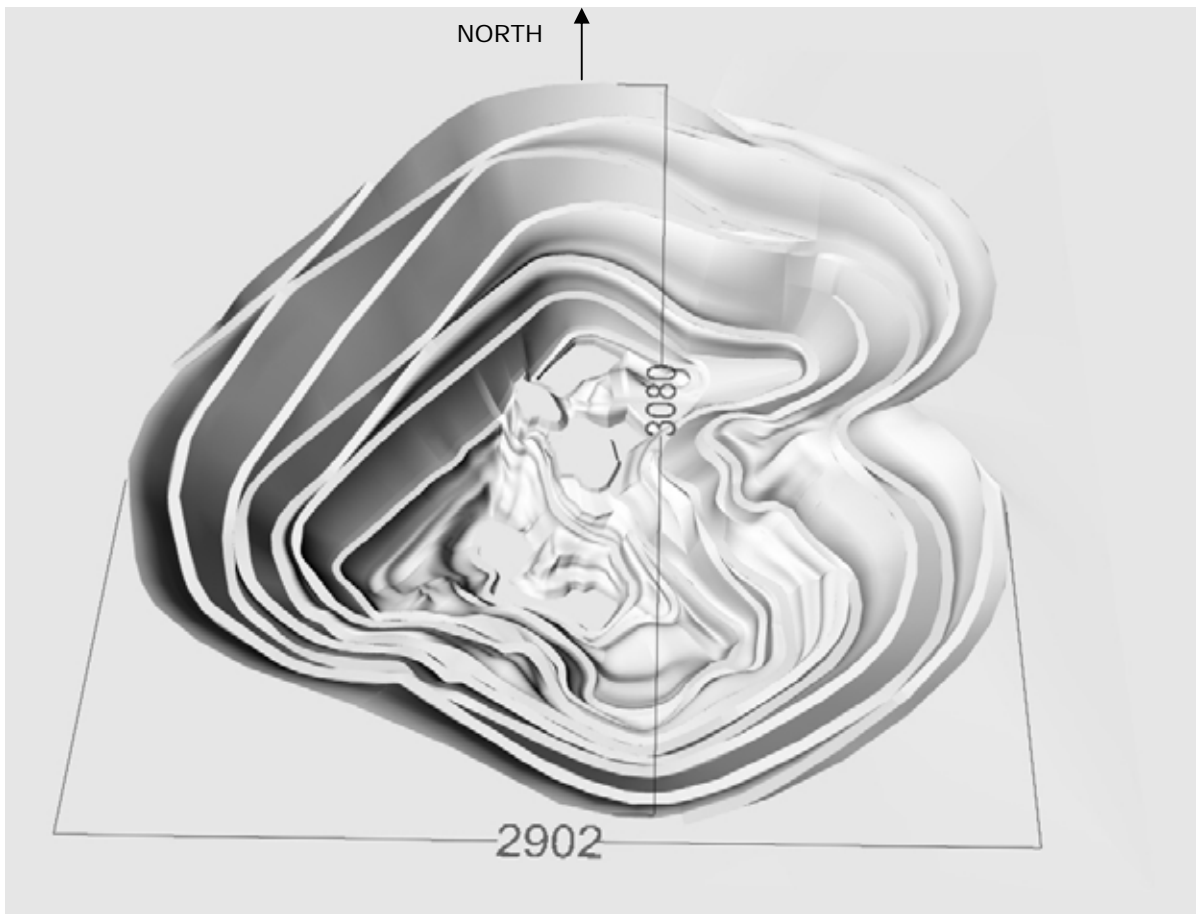


Figure 3.1: Aerial view of the proposed pit configuration looking from the south.

4 IN-PIT PARTICULATE EMISSIONS

Particulate emissions (dust) are a problem in almost all mining operations. Dust is produced in most mining operations from blasting, handling, transport, preparation and processing. Dust can be hazardous to human health, and thus can affect working conditions and productivity within and around a mine site. If the dust that is generated within a mine pit is unable to escape, working conditions can be severely affected. The dust that escapes the pit can also be detrimental to the above-pit environment.

In-pit dust primarily arises from two types of activity:

- Excavation, including blasting and loading of the rock into haul trucks. These emissions generally occur at a number of discrete points within the pit, the locations of which vary slowly as the pit evolves, and
- Wheel generated dust arising through transport of the rock by the haul trucks. Wheel generated dust occurs along the generally unsealed roads used by the haul trucks to transport the rock from the excavation areas to the surface of the pit for processing and returning to the excavation sites.

Details of estimated dust emissions during the first 24-years of the Olympic Dam expansion pit operation were supplied by Dave Winterburn of the Olympic Dam EIS Project^a. Estimated in-pit dust emissions for the Year 24 pit operations are summarised in Table 4.1. Emissions from in-pit haulage roads are seen to increase as the haulage distance increases due to the depth of the pit, while excavation activity emissions remain consistent over the life of the pit.

This investigation has used the average Year 24 emissions for the Year 40 pit configuration. Average Year 40 dust emissions were not available at the commencement of the investigation.

Table 4.1: Summary of estimated dust emissions for the Year 24 pit operations as used for the Year 40 dust behaviour simulations.

Activity	TSP (kg/hr)	PM10 (kg/hr)	PM2.5 (kg/hr)
In-pit excavation areas	2,347	975	95
In-pit haulage roads	3,005	858	132
Total Year 24 Operations	5,352	1,834	226

^a 060817_BaseCase_Dust.xls

5 MODEL CONFIGURATION

5.1 The CFD Model

The fluid flow and thermodynamic modelling undertaken in this study used the Computational Fluid Dynamics (CFD) modelling software AVL SWIFT Version 8.41 (Swift). Swift employs a Finite Volume discretisation method to solve the fundamental physical conservation laws (mass, momentum, energy) in their integral form.

The conservation laws for mass (continuity), momentum and energy form a closed set of modelling equations that can be solved for specified initial and boundary conditions. The exact solution of the equations provides a continuous distribution of the conservation variables (i.e. total enthalpy, species concentration, turbulent kinetic energy and dissipation of turbulent energy, or vector components such as the fluid velocity) in terms of the spatial co-ordinates (x,y,z) and time t . However, it is well known that an exact solution is rarely available, with various numerical methods used to replace the continuous distribution by one at a set of discrete points in space and time. Through the discretisation of the modelling equations over the solution domain (space and time), the modelling equations are converted into a system of algebraic equations for which a general numerical method solution can be formulated.

The computational domain is established and divided into a number of non-overlapping control volumes, which constitute the numerical grid. A control volume bounded by an arbitrary number of surfaces, i.e. a general convex polyhedron, can be used. A numerical grid, composed from a finite number of control volumes (cells), is obtained through the discretisation in space of the solution domain. The calculation of dependent variable values on the cell faces involves interpolation from adjacent cell centre values through an appropriate differencing scheme. The adopted discretisation practice is formally second order accurate in space, but this can be relaxed.

SWIFT solves the governing equations using a Finite Volume approach whereby the conservation equations for the fluid entering and leaving the volume are integrated over the finite control volumes (cells generated by the adopted numerical mesh). A steady state solution of the conservation equations is obtained using the $k-\epsilon$ turbulence model. This is the most widely used turbulence model, particularly for industrial computations. It is numerically robust and has been tested in a wide range of flow scenarios including heat transfer, combustion, and two-phase flows. It is generally accepted that the $k-\epsilon$ model usually yields realistic predictions of major mean flow features in most situations.

The flow was treated as incompressible. An upwind differencing scheme was used for the solution of the energy, turbulence and scalar transport equations, while the momentum and continuity equations use a central differencing scheme.

5.2 Representation of Particulate

The particulate, or dust, was represented as a second flow phase within the model. This approach uses volume fraction to represent the distribution of the two flow phases (air and dust) in addition to all other flow variables for each phase.

Wallis (1969) states: "A phase is simply one of the states of matter and can be either a gas, a liquid or a solid. Multiphase flow is the simultaneous flow of several phases. Two-phase flow is the simplest case of multiphase flow." (AVL 2005).

Most flows are in fact multiphase, with the single phase flow assumption made to avoid the additional complexity of multiphase simulations. Air, for example, naturally contains particles, however they are at such low concentrations that they do not affect the flow and thus can be neglected.

There are two approaches to the simulation of multiphase flows:

- Euler-Euler: the most general approach whereby the volume fraction equations remain coupled, allowing the solution of any multiphase in principle; and
- Euler-Lagrangian: allows for simplification of the solution procedure through decoupling of the volume fraction equations. This approach is often used for flows with low dispersed phase volume fractions.

The Euler-Euler approach is employed in the current study.

The particulate is represented as a second phase of fluid comprising discrete 'bubbles' of defined radius and density within the continuous primary fluid phase (air). Momentum exchange occurs between the two fluid phases due to drag and turbulence dispersion forces.

A momentum interfacial exchange parameterisation controls the transfer of momentum between the two fluid phases. In this study, a gas-liquid parameterisation based on bubbly flow was employed. The drag coefficient correlation of Schlichting, (1979) was used:

$$C_D = \begin{cases} \frac{24}{Re_b} (1 + 0.15 Re_b^{0.687}) & Re_b \leq 1000 \\ 0.438 & Re_b > 1000 \end{cases} \quad \text{Equation 5-1}$$

The bubble-induced viscosity from the Sato model is also defined at the interface through the specification of the Sato coefficient, C_{SATO} . The use of the Sato coefficient is a simple and effective way to calculate turbulence viscosity whereby Sato's viscosity (Sato & Sekaguchi, 1975; Theofanus & Sullivan, 1982) is added to the shear-induced turbulent viscosity (SI) due to bubble-induced (BI) turbulence. A Sato coefficient of 0.6 was used in the study. A more detailed description of the approach is available from the AVL SWIFT Multiphase Flow manual (AVL 2005).

5.3 CFD Domain Configuration

A view of the proposed pit configuration is shown in Figure 3.1.

The size of the pit places constraints on the configuration and development of the representation of the pit within the CFD model. Ideally, to best represent the flow behaviour, the CFD domain needs to consider a number of issues, including:

- The overall domain size in relation to the pit dimensions to avoid boundary influences on the critical region of flow;

- The characteristic size of the flow features the simulations are attempting to represent and the appropriate domain and grid sizes to capture these features; and
- The size of the grid elements in the critical regions of flow, which for atmospheric flows is typically in the region adjacent to the surface where gradients, or changes, in flow parameters are usually highest.

These requirements can place conflicting priorities on the development of the domain, the size (number of grid cells) of which is ultimately limited by the available computing resources.

5.3.1 Open Pit Domains

In developing the domain for the current study, the above issues were a significant consideration. There was a need to capture and resolve the near-surface flow relatively well, particularly under nocturnal stable atmospheric conditions. However, the size of the domain was also a consideration to minimise any influence of the domain boundary conditions on the developed flow characteristics.

The CFD model domain for the proposed Olympic Dam open-pit was developed to the limit of the available computing resources, with consideration to the above restrictions and compromises. The major dimensions of the domain configurations are detailed in the schematic presented in Figure 5.1. The simulations considered the pit as the primary feature of the domain. It was felt that inclusion of features such as the WRD and other infrastructure likely to develop around the pit would require a significant expansion of the domain and, consequently, compromise the ability to adequately capture near-surface flow characteristics immediately around and within the pit.

Due to the size of the proposed mine pit, it was not considered feasible to attempt to capture the terraces that develop around the mine wall. Hence the walls of the pit were considered as a rough wall, with the influence of the terracing represented through the surface roughness.

The roads, one of the major dust sources within a mine operation, are generally larger than the wall terraces. The domain was developed with the intent of capturing road surfaces sufficiently to enable their characteristics to influence the flow within the pit if they are significant. The more horizontal road sections are evident spiralling down the schematic view of the pit.

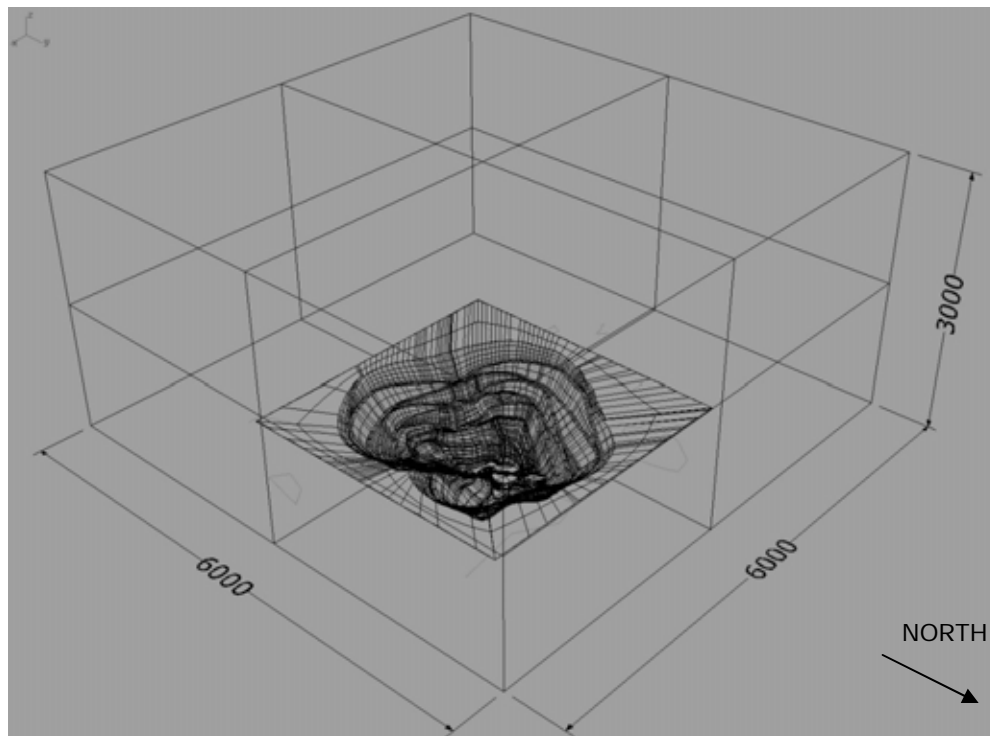


Figure 5.1 Schematic of the CFD model domain for the proposed pit configuration (dimensions in metres).

5.3.2 Domain Grid

For the simulation of the flow and dust behaviour within the proposed Olympic Dam Expansion open pit mine, both domains were meshed with approximately 700,000 cells, with the highest cell density (smaller cells) at ground level immediately around and within the pit. Multi-phase simulations require approximately twice the computer resources as single-phase as the solution of two sets of equations is generally required. Thus, the available computing resources limited the number of cells within the domain. A section through the domain demonstrating the structure of the grid is presented in Figure 5.2, while a close-up image showing more detail of the in-pit computational grid configurations is presented in Figure 5.3.

The increased cell density close to the ground and pit surface is evident. Smaller cells near the surface enhance the resolution in this region of higher vertical gradient, where the surface deposition and thus pit retention takes place.

The smallest cell size within the domain was in the order of 12 m and 16 m. However, it must be remembered that halving the cell size is effectively an increase in the number of cells by a factor of 8 (2^3). Similarly, increasing the domain extent can significantly increase the number of cells. As discussed above, the final domain configuration was a compromise of a number of conflicting requirements based on personal judgement. Detailed investigation of the influence of these issues would likely require significantly enhanced computing resources, even if dust was not represented in the model.

Cells in the upper regions of the domain were up to 250 m in dimension in order to maximise the domain size relative to the pit dimensions. The larger the domain

relative to the size of the primary feature, the less likely it is the domain boundary conditions will adversely affect the flow.

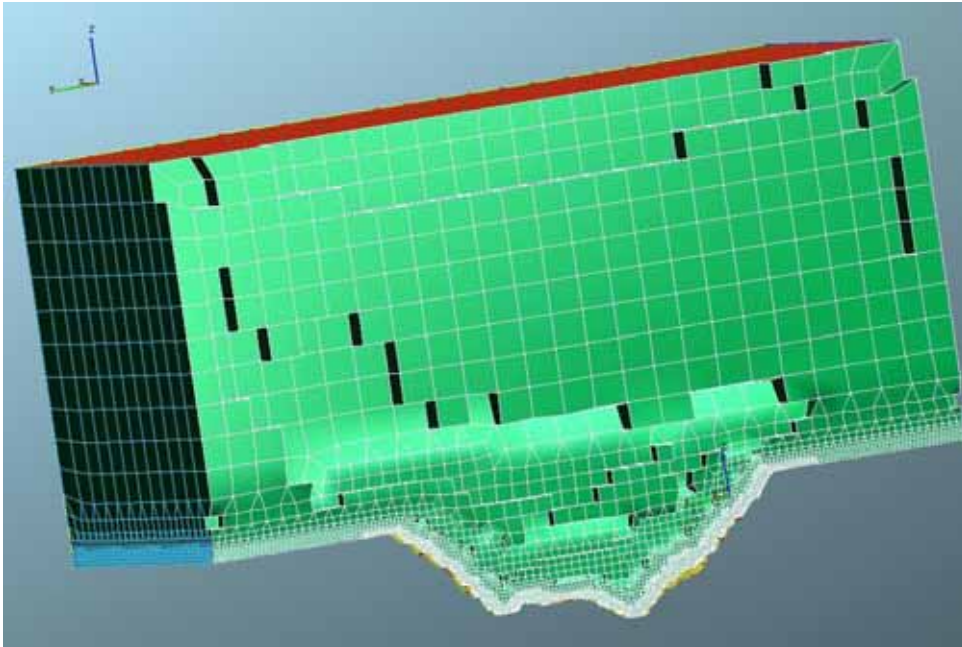


Figure 5.2: Open pit configuration CFD domain grid section.

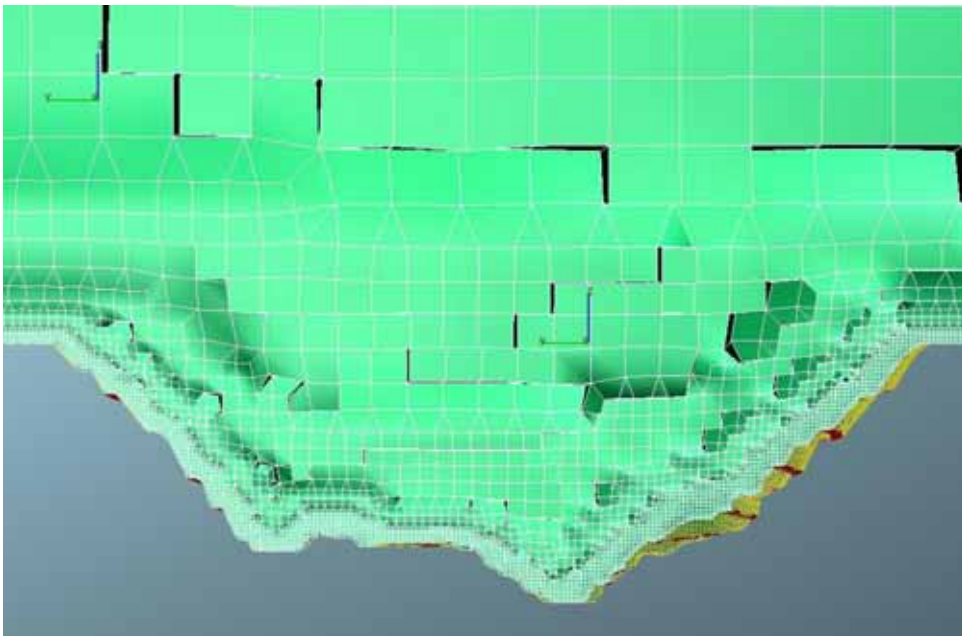


Figure 5.3: Section through the open pit detailing the configuration of the computational grid within the pit.

5.3.3 General Domain Boundary Conditions

Atmospheric velocity turbulence and temperature profiles were applied to the domain inlet flow boundary (see Section 5.4 for specific detail) while a zero pressure gradient condition was imposed at the model domain flow outlet. The boundary at the top of the domain was 3 km above ground level and as such would not be expected to distort significantly as a result of the pit. This domain boundary was configured as a slip wall, thus only enabling flow of a set wind speed and direction and not enabling flow to enter or leave the domain through this boundary.

The side boundaries, parallel to the primary flow direction were configured as symmetrical such that flow conditions are mirrored through the wall. For the oblique angle wind direction simulations (45° and 135°) no domain sidewalls existed, with two domain walls classed as flow inlet regions and two classed as outlet regions.

The bottom of the domain represents the ground surface containing the pit. The surface roughness for the study was maintained at a constant value of $z_0 = 0.2$ m outside the pit, representing the general region surrounding the site as opposed to the direct influence of the Olympic Dam site on the flow. Regions within the pit not classed as dust sources (i.e. not roads and excavation areas) were also parameterised as zero flow rough walls. These regions consisted of both pit wall and base sections. The surface roughness was set at $z_0 = 0.1$ m, a level estimated to take account of the wall terracing and other features likely to exist within the open pit mine environment.

5.3.4 Dust Emissions

As discussed above, the primary sources of in-pit dust generation are related to the excavation and haulage of rock and ore from the mine pit.

Dust emissions arising from excavation activities were established at agreed discrete locations within the pit. A total of seven locations were used for the pit configuration.

The roads used by the haul trucks to transport material to the pit surface are also a primary source of dust emission. Dust was emitted through a low concentration (volume fraction 1e-08), low velocity flow inlet to the model through the in-pit road and excavation surfaces based on the emission rates summarised in Table 4.1. Emission rates were uniform per unit area of emission surface. The dust emission locations are presented in Figure 5.4.

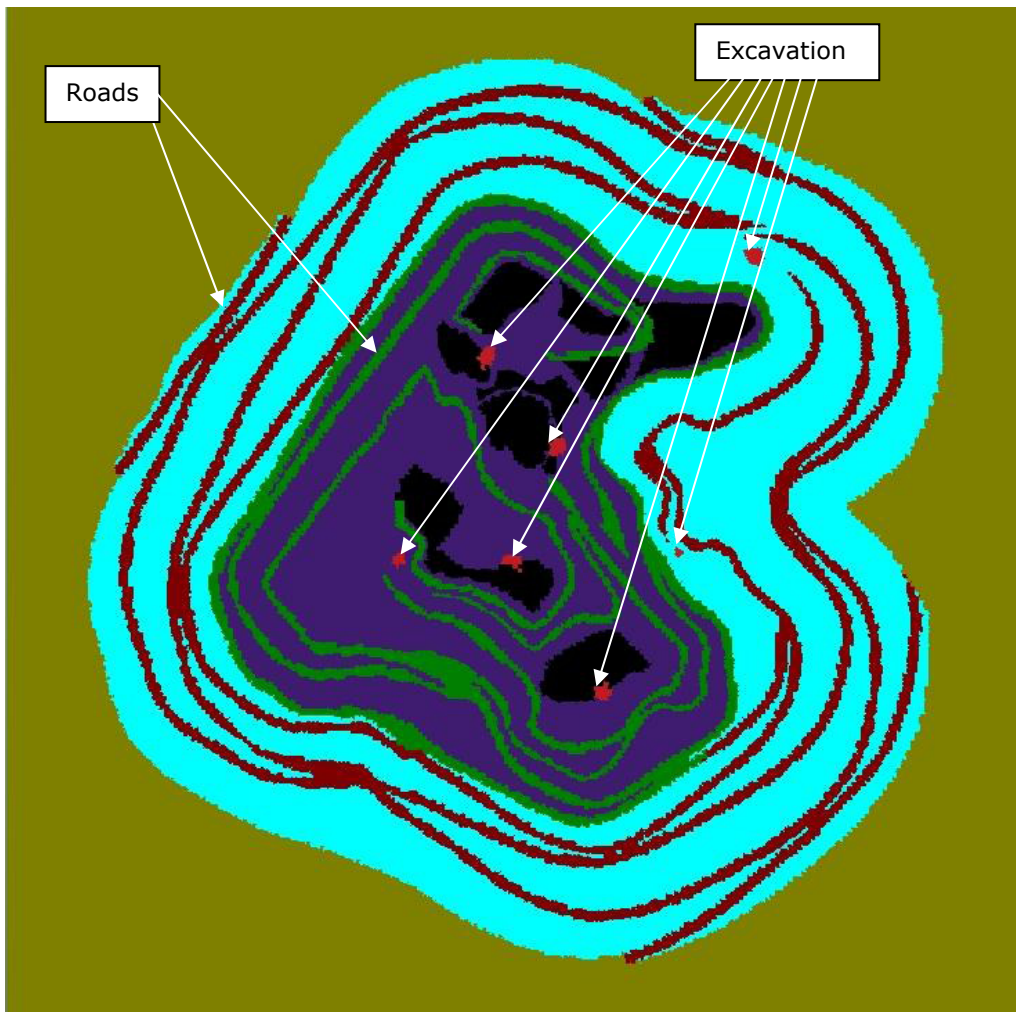


Figure 5.4: Plan of the model pit configuration detailing the excavation and road dust emission locations.

5.4 Atmospheric Flow Initialisation

Investigations were centred upon a base case ambient flow condition with perturbations of wind speed, atmospheric stability and wind direction around the base case. The approaching ambient flow was established as an idealised representation of conditions observed in the first few hundred meters of the atmospheric boundary layer over uniform flat terrain. The description of the flow, taken from Panofsky and Dutton (1984), is based on Monin-Obukhov theory and depends mainly on the height, z ; roughness length, z_0 ; friction velocity, u_* ; and the Monin-Obukhov length, L , as detailed in Equation 5-2:

$$u_0(z) = \begin{cases} \frac{u_*}{K} \left[\ln\left(\frac{z}{z_0}\right) - \ln\left[\left(\frac{1+x^2}{2}\right)\left(\frac{1+x}{2}\right)^2\right] - \frac{\pi}{2} + 2\arctan x \right] & L < 0 \\ \frac{u_*}{K} \left[\ln\left(\frac{z}{z_0}\right) + 5\frac{z}{L} \right] & L > 0 \end{cases} \quad \text{Equation 5-2}$$

Where x is given by $x = (1 - 16z/L)^{1/4}$ and K is the von Karman constant ($K = 0.41$ for this study). A neutrally-stable boundary layer profile, with no thermal gradient, was simulated. Thus a uniform temperature profile was used for all model configurations.

Initial turbulent dissipation of energy, ε_0 , was based on measurements of turbulent kinetic energy budget terms in the atmospheric surface layer (Panofsky and Dutton 1984) for neutral conditions (as $L \rightarrow \infty$) as shown in Equation 5-3.

$$\varepsilon_0(z) = \frac{u_*^3}{Kz} \quad \text{Equation 5-3}$$

The initial turbulent kinetic energy, k , can be obtained from the k - ε model for neutral conditions ($L \rightarrow \infty$) as given in Equation 5-4.

$$k_0(z) = 3.33u_*^2 \quad \text{Equation 5-4}$$

The constant surface roughness value of $z_0 = 0.2$ m representing the general region surrounding the site was used to parameterise the initial atmospheric flow.

Simulation of the stable atmospheric conditions was based upon a Monin-Obukhov length of $L_{MO} = 7$ m and a surface temperature (2 m reference height) of 277 K with the wind speed, $U_{10m} = 1.5$ m/s. To minimise the variation of the stable boundary layer from that of the base case neutral conditions, the neutral wind profile was used above the height for which the stable profile velocities were higher than those used in the base case simulation. This level was about 61 m above the surface. The temperature scale, T_* , was calculated from the definition of L_{MO} , with the initial temperature profile calculated from Equation 5-5 up to a level of 200 m, above which a reduced temperature gradient was applied.

$$T_0(z) = \frac{T_*}{K} \left[\ln\left(\frac{z}{z_0}\right) + 5\frac{z}{L} \right] \quad \text{Equation 5-5}$$

A constant surface temperature could be applied to the surface external to the pit, however the behaviour within the pit is less well understood. To encourage stratification within the pit, cooling of the flow within the pit was enhanced through the use of decreasing pit surface temperatures with depth by a rate of 2.5 K per 100 m. The use of detailed parameterisations of in-pit thermal behaviour may be possible, however for the purpose of these investigations the simplified boundary condition is believed to be suitable provided flow entrapment due to stratification is not observed.

The k - ε turbulence model does not represent the turbulent structure of the unstable or convective boundary layer correctly. The aim of the current study was to investigate the influence of enhanced turbulence within the incident flow for unstable conditions. To provide the least variation from the base case scenario, the initial velocity profile was based upon idealised neutral conditions with enhanced initial turbulence and a heat-flux of 400 W/m² applied through the ground surface. A simplified boundary condition was also used to represent the thermal behaviour within the pit. The surface heat flux of 400 W/m² was applied to horizontal surfaces such as the pit base, while a value of half this amount was used for the pit walls

that are at an angle of about 60° to the horizontal. A heat flux of 400 W/m² is representative of peak solar insolation. Again, a more detailed representation of the variation of pit surface thermodynamics would be possible, however as an initial investigation and with the use of the k- ε turbulence model, the current simplification is considered suitable.

A summary of the simulation boundary layer configurations is presented in Table 5.1. Idealised initial velocity and temperature profiles are presented in Figure 5.5 and Figure 5.6.

Table 5.1: Summary of wind speeds and temperature profiles of the ambient flow for the simulation configurations.

Configuration	Wind Speed, U10m (m/s)	Initial Vertical Temperature Gradient (°C/100 m)	Wind Direction (°)
Base Case	5	0.0	0
Wind Direction	5	0.0	45, 90, 135, 180
Wind Speed	2, 10	0.0	0
Stable	1.5	5.3	0
Unstable	3	0.0	0

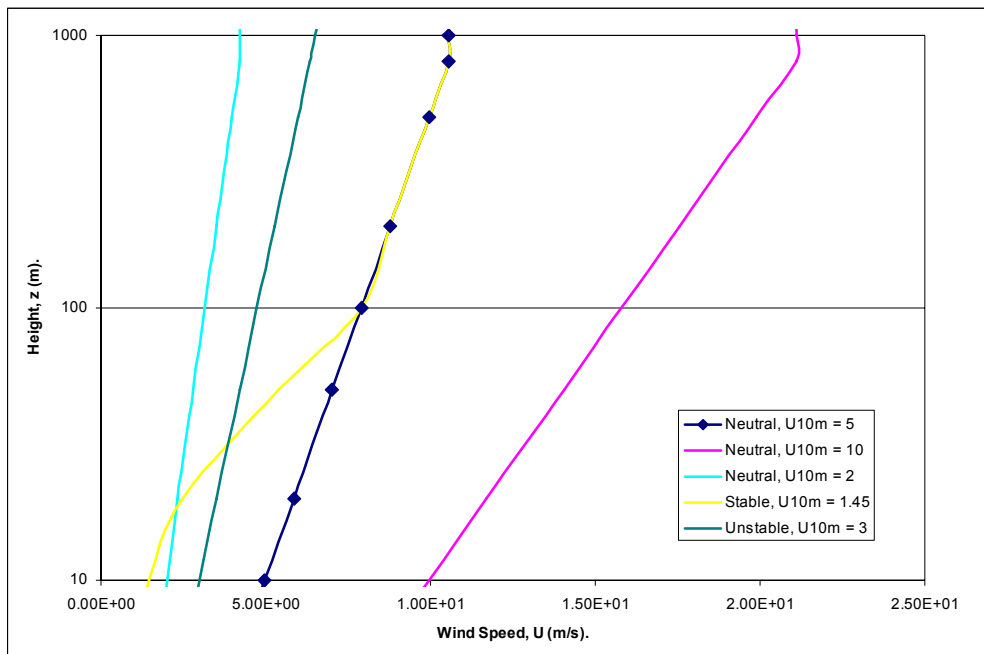


Figure 5.5: Initial atmospheric flow velocity profiles.

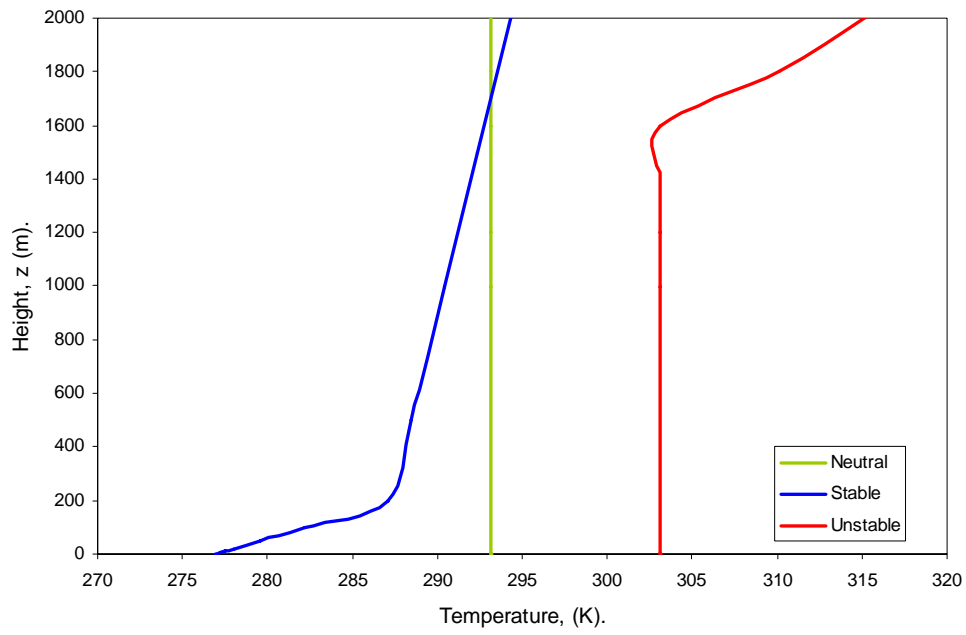


Figure 5.6: Initial atmospheric temperature profiles.

6 MODEL FLOW BEHAVIOUR

6.1 Upwind Flow Characteristics

The behaviour of dust within the pit is dependent upon the in-pit flow characteristics. Of particular interest in relation to dust deposition are the in-pit wind speed and the potential for in-pit recirculation. Also of interest is the behaviour of the in-pit flow under various atmospheric conditions, wind speed, wind direction, atmospheric stability.

Simulations of flow and dust behaviour were conducted for a base case meteorological scenario, with simulations also performed for a limited number of perturbation meteorological conditions. As the CFD simulations provide a full description of a large number of flow parameters across the entire domain, it is unfeasible to attempt to present all the information. However, an understanding of in-pit flow and dust behaviour is considered important in relation to understanding the model deposition processes and thus pit retention predictions. Analyses of the in-pit flow and dust behaviour across the range of atmospheric stability and wind direction simulations are presented below.

6.1.1 North Wind, $U_{10m} = 5 \text{ m/s}$

Streamlines of flow through the pit for the base case meteorological conditions (north wind, $U_{10m} = 5 \text{ m/s}$ neutral boundary layer) are presented in Figure 6.1. It is evident the pit significantly influences the flow behaviour within and immediately downwind. Lateral displacement of the flow is evident on both pit sides as well as displacement of flow toward the downwind pit centre.

Strong spiralling vortex structures are observed to develop within the lee of the upwind wall, beneath the main cross flow that descends into the pit to impact on the upper proportion of the downwind pit walls. The primary spirals within the pit are orientated laterally to the flow and again convergence and exit the pit on the downwind side walls forming a region of low velocity over and immediately downwind of the pit. The region of low velocity over the pit is more evident in Figure 6.2 looking along the direction of flow from an upwind location. The streamlines show the spiral flow behaviour within the pit, with a major lateral spiral evident on the western side of the pit. The spiral structures in the pit are generally of the order the size of the pit, with no smaller recirculation zones observed to form in the immediate lee of the upwind pit wall.

Contours of the velocity in the surface cell within and around the pit are presented in Figure 6.3. Very high velocities are observed on the up and down wind rims of the pit, with magnitudes in the order of 1.5 to 2 times the background wind speed of $U_{10m} = 5 \text{ m/s}$. Regions of highest velocity within the pit are observed to be on the upper regions of the downwind walls of the pit and across the ridge on the eastern side. Greater elevation atmospheric flow of higher velocity is observed to descend directly into the pit, virtually un-attenuated, in both regions.

The magnitude of the velocity over the surface of the remainder of the pit is seen to be relatively low, less than half the velocity over the ground above the pit. Higher velocities are observed in some locations, most likely due to geophysical influences; however, the flow is close to stagnant in other regions. Again, the velocity over the

road sections is observed to be low. It is unclear if this is due to the structure of the road platforms or their use as a low velocity inlet to the model domain to represent the emission of dust along the roads. Interestingly, the velocity over other horizontal regions within the lower sections of the pit are also observed to be low, and thus the low velocities are more likely to be due to the geophysical structure. Regions of lower surface velocity immediately downwind of the pit are also evident.

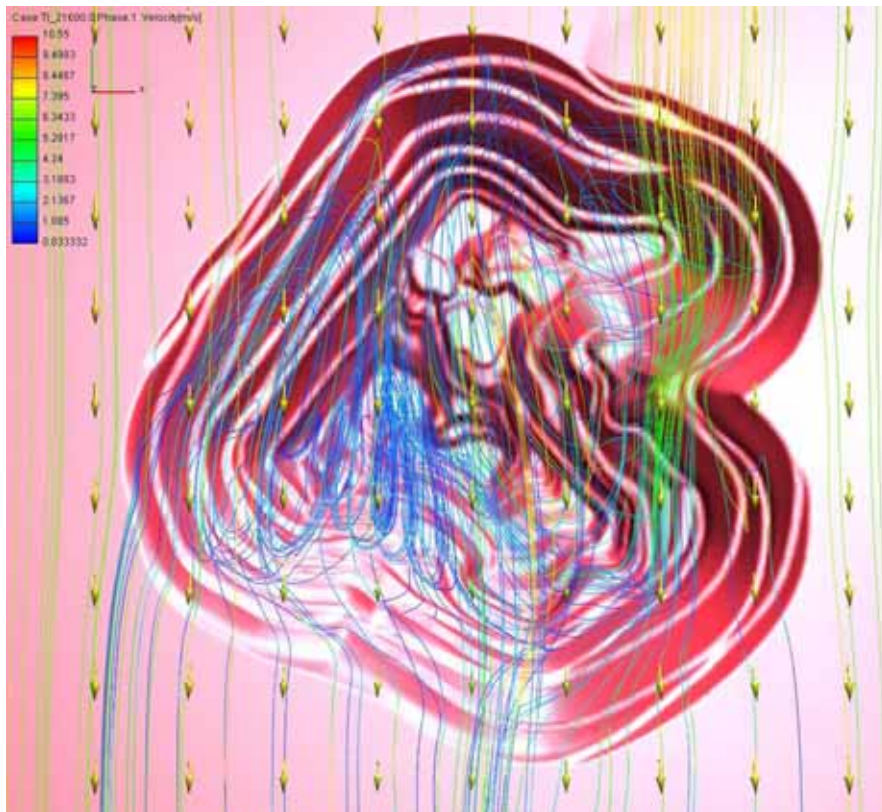


Figure 6.1: Streamlines of flow through the pit for the base case neutral boundary layer with $U_{10m} = 5$ m/s.

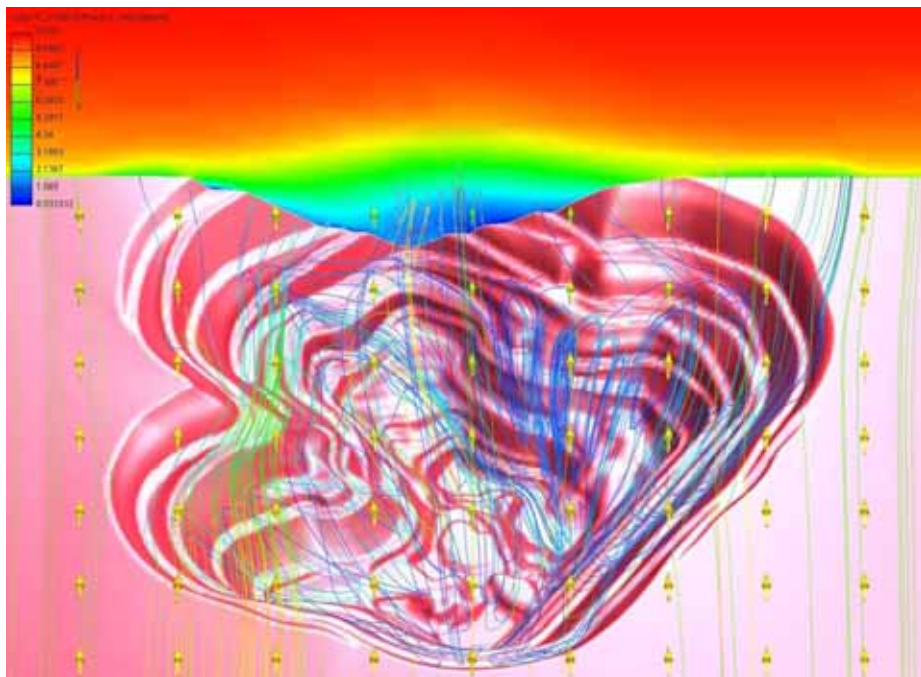


Figure 6.2: Streamlines of flow through the pit for the base case neutral boundary layer with $U_{10m} = 5$ m/s with velocity magnitude contours on a section near the downwind end of the pit ($Y = -1100$).

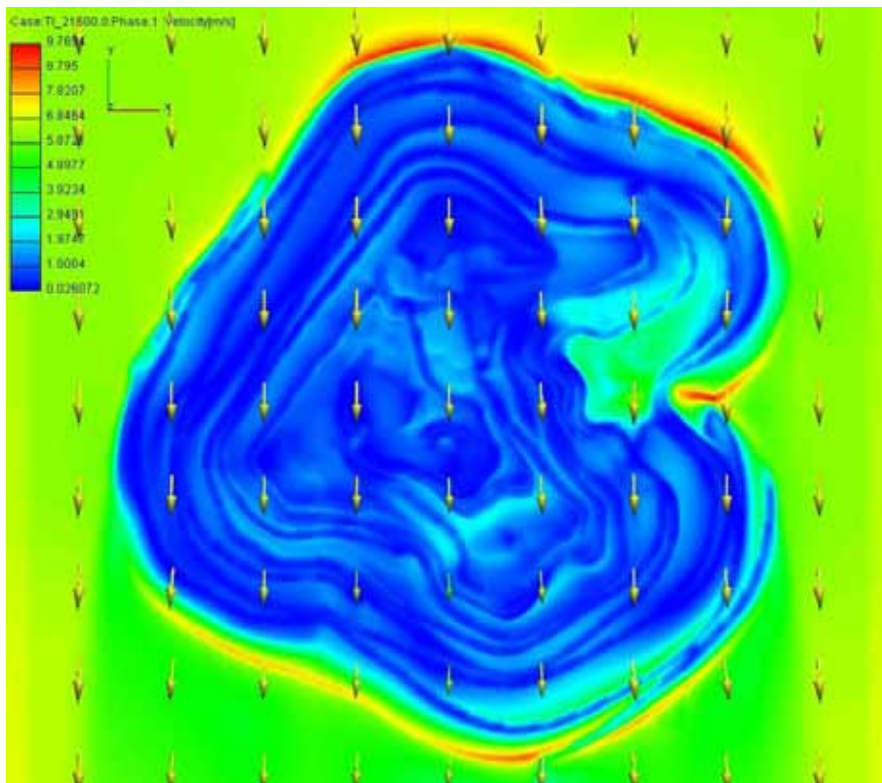


Figure 6.3: Velocity magnitude in the surface cell within and around the pit for the base case neutral boundary layer with $U_{10m} = 5$ m/s.

Profiles of velocity magnitude, turbulence intensity and the individual velocity components upwind, through and downwind of the pit are presented in Figure 6.4 to Figure 6.8. The figures provide profiles through the domain centre, essentially the pit centre, along a line parallel to the wind direction. The location '1.5kmN' is located just inside the upwind pit edge, while the location '1.5kmS' is located just downwind of the pit edge.

The profiles show that there is only a minor variation in along-wind flow characteristics above the level of the pit top. The lower level flow accelerates as it approaches the pit, with the lower level velocities at a maximum as the flow enters the pit itself. The above pit flow decelerates as it passes over the pit, and apart from a small region of accelerated lower level flow on the immediate downwind edge of the pit, lower level velocities are minimum over the downwind regions and further downwind of the pit. Decelerated velocity is observed over the pit to heights of over 1 km.

Flow within the pit is dominated by the formation of a major spiral structure in order of the pit size. This is clearly evident in the longitudinal velocity profiles (Figure 6.6) where a region of reverse flow is observed to develop and descend into the pit. Towards the middle of the pit, the spiral is centred about 300 m below ground level, with maximum reverse flows of the order 2 m/s at a depth of about 700 m. The external boundary layer flow tends to pass over the major recirculation zone within the pit.

Turbulence intensity levels within the pit are observed to significantly increase below the pit surface (Figure 6.5), with again, the velocity fluctuations generally in

the order of the mean velocity throughout much of the pit depth. Significant lateral and vertical velocity components are also evident below the level of the pit, suggesting the existence of spiral circulation of the in-pit flow. This flow structure will provide good flushing of contaminants or pollutants from within the pit.

Modification of lateral and vertical velocity components is also observed above the level of the pit. Relatively significant lateral components are observed up to about 200 to 300 m above the ground, while significant vertical components are observed 600 m or further above the ground. Very significant vertical components of the order 1 m/s and even greater are observed in the 200 m immediately above the ground, as the flow immediately enters or leaves the pit. Peak vertical velocities in the order of 1.5 m/s are observed just downwind of the pit, with vertical velocities in the order of 0.8 m/s observed as the flow enters the upwind edge of the pit. With such significant vertical velocity components observed in regions of relatively strong longitudinal flow, it would be anticipated that thermal stratification of the atmospheric boundary layer will have little influence on the flow characteristics in and immediately around the pit.

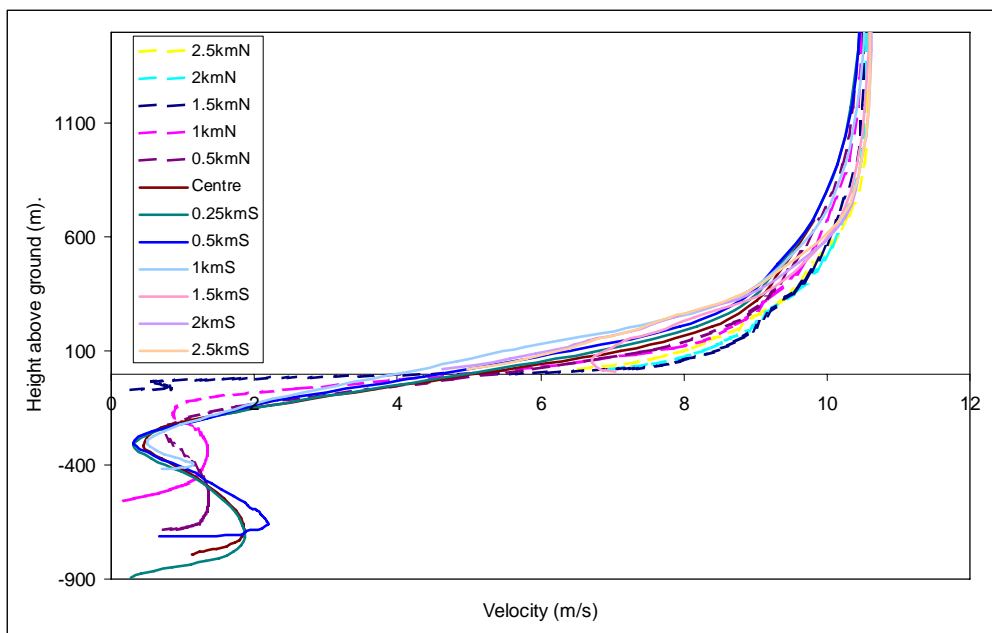


Figure 6.4: Velocity magnitude profiles through the centre of the pit for the base case neutral boundary layer with $U_{10m} = 5$ m/s.

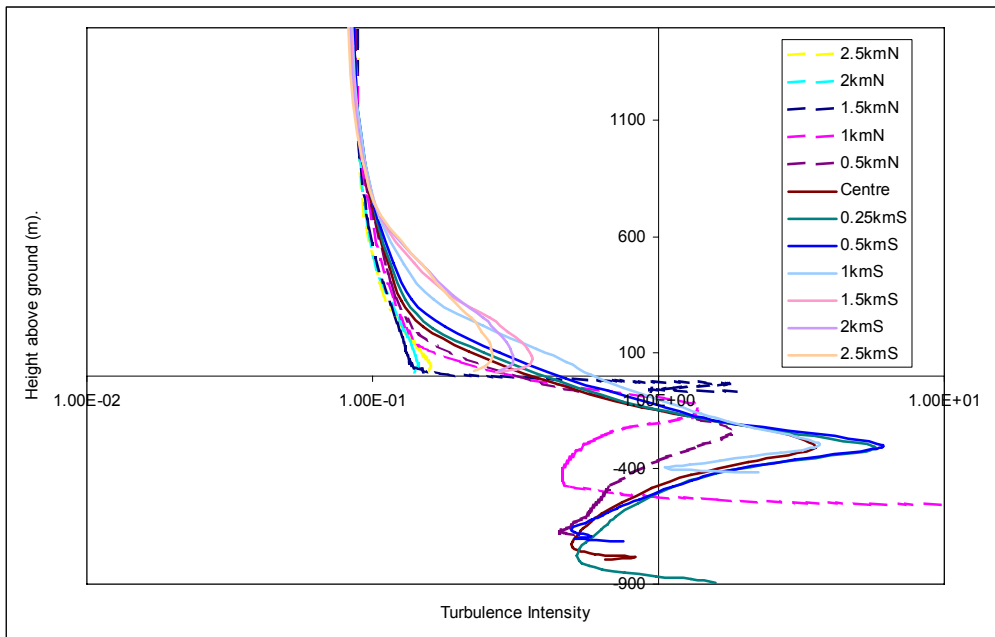


Figure 6.5: Turbulence intensity profiles through the centre of the pit for the base case neutral boundary layer with $U_{10m} = 5$ m/s.

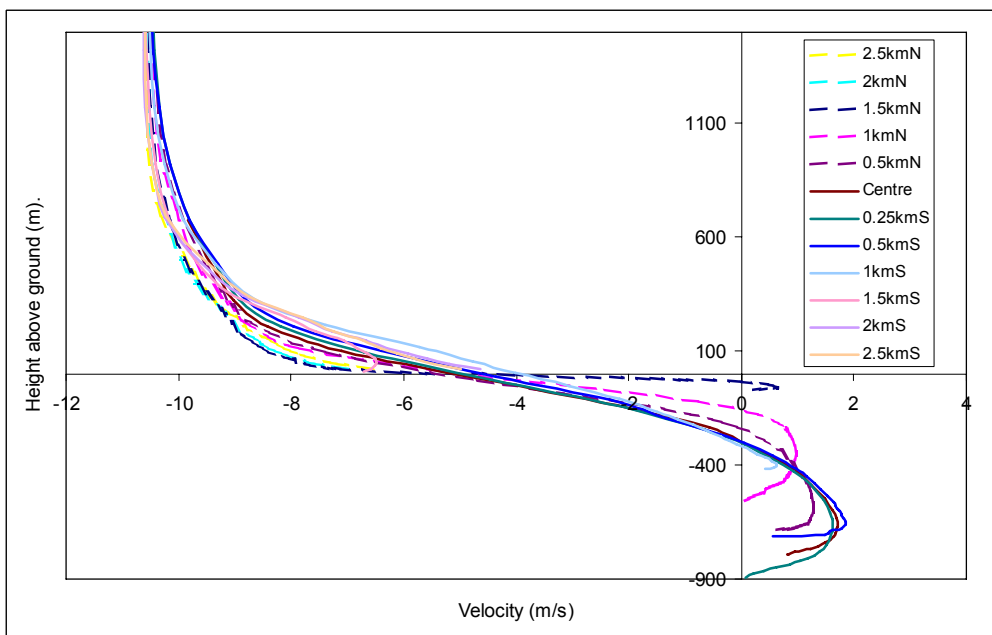


Figure 6.6: Longitudinal velocity profiles through the centre of the pit for the base case neutral boundary layer with $U_{10m} = 5$ m/s.

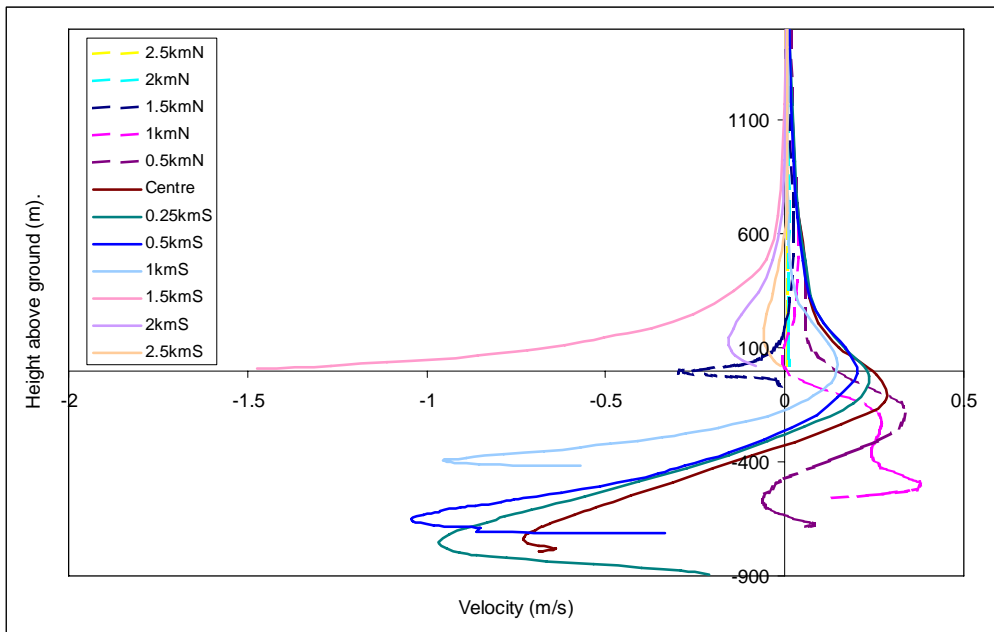


Figure 6.7: Lateral velocity profiles through the centre of the pit for the base case neutral boundary layer with $U_{10m} = 5$ m/s.

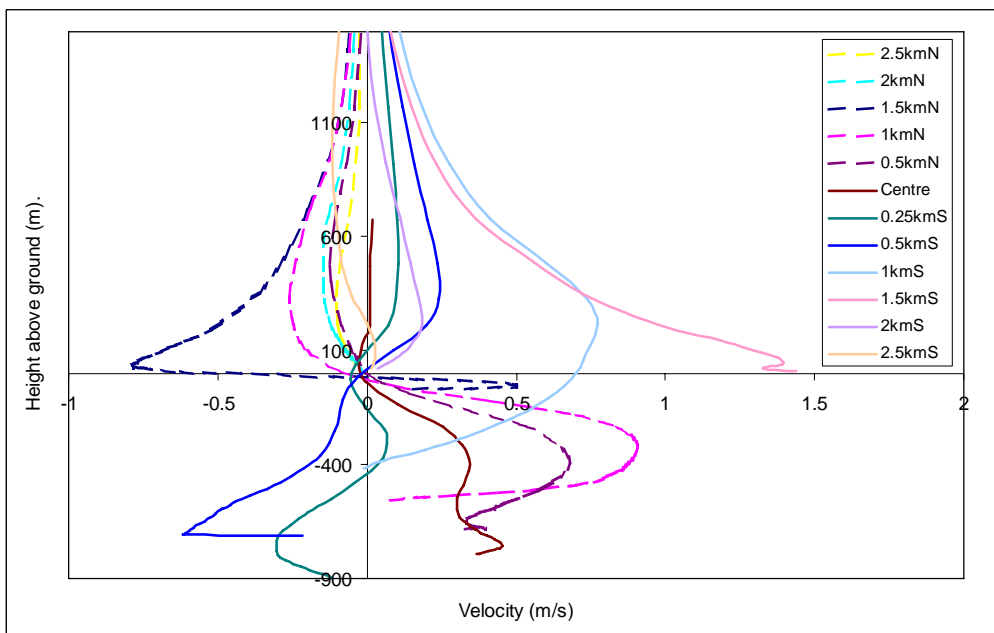


Figure 6.8: Vertical velocity profiles through the centre of the pit for the base case neutral boundary layer with $U_{10m} = 5$ m/s.

Iso-surfaces of Phase II fluid volume fraction (dust concentration) in the pit for the base case north wind with $U_{10m} = 5$ m/s are presented in Figure 6.9 to Figure 6.11. The iso-surface provides a three dimensional representation of the structure of the dust or particulate clouds as predicted by the CFD simulations.

In Figure 6.9, dust is seen to accumulate on the upwind walls of the pit, with concentrations on the more exposed downwind walls remaining lower. Ground level or pit surface Phase II volume fraction concentrations, presented in Figure 6.12, substantiate this observation, with very low concentrations evident, particularly on the eastern side of the downwind pit walls.

The regions of excavation are the primary contributors to regions of higher dust concentration. These are all positioned toward the base of the pit, with a larger number of sites used to distribute the dust sources more uniformly. These are evident in Figure 6.12 as seven red regions generally toward the pit base, although one is higher on the northeast corner of the pit.

Dust emitted from excavation regions toward the base of the pit is seen to travel in a northerly or 'upwind' direction across the base of the pit and up the northern walls (Figure 6.9 and Figure 6.12). It would appear the vortex structures on each side of the pit are independent and converge toward the centre of the pit. A ridge of dust is evident near the centre of the pit in Figure 6.9. As the flow containing the dust travels up the northeast and northwest walls it converges at the northern end of the pit, causing a welling up of the dust into the main atmospheric flow above. The dust then passes back over the pit at elevation, with ground level concentrations immediately downwind of the pit relatively low. An elevated plume of dust over the centre of the pit is evident in Figure 6.11.

The CFD simulations would suggest that the pit is an effective shape for the efficient flushing of the pit of pollutants generated within the pit due to in-pit activities under northerly winds.

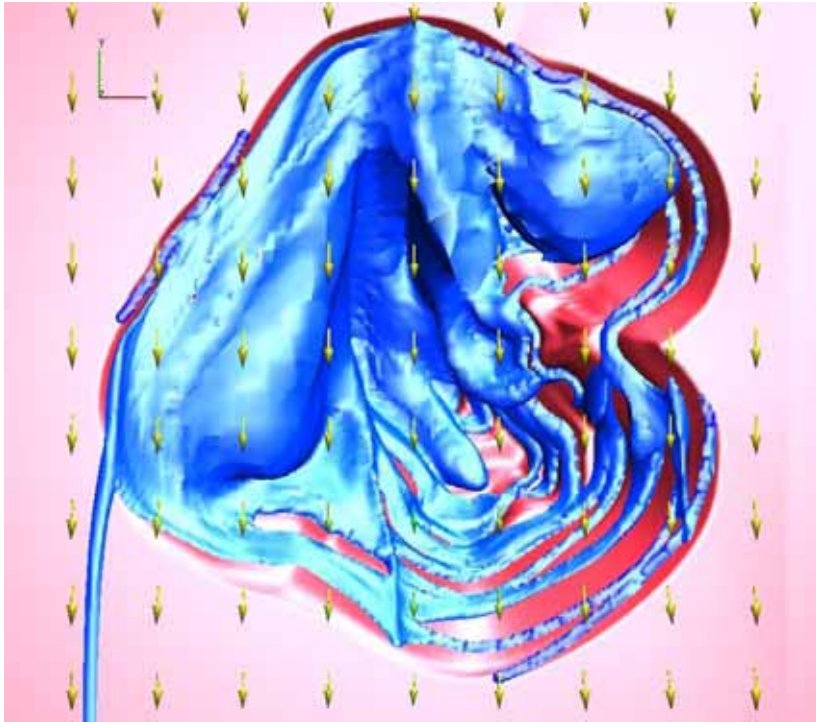


Figure 6.9: Iso-surface of Phase II volume fraction (dust concentration) ($1e-9$) within the pit for the base case neutral boundary layer with $U_{10m} = 5$ m/s, $10 \mu\text{m}$ particles.

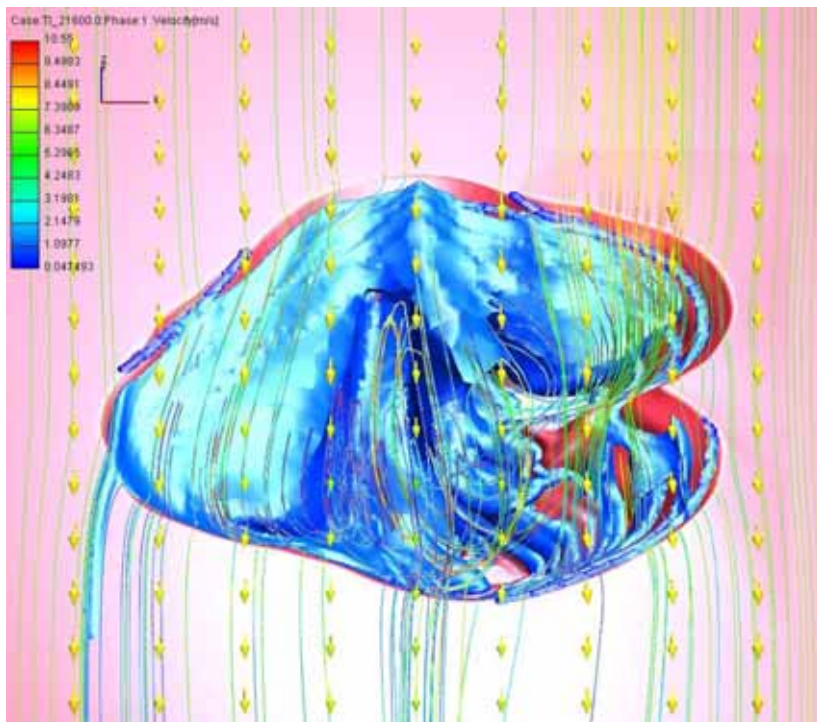


Figure 6.10: Iso-surface of Phase II volume fraction (dust concentration) ($1e-9$) within the pit and flow streamline for the base case neutral boundary layer with $U_{10m} = 5$ m/s, $10 \mu\text{m}$ particles.

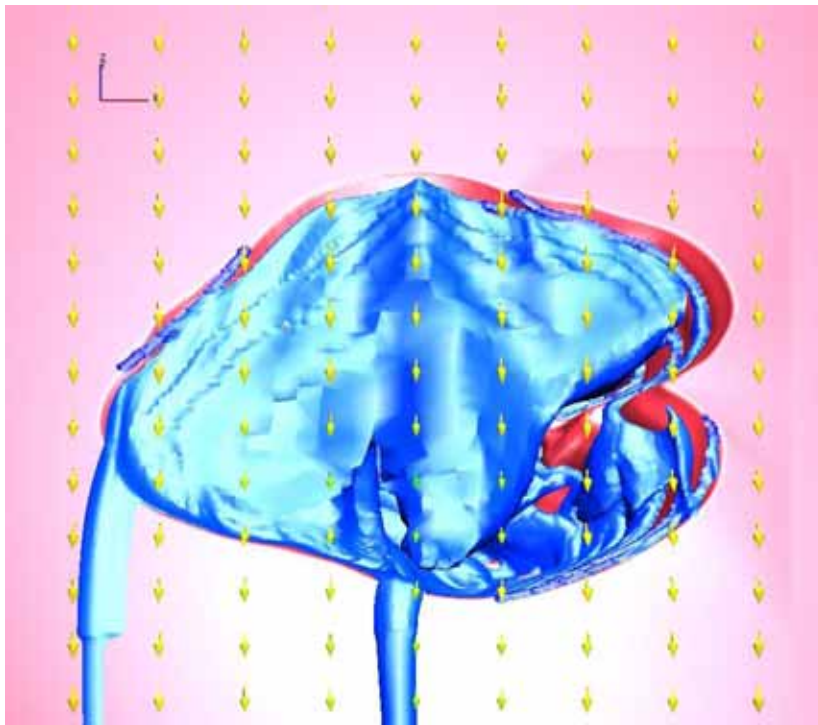


Figure 6.11: Iso-surface of Phase II volume fraction (dust concentration) ($7e-10$) within the pit for the base case neutral boundary layer with $U_{10m} = 5$ m/s, $10 \mu\text{m}$ particles.

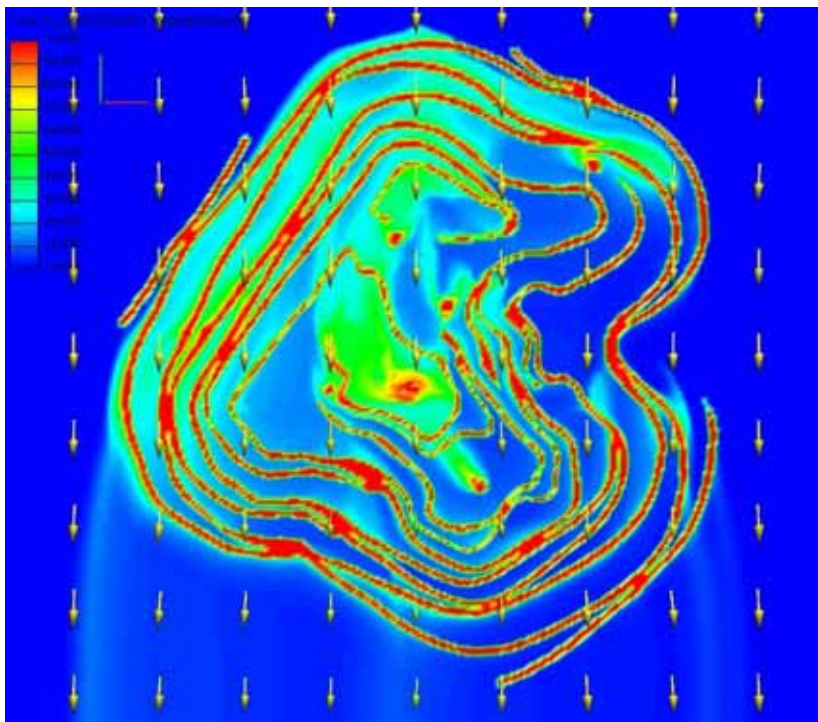


Figure 6.12: Pit surface and ground level Phase II volume fraction (dust concentrations) for the pit base case neutral boundary layer with $U_{10m} = 5$ m/s, $10 \mu\text{m}$ particles.

6.1.2 North Wind, Stable, $U_{10m} = 1.5$ m/s

Figure 6.13 and Figure 6.14 present streamlines through the pit for a simulated stable atmospheric boundary layer flow with $U_{10m} = 1.5$ m/s. They are equivalent to Figure 6.1 and Figure 6.2 for the neutral boundary layer base case with $U_{10m} = 5$ m/s. While there are some minor variations in the in-pit flow due to the alteration of the lower level atmospheric flow, the general features are essentially equivalent to those observed with the neutral boundary layer flow. Major spiral vortex structures, in the order of the size of the pit, form generally lateral to the mean flow direction, and thus are driven by the ambient wind flow across the pit.

Contours of the velocity in the surface cell within and around the pit are presented in Figure 6.15. As with the neutral boundary layer case, very high velocities are observed on the up and down wind rims of the pit, with magnitudes in the order of 1.5 to 2 times the background reference wind speed. Although the wind speed was configured as $U_{10m} = 1.5$ m/s at the domain inlet, there is a clear acceleration of the flow toward the pit for all boundary layer configurations, however this is most pronounced in the simulated stable conditions. Regions of highest velocity within the pit are observed to be on the downwind walls of the pit and across the ridge on the eastern side, as observed with the neutral boundary layer.

The magnitude of the velocity over the surface of the remainder of the pit is seen to be relatively low, generally less than half the velocity over the ground above the pit. Higher velocities are observed in some locations, most likely due to geophysical influences; however, the flow is close to stagnant in other regions, particularly the horizontal regions in the lower sections of the pit.

Velocity and turbulence profiles along the domain centreline for the stable boundary layer flow are presented in Figure 6.16 to Figure 6.21 for comparison with similar profiles for the neutral boundary layer presented in Figure 6.4 to Figure 6.8. Again, only minor variations are evident in the flow characteristics, with the broad features of magnitude and direction of the in-pit flow essentially equivalent for both the neutral and stable atmospheric boundary layer simulations.

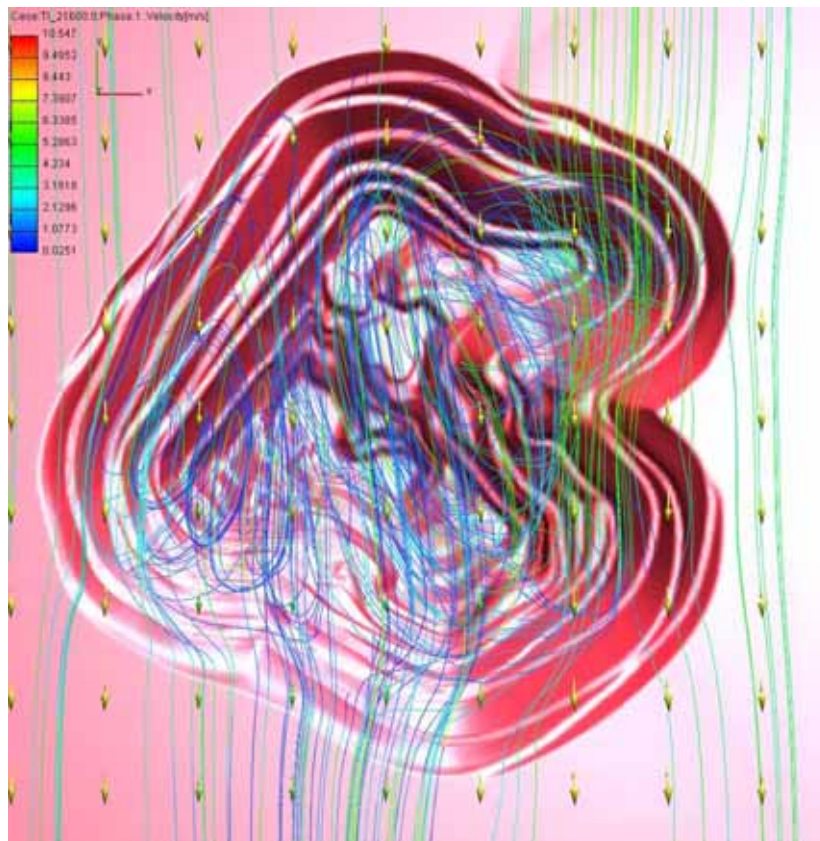


Figure 6.13: Streamlines of flow through the pit for stable atmospheric boundary layer flow with $U_{10m} = 1.5$ m/s.

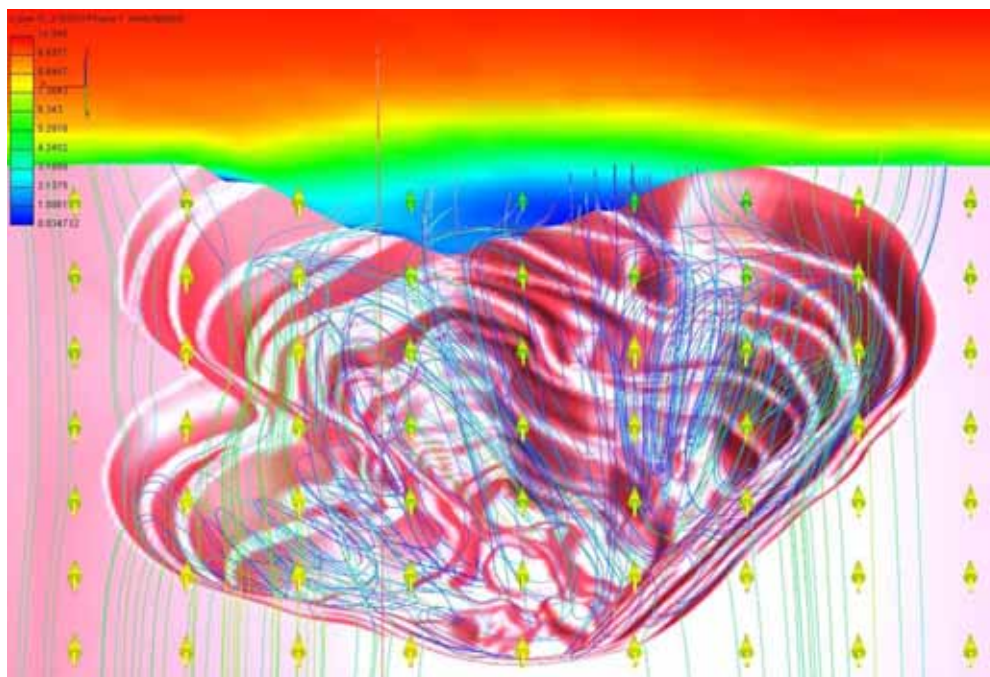


Figure 6.14: Streamlines of flow through the pit for stable atmospheric boundary layer flow, $U_{10m} = 1.5$ m/s, and velocity magnitude contours on a section near the downwind end of the pit ($Y = -1100$).

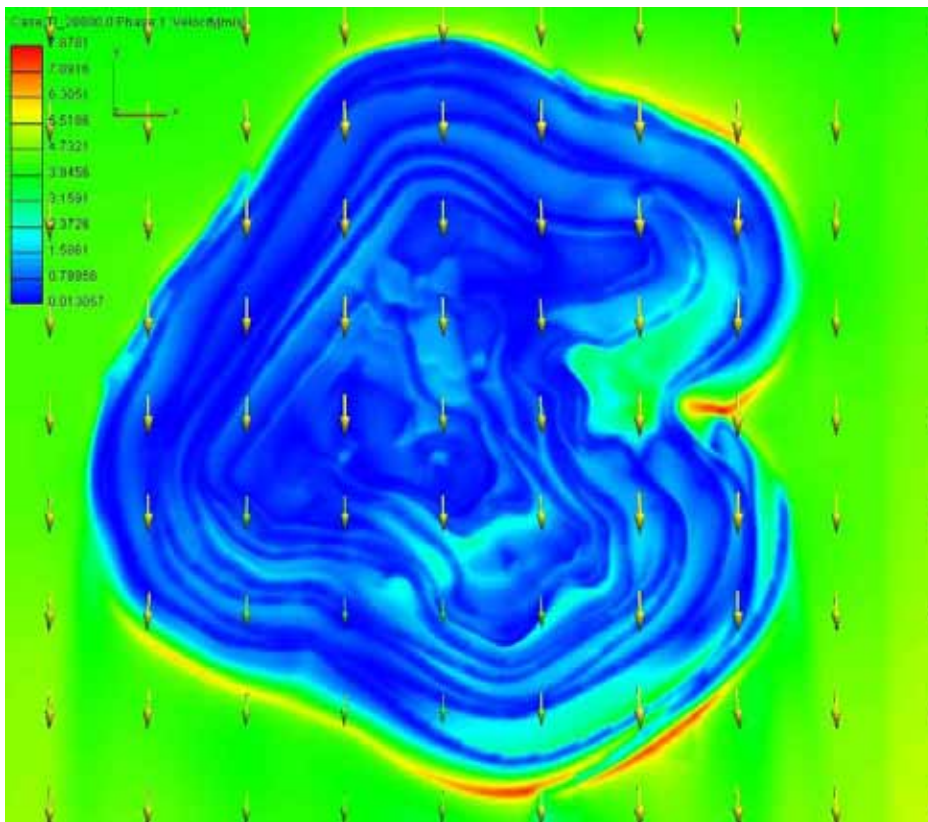


Figure 6.15: Velocity magnitude in the surface cell within and around the pit for stable atmospheric boundary layer flow, $U_{10m} = 1.5 \text{ m/s}$.

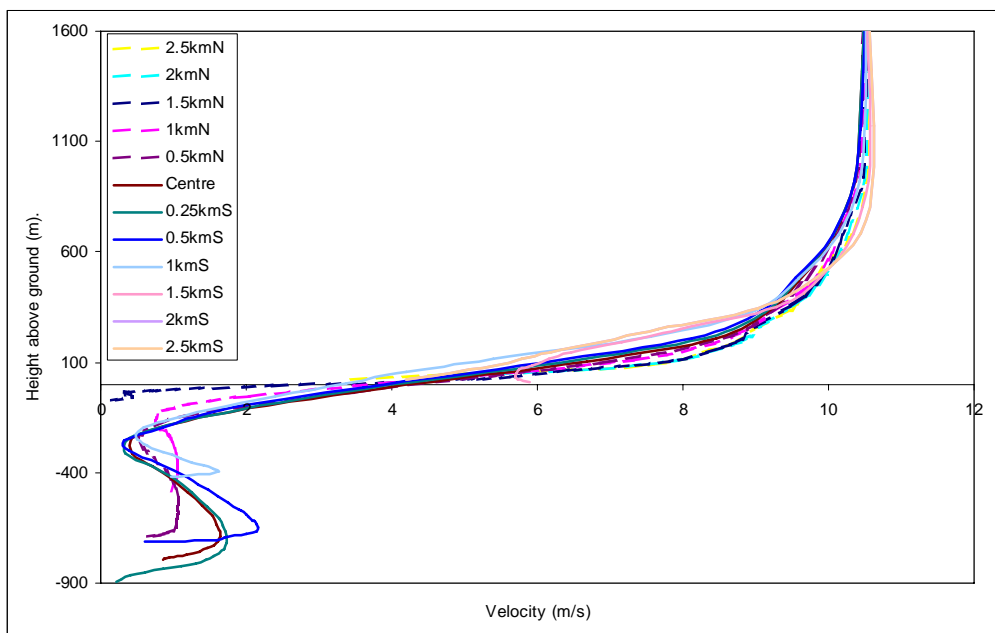


Figure 6.16: Velocity magnitude profiles through the centre of the pit for stable atmospheric boundary layer flow, $U_{10m} = 1.5 \text{ m/s}$.

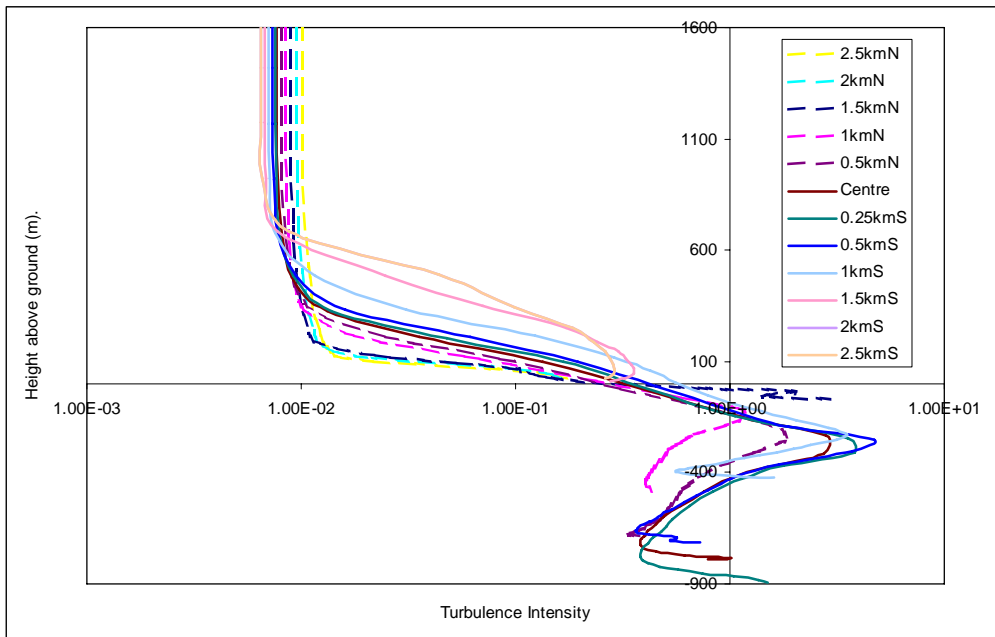


Figure 6.17: Turbulence intensity profiles through the centre of the pit for stable atmospheric boundary layer flow, $U_{10m} = 1.5$ m/s.

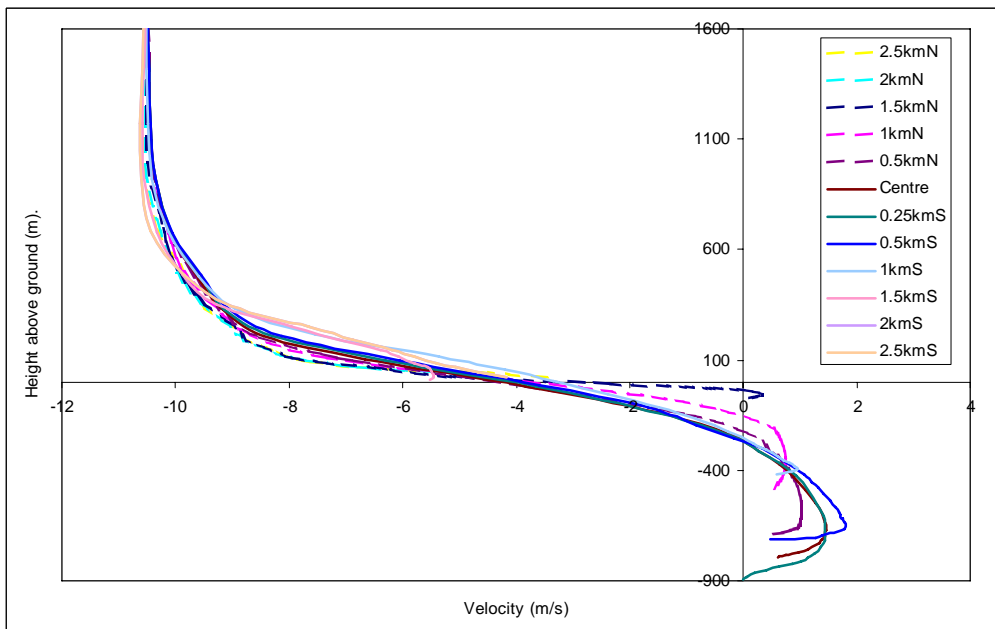


Figure 6.18: Longitudinal velocity profiles through the centre of the pit for stable atmospheric boundary layer flow, $U_{10m} = 1.5$ m/s.

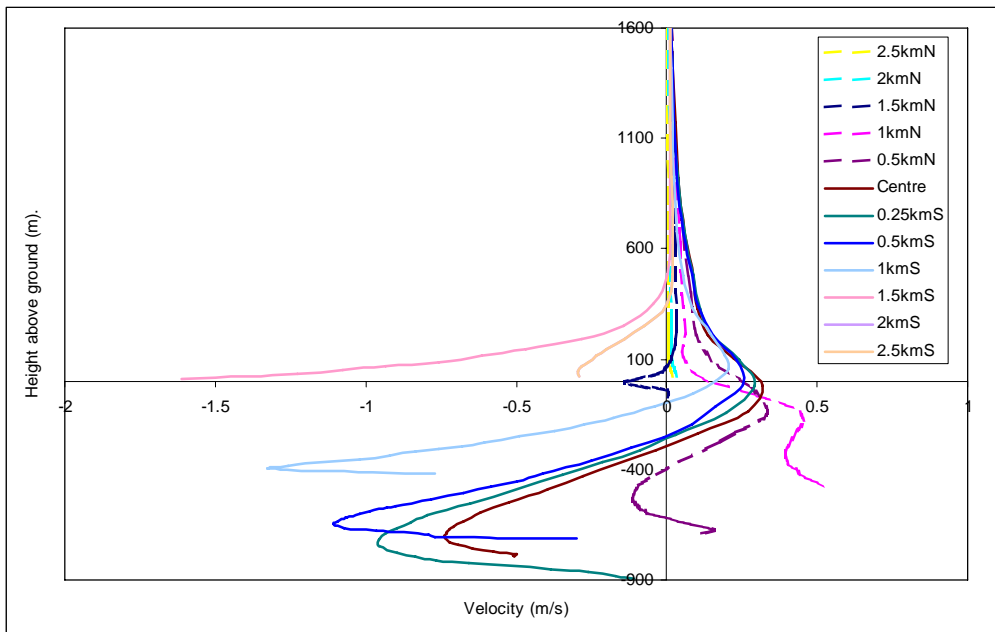


Figure 6.19: Lateral velocity profiles through the centre of the pit for stable atmospheric boundary layer flow, $U_{10m} = 1.5$ m/s.

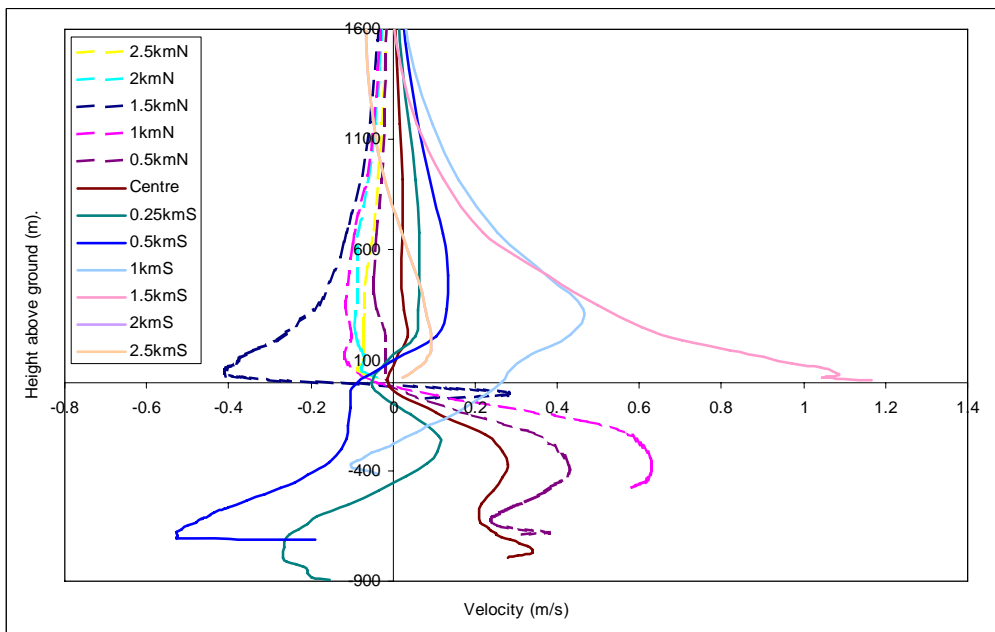


Figure 6.20: Vertical velocity profiles through the centre of the pit for stable atmospheric boundary layer flow, $U_{10m} = 1.5$ m/s.

Profiles of temperature along the centreline of the domain for the stable atmospheric boundary layer flow are presented in Figure 6.21. The profiles are

warmer on the downwind side of the pit, suggesting entrainment of warmer elevated air from above by the recirculating spirals. The air is then cooled as it travels through the lower sections of the pit in essentially an upwind direction. Again, the surface temperature within the pit, including the road and excavation sources, was configured to decrease with depth at a rate of 0.025 K/m to enhance the possibility of decoupled stratified flow regions forming within the lower regions of the pit. Again, there are a few locations where significantly lower temperatures are observed close to the pit surface, however these are believed to be more a reflection of the parameterisation of the pit wall and dust source boundary condition temperatures. The simulations do not suggest the formation of a stationary recirculation cell within the pit, however such a feature may occur under conditions of lower elevated wind speeds.

Contours of temperature on a section at the downwind end of the pit are presented in Figure 6.22. This is essentially an equivalent image to Figure 6.14, however presenting temperature as opposed to velocity on the contoured section across the domain. Both images show evidence of entrainment of the boundary layer flow into the pit, resulting in a reduction of the flow velocity above the pit level and an increase in temperature at the pit top and within the downwind half of the pit. The cooling effect of the pit surface is also evident close to the pit walls and on the upwind side of the pit where temperatures are observed to be lower. Even with the significantly low temperatures in the base of the pit, flushing of the lower level air was still evident.

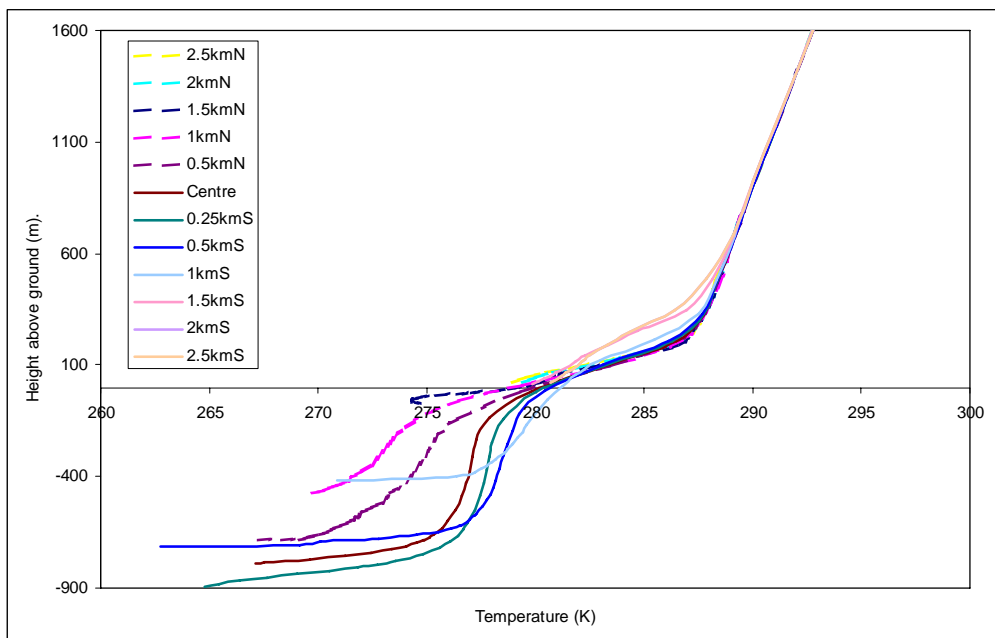


Figure 6.21: Temperature profiles through the centre of the pit for stable atmospheric boundary layer flow, $U_{10m} = 1.5$ m/s.

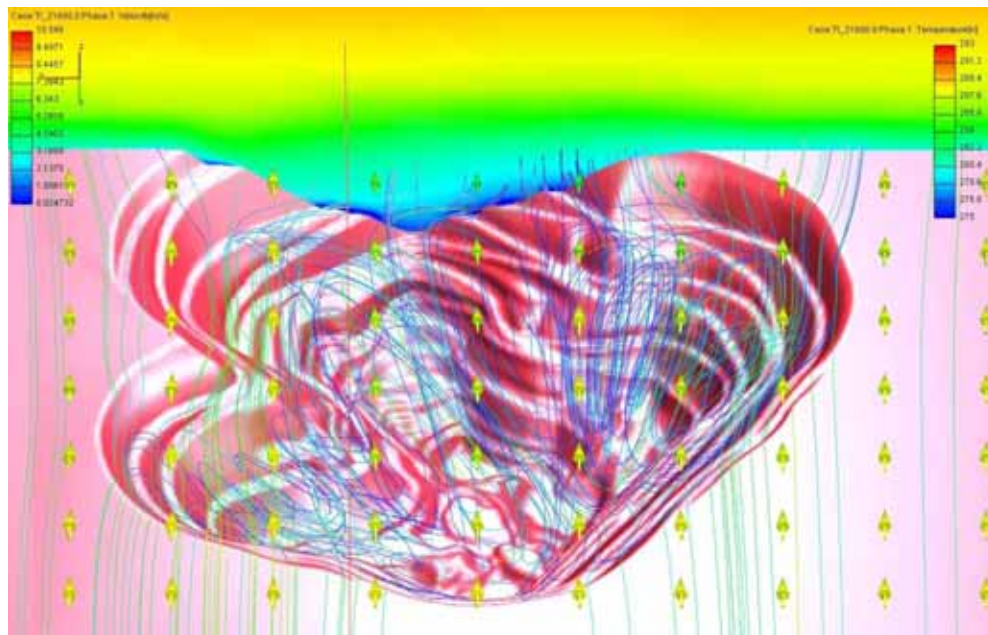


Figure 6.22: Streamlines of flow through the pit for stable atmospheric boundary layer flow, $U_{10m} = 1.5$ m/s, colour contours of flow temperature on a section near the downwind end of the pit ($Y = -1100$).

Iso-surfaces of Phase II fluid volume fraction (dust concentration) with the pit stable atmospheric boundary layer are presented in Figure 6.23 to Figure 6.25. Again high dust concentrations are seen in the lee of the upwind wall as the recirculating flow within the pit transports the dust up the pit face. As with the neutral boundary layer flow, concentrations on the more exposed downwind walls remain lower. Ground level or pit surface Phase II volume fraction concentrations, presented in Figure 6.26, support this observation, with (as observed for the neutral boundary layer flow) very low concentrations evident particularly on the eastern side of the downwind pit wall.

Essentially the behaviour of the flow and dust within the pit is seen to be equivalent under the stable and neutral flow configurations. Only subtle differences exist as a result of the thermal stratification and lower ambient turbulence. One such difference is in relation to the exit of the dust from the pit. As discussed above for the neutral flow scenario, the spirals within the pit appear to converge in the upwind centre of the pit causing an up-welling of the dust into the main ambient flow across the pit (Figure 6.11). The initial up-welling is observed in the stable flow configuration as well, however, in the stable scenario the up-welling is observed to subside as it crosses the pit, forming a more horizontal dust cloud as it exits the pit region (Figure 6.25). It is most likely that the subsidence of the dust is due to the thermal stratification of the flow, with the cooler flow from within the pit rising into warmer air above, buoyancy forces are causing the cooler air to then subside. The dust plume is then slightly lower as it exits the pit, creating a large footprint on the surface and slightly increased surface concentrations.

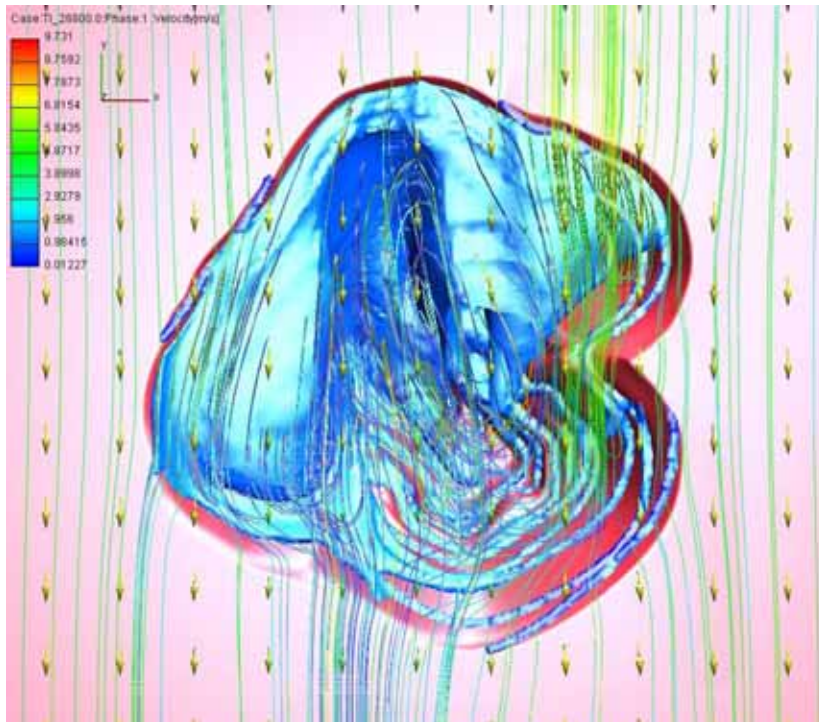


Figure 6.23: Iso-surface of Phase II volume fraction (dust concentration) ($1.5e-9$) and streamlines in the pit for stable atmospheric boundary layer flow, $U_{10m} = 1.5$ m/s, $10 \mu\text{m}$ particles.

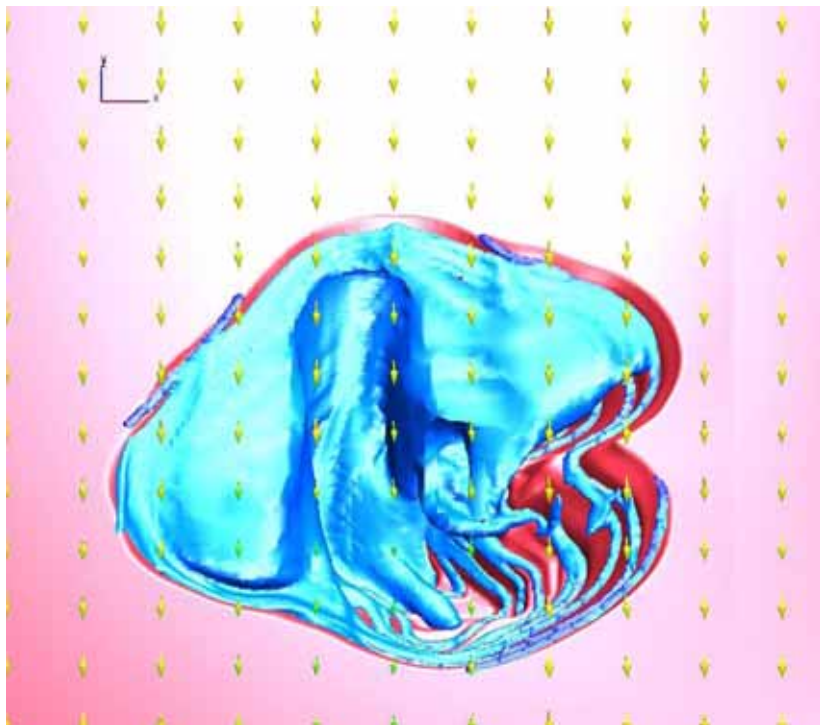


Figure 6.24: Iso-surface of Phase II volume fraction (dust concentration) ($1e-9$) in the pit for stable atmospheric boundary layer flow, $U_{10m} = 1.5$ m/s, $10 \mu\text{m}$ particles.

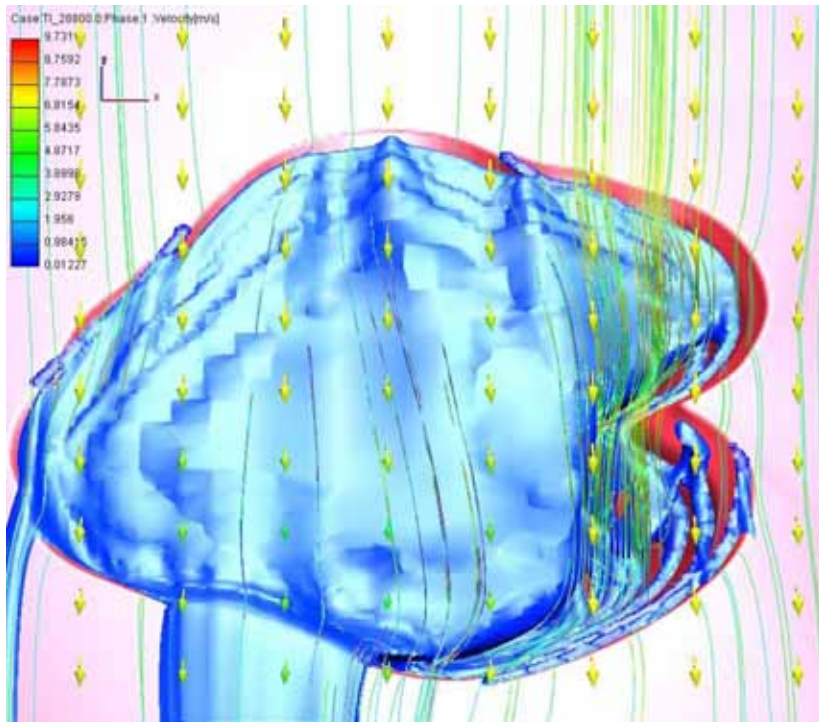


Figure 6.25: Iso-surface of Phase II volume fraction (dust concentration) ($7e-10$) and streamlines in the pit for stable atmospheric boundary layer flow, $U_{10m} = 1.5$ m/s, $10 \mu\text{m}$ particles.

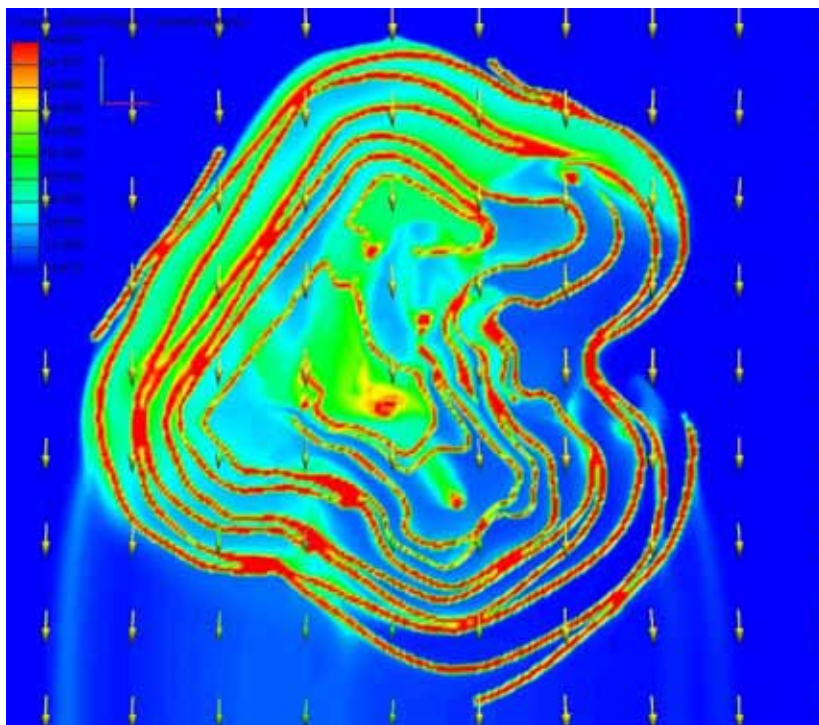


Figure 6.26: Pit surface and ground level Phase II volume fraction (dust concentration) pit for stable atmospheric boundary layer flow, $U_{10m} = 1.5$ m/s, $10 \mu\text{m}$ particles.

6.1.3 North Wind, Unstable, $U_{10m} = 3$ m/s

Figure 6.27 and Figure 6.28 present streamlines through the pit for simulated unstable atmospheric boundary layer flow with $U_{10m} = 3$ m/s. They are equivalent to Figure 6.1 and Figure 6.2 for the neutral boundary layer base case and Figure 6.13 and Figure 6.14 of the stable boundary layer scenario. In addition to the difference in the thermal characteristics of the boundary layers, the unstable boundary layer has lower wind speeds through the depth of the boundary layer apart from the very lower regions of the stable boundary layer. Thus the more elevated driving winds are of lower wind speed in the unstable boundary layer.

Again, while there are some minor variations of the in-pit flow with the alteration of the atmospheric boundary layer characteristics, the general features are essentially equivalent to the neutral and stable boundary layer simulations. A large recirculation forms through the depth of the pit, driven by the atmospheric flow above.

Contours of the velocity in the surface cell within and around the pit are presented in Figure 6.29. As with the neutral and stable boundary layer cases, very high velocities are observed on the up- and downwind rims of the pit. Regions of highest velocity within the pit are observed to be on the downwind walls of the pit and across the ridge on the eastern side, as observed for the neutral and stable boundary layers.

Velocity and turbulence profiles along the domain centreline for the unstable boundary layer flow are presented in Figure 6.30 to Figure 6.31 for comparison with similar profiles for the neutral boundary layer presented in Figure 6.4 to Figure 6.8 and the profiles of the stable boundary layer presented in Figure 6.16 to Figure 6.20. Again, only minor variations are evident in the flow characteristics, with the broad features of relative magnitude and direction of the in-pit flow essentially equivalent for the neutral, stable and unstable atmospheric boundary layer configurations. The most significant variations in flow behaviour relate to the lateral (cross pit) flow component, with the unstable configurations demonstrating different behaviour in the 0.5 to 1 'kmS' region in particular.

The flow structure within the pit is clearly primarily responsive to the mechanical influence of the pit structure, with the thermal profile of the upwind boundary layer flow or the pit surface having very little influence on the developed flow characteristics for the simulations performed.



Figure 6.27: Streamlines of flow through the pit for unstable atmospheric boundary layer flow, $U_{10m} = 3 \text{ m/s}$.

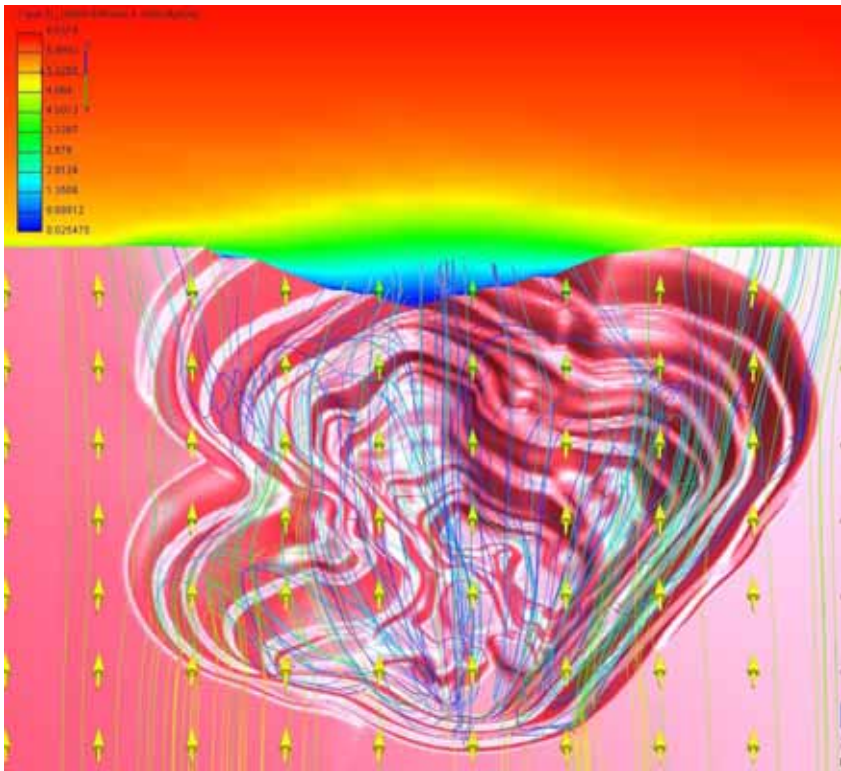


Figure 6.28: Streamlines of flow through the pit for unstable atmospheric boundary layer flow, $U_{10m} = 3 \text{ m/s}$ and velocity magnitude contours on a section near the downwind end of the pit ($Y = -1100$).

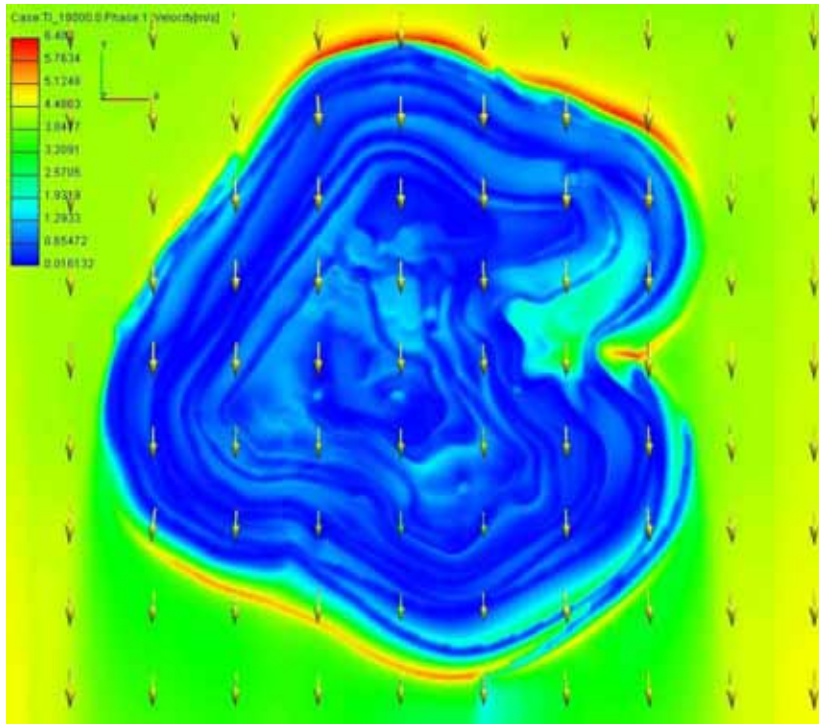


Figure 6.29: Velocity magnitude in the surface cell within and around the pit for unstable atmospheric boundary layer flow, $U_{10m} = 3$ m/s.

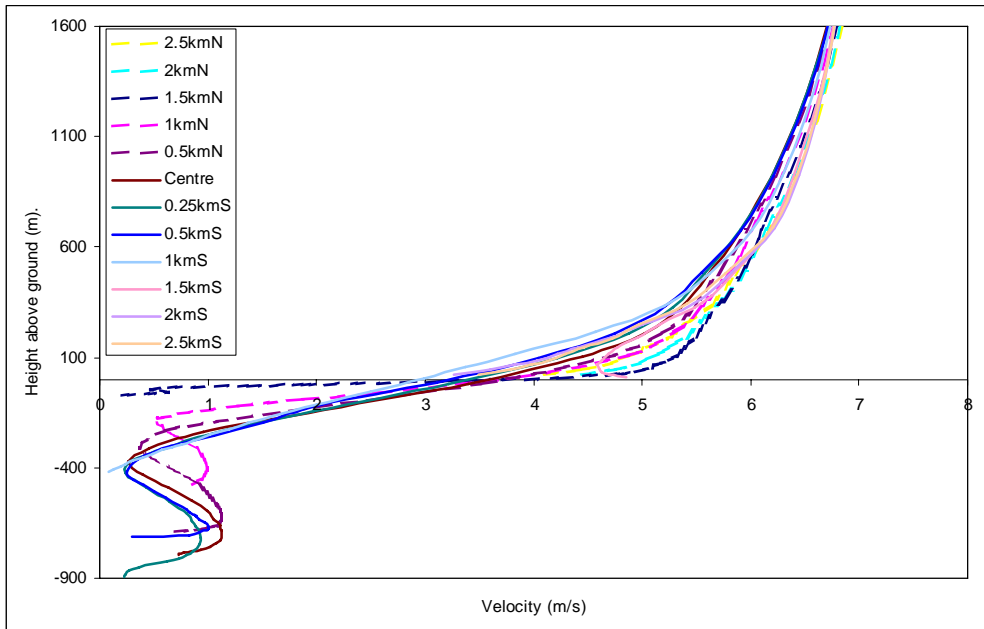


Figure 6.30: Velocity magnitude profiles through the centre of the pit for unstable atmospheric boundary layer flow, $U_{10m} = 3$ m/s.

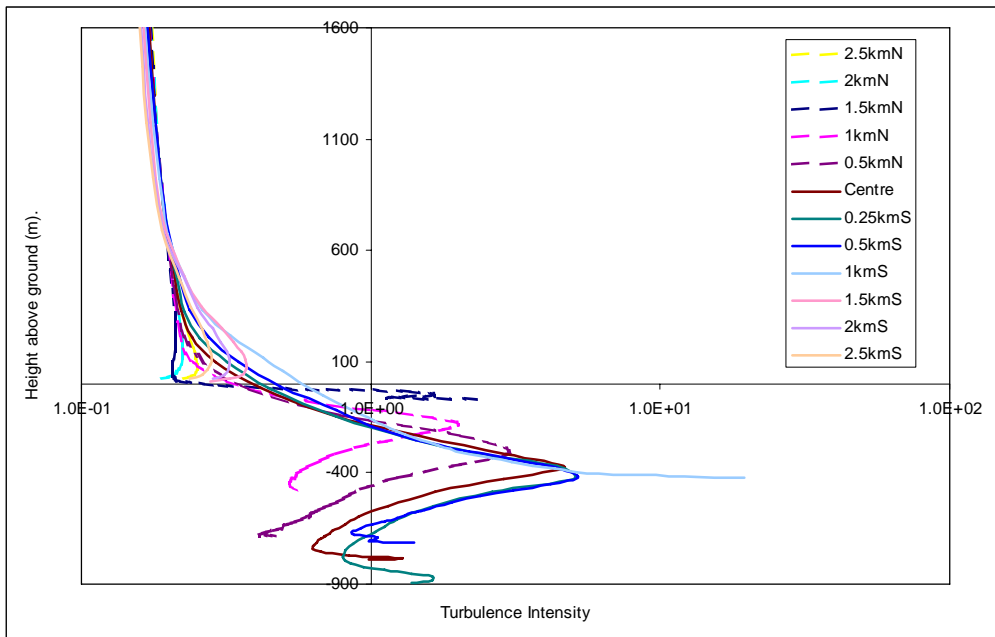


Figure 6.31: Turbulence intensity profiles through the centre of the pit for unstable atmospheric boundary layer flow, $U_{10m} = 3 \text{ m/s}$.

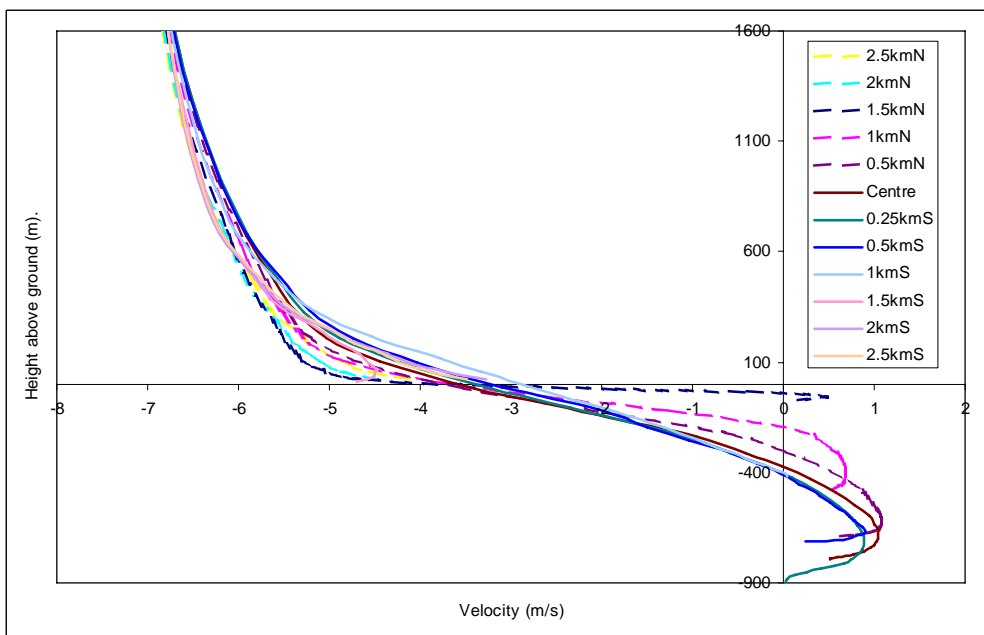


Figure 6.32: Longitudinal velocity profiles through the centre of the pit for unstable atmospheric boundary layer flow, $U_{10m} = 3 \text{ m/s}$.

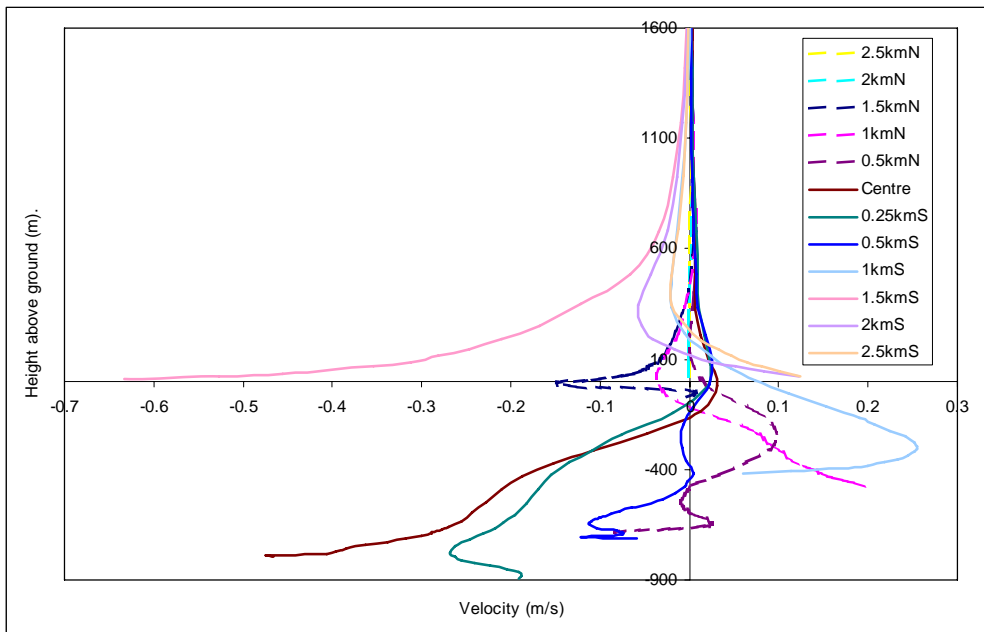


Figure 6.33: Lateral velocity profiles through the centre of the pit for unstable atmospheric boundary layer flow, $U_{10m} = 3$ m/s.

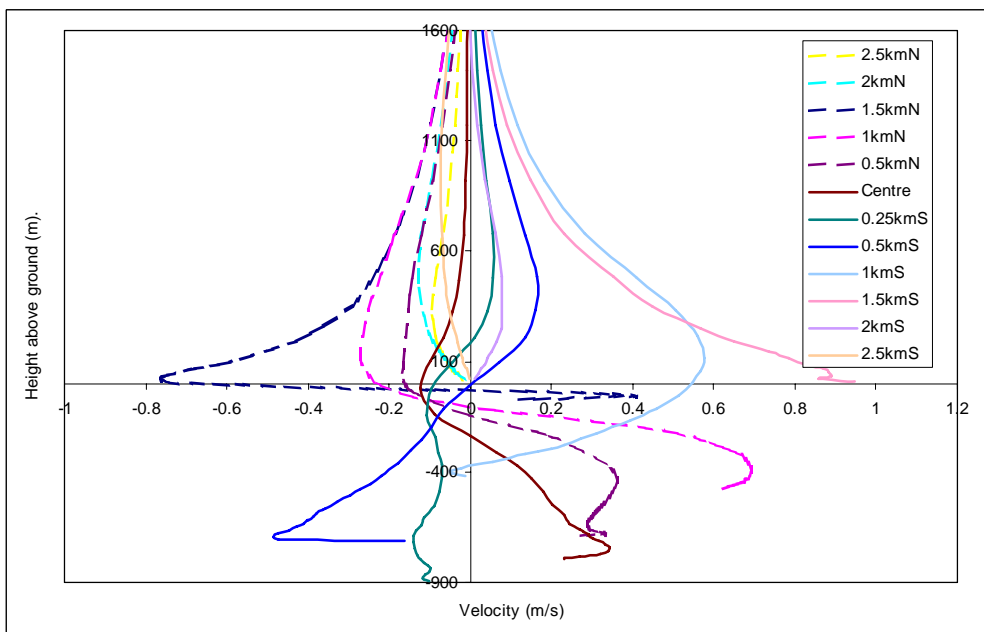


Figure 6.34: Vertical velocity profiles through the centre of the pit for unstable atmospheric boundary layer flow, $U_{10m} = 3$ m/s.

Profiles of temperature along the centreline of the pit domain for the unstable atmospheric boundary layer flow are presented in Figure 6.35. The profiles suggest a general dropping, or lowering, of the external upwind temperature profile into the pit. Generally the temperatures within the pit are observed to be higher than the temperatures leading up to the pit, particularly on the upwind side of the pit, due to

warming of the flow as it recirculates through the pit. Elevated temperatures close to the surface are also very evident, particularly in the low and upwind sections of the pit.

Contours of temperature on a section at the downwind end of the pit are presented in Figure 6.36. This is essentially an equivalent image as Figure 6.28, however presenting temperature as opposed to velocity on the contoured section across the domain. Again, a reduction in velocity and increase in temperature over the pit is evident as the atmospheric boundary layer flow entrains lower velocity, higher temperature recirculating air from within the pit. Figure 6.37 presents a similar image through the centre of the pit. Elevated temperatures in the lower sections of the pit are evident.

Areas of higher surface temperature in the base of the pit can also be seen in Figure 6.38 presenting contours of the surface temperature within and around the pit. While generally the pit surface temperature is no hotter than the surface temperature of the ground surrounding the pit, and actually cooler on the downwind pit walls, significantly elevated temperatures are evident in small regions of the lower section of the pit. The higher temperatures are observed on the horizontal in-pit surfaces, the regions of higher in-pit surface heat flux. Maximum predicted surface temperatures within the pit are in the order of 30 K above the ground level surface temperature, with significant areas in the base of the pit with surface temperatures between 10 and 20 K above the ground level surface temperature. It should also be noted the simulations do not account for adiabatic warming of the air with increased depth, further increasing temperature by 1 K per 100m depth. Thus, the modelling would suggest that temperatures in the order of 20 to 30°C, and potentially 40°C over very small areas, above ambient ground level temperatures could be experienced at the base of the pit. Thus on hotter days, input temperatures of 70°C or more may be experienced in base regions of the pit.

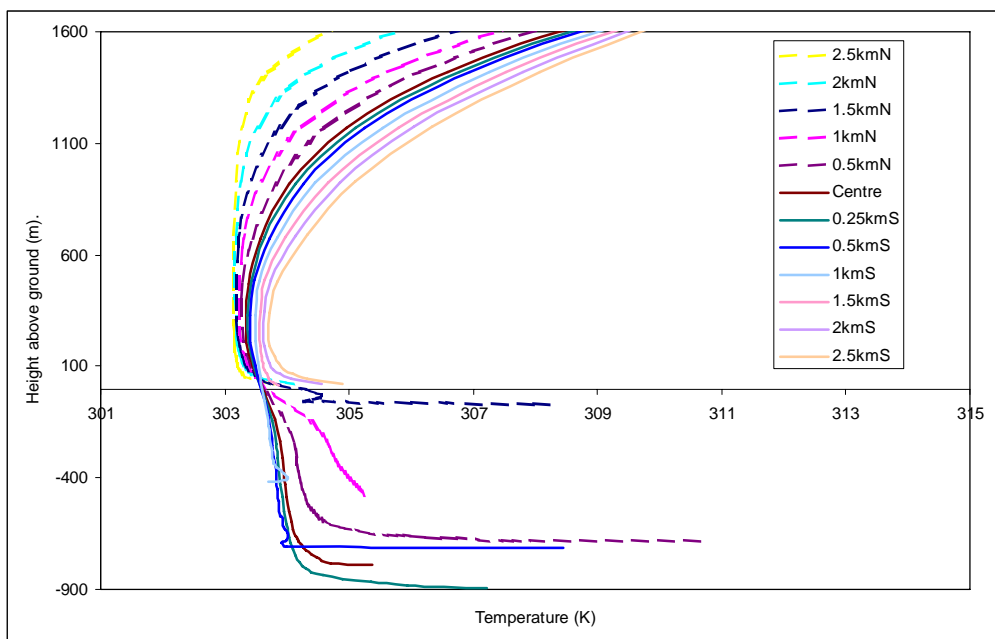


Figure 6.35: Temperature profiles through the centre of the pit for unstable atmospheric boundary layer flow, $U_{10m} = 3$ m/s.

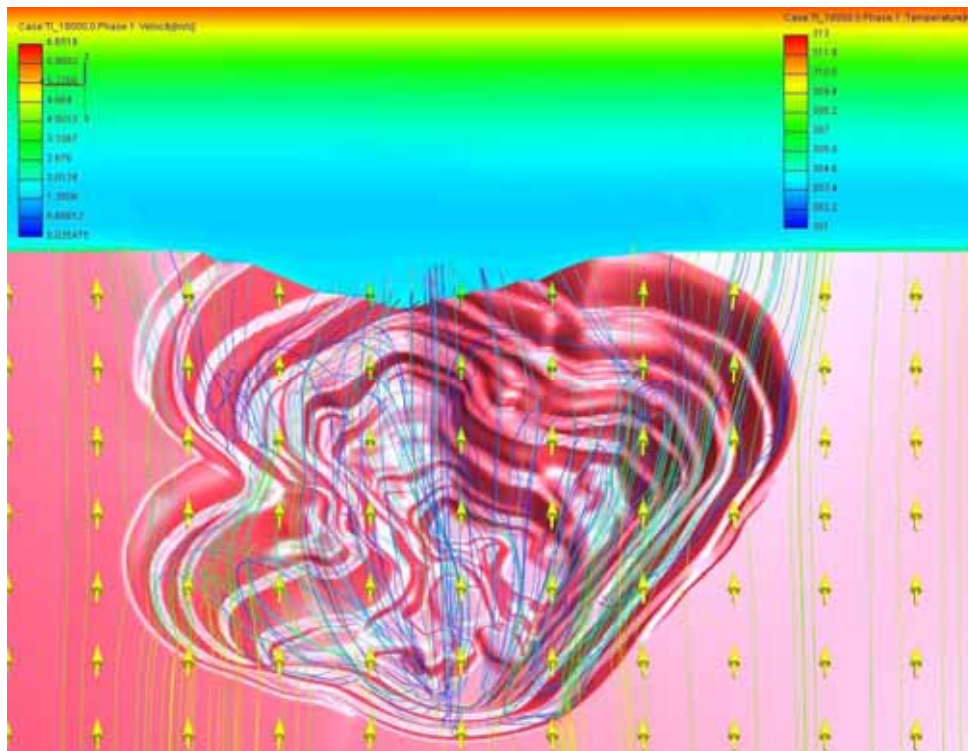


Figure 6.36: Streamlines of flow through the pit for unstable atmospheric boundary layer flow, $U_{10m} = 3$ m/s, colour contours of temperature on a section near the downwind end of the pit ($Y = -1100$).

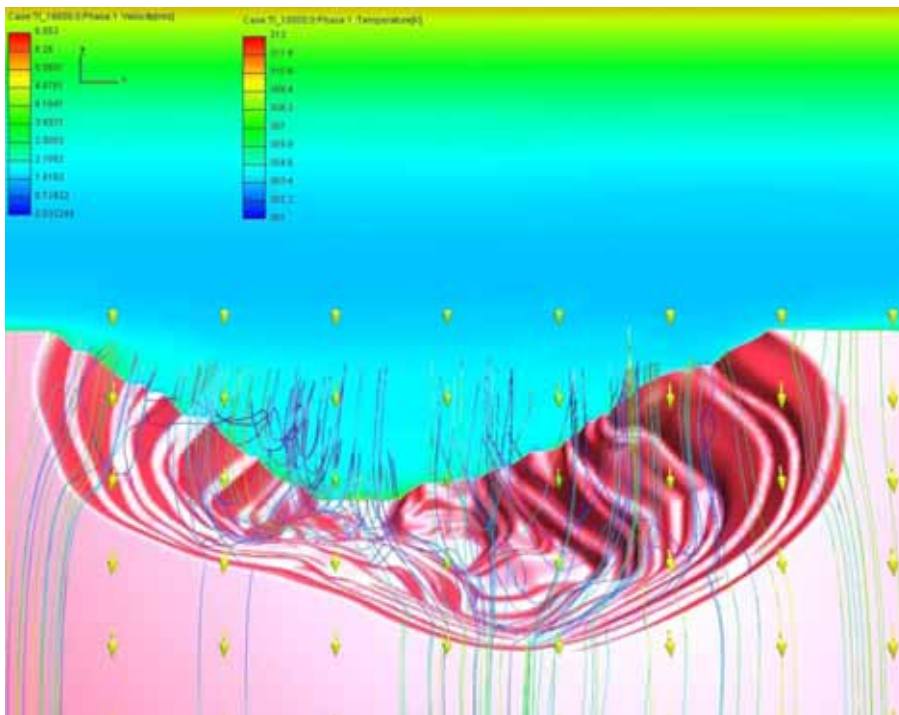


Figure 6.37: Streamlines of flow through the pit for unstable atmospheric boundary layer flow, $U_{10m} = 3$ m/s, colour contours of temperature on a section near the downwind end of the pit ($Y=0$).

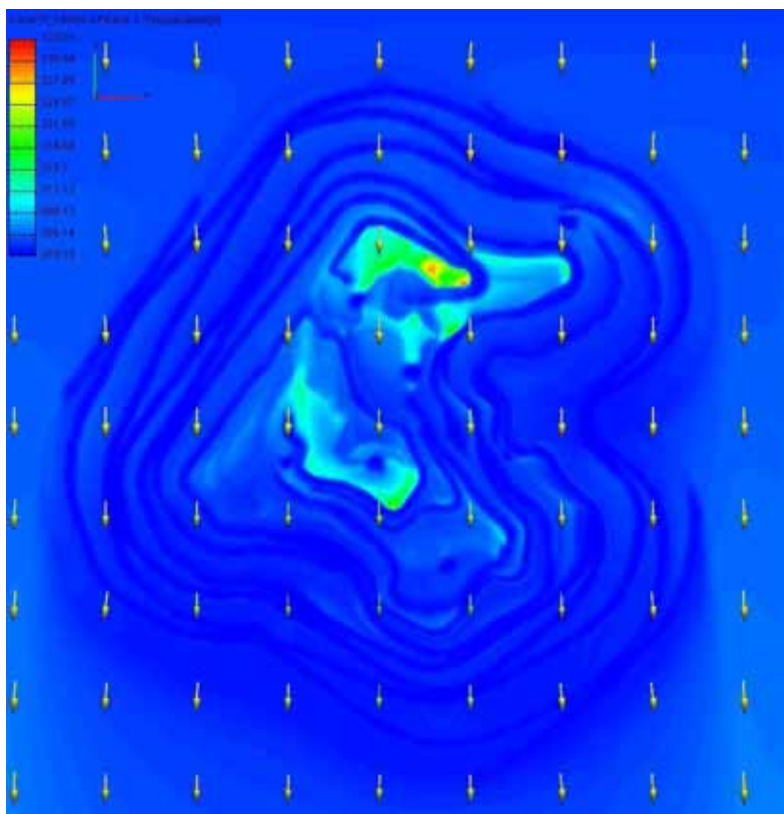


Figure 6.38: Ground surface temperature contours for the unstable atmospheric boundary layer flow, north winds, $U_{10m} = 3$ m/s.

Iso-surfaces of Phase II fluid volume fraction (dust concentration) with a simulated unstable atmospheric boundary layer (north wind, $U_{10m} = 3$ m/s) are presented in Figure 6.39 to Figure 6.41. Again, higher dust concentrations are seen in the lee of the upwind wall as the recirculating flow within the pit transports the dust up the upwind pit face. As with the neutral and stable boundary layer flow, concentrations on the more exposed downwind walls remain lower. Ground level or pit surface Phase II volume fraction concentrations, presented in Figure 6.41, substantiate this observation, with very low concentrations evident, particularly on the eastern side of the downwind pit wall.

Essentially, the behaviour of the flow and dust within the pit is seen to be equivalent under the three boundary layer stability flow configurations simulated. Subtle differences do exist as a result of the thermal stratification and differences in ambient turbulence levels, with, for instance the dust clouds dispersing more quickly in the higher ambient turbulence unstable flow. However, the main characteristic re-circulations are evident across the full stability range of the simulations.

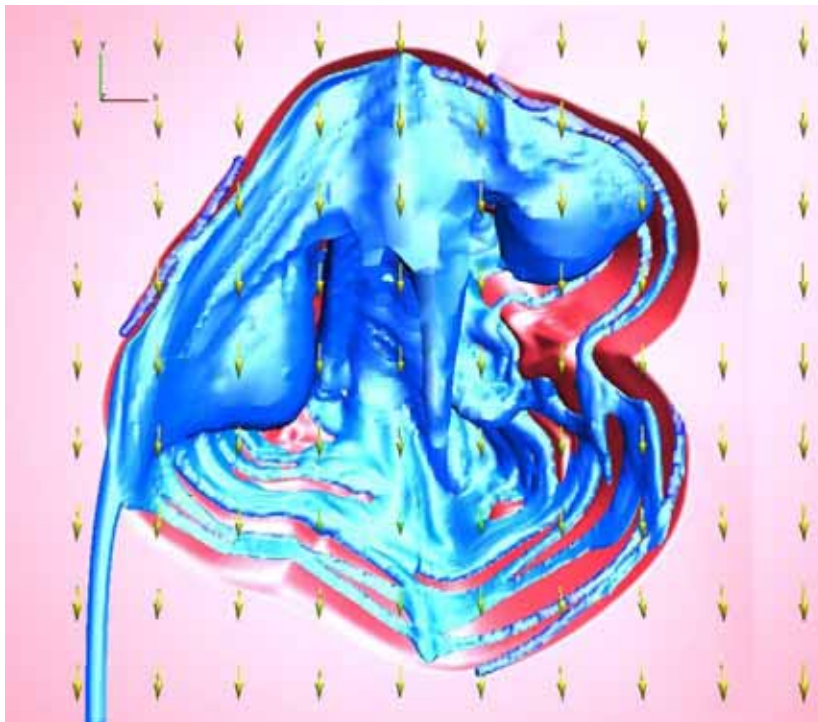


Figure 6.39: Iso-surface of Phase II volume fraction (dust concentration) ($1.5e-9$) in the pit for unstable atmospheric boundary layer flow, $U_{10m} = 3$ m/s, $10 \mu\text{m}$ particles.

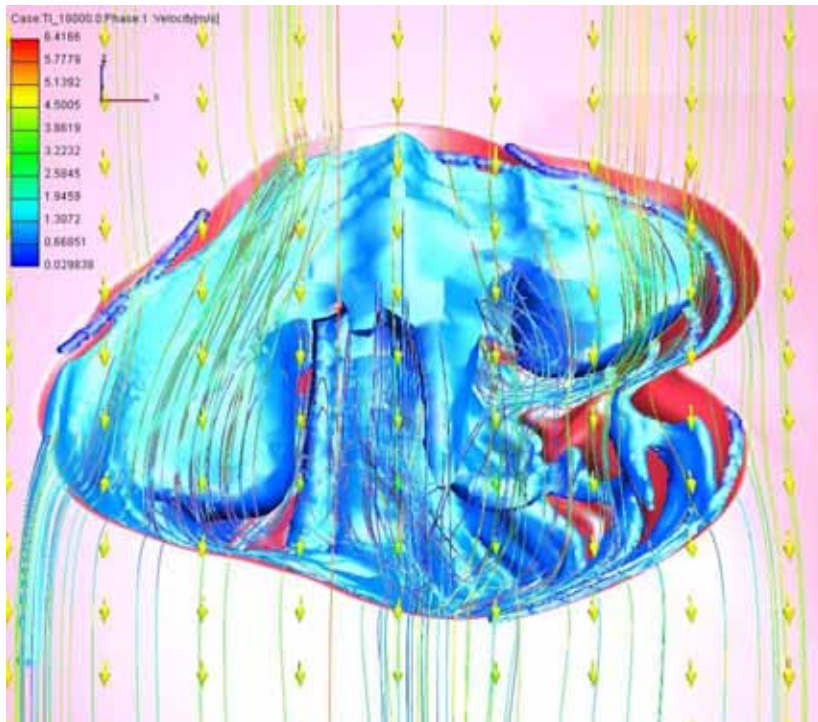


Figure 6.40: Iso-surface of Phase II volume fraction (dust concentration) ($1.5e-9$) in the pit for unstable atmospheric boundary layer flow, $U_{10m} = 3$ m/s, $10 \mu\text{m}$ particles.



Figure 6.41: Iso-surface of Phase II volume fraction (dust concentration) ($2e-9$) and streamlines in the pit for unstable atmospheric boundary layer flow, $U_{10m} = 3$ m/s, $10 \mu\text{m}$ particles.

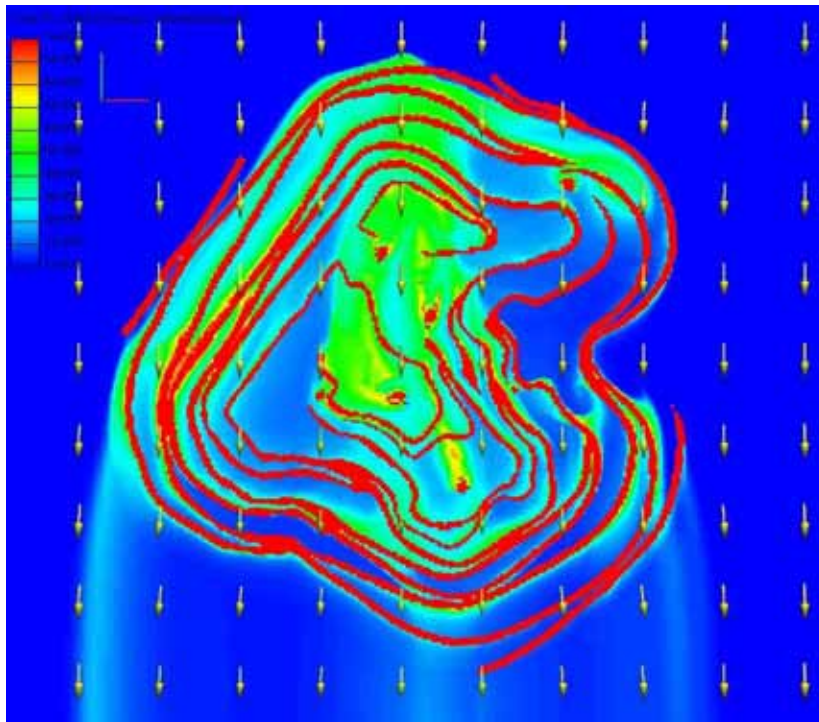


Figure 6.42: Pit surface and ground level Phase II volume fraction (dust concentration) for unstable atmospheric boundary layer flow, $U_{10m} = 3$ m/s, $10 \mu\text{m}$ particles.

6.1.4 East Wind, $U_{10m} = 5$ m/s

Streamlines for easterly winds ($U_{10m} = 5$ m/s) are presented in Figure 6.43. A major recirculation throughout the entire pit is evident, with the atmospheric flow striking the rear northwest wall, passing diagonally across in a southeast direction, and back upwind across the base of the pit. The flow then ascends in the two lobes on the eastern side of the pit, prior to passing across the top of the pit and converging toward the western corner as it leaves the pit. Two smaller vertically-orientated vortex structures are also evident in more stagnant regions.

Iso-surfaces of Phase II fluid volume fractions for the simulated easterly wind configuration are presented in Figure 6.44 and Figure 6.45. Contours of the pit surface and ground level concentrations are presented in Figure 6.46. The Phase II fluid or dust is again seen to accumulate in the recirculation regions in the lee of the upwind walls of both pit sections, with concentrations on the more exposed downwind walls remaining lower. As with the north wind scenarios, the dust then passes back over the pit, clear of the surface, and exits the pit on the western corner. It would appear that the dust in the northern end of the pit is spiralled in a southerly direction prior to joining the main cloud that exits the pit.

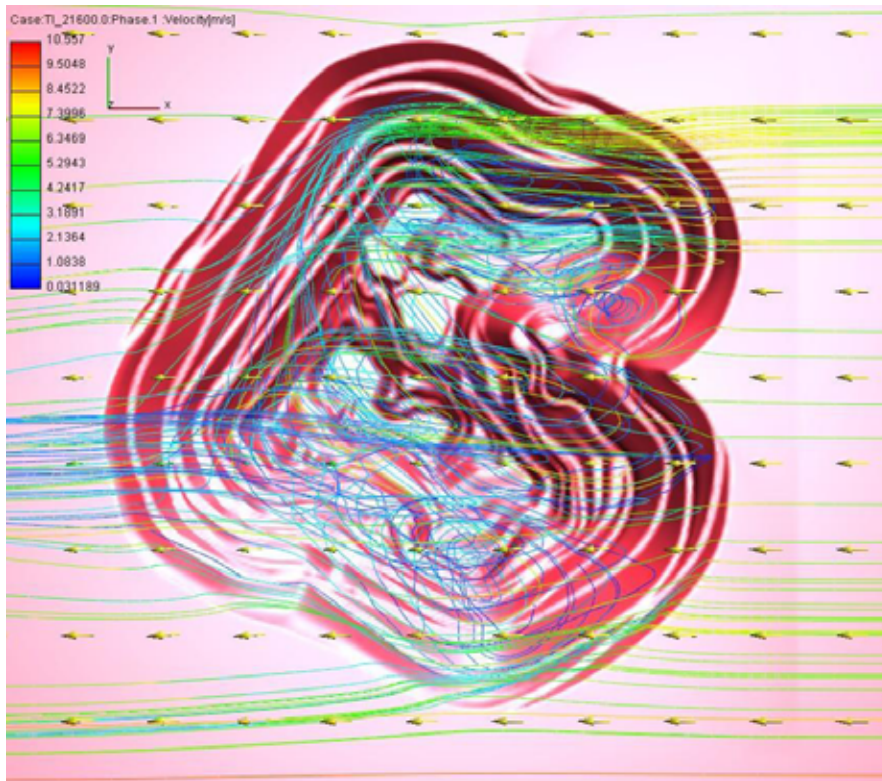


Figure 6.43: Streamlines of flow through the pit for easterly winds, neutral boundary layer, $U_{10m} = 5$ m/s.

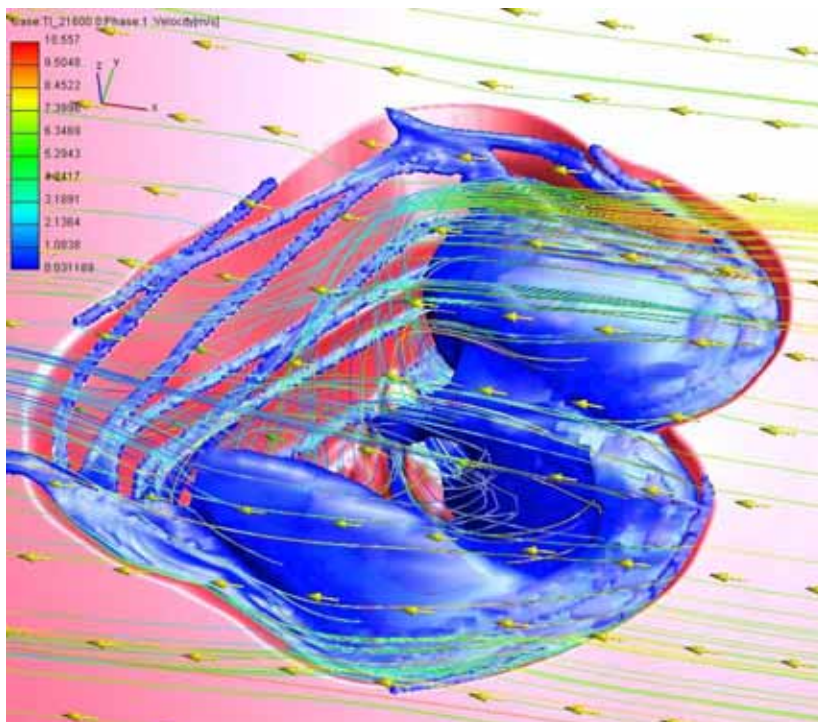


Figure 6.44: Iso-surface of Phase II volume fraction (dust concentration) ($7.5e-10$) and streamlines in the pit for easterly winds, neutral boundary layer, $U_{10m} = 5$ m/s, $10 \mu\text{m}$ particles.

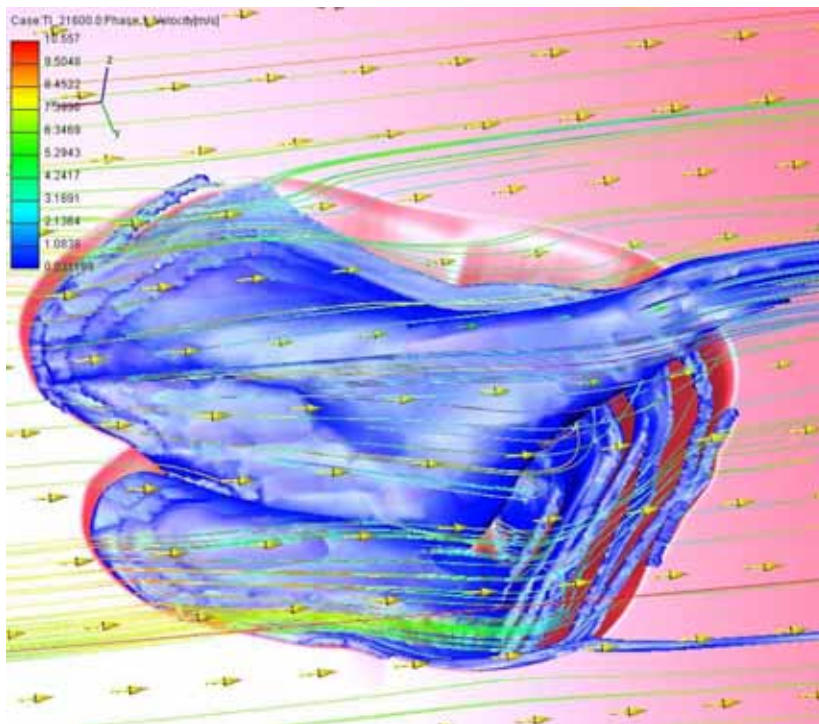


Figure 6.45: Iso-surface of Phase II volume fraction (dust concentration) ($5e-10$) and streamlines in the pit for easterly winds, neutral boundary layer, $U_{10m} = 5$ m/s, $10 \mu\text{m}$ particles.

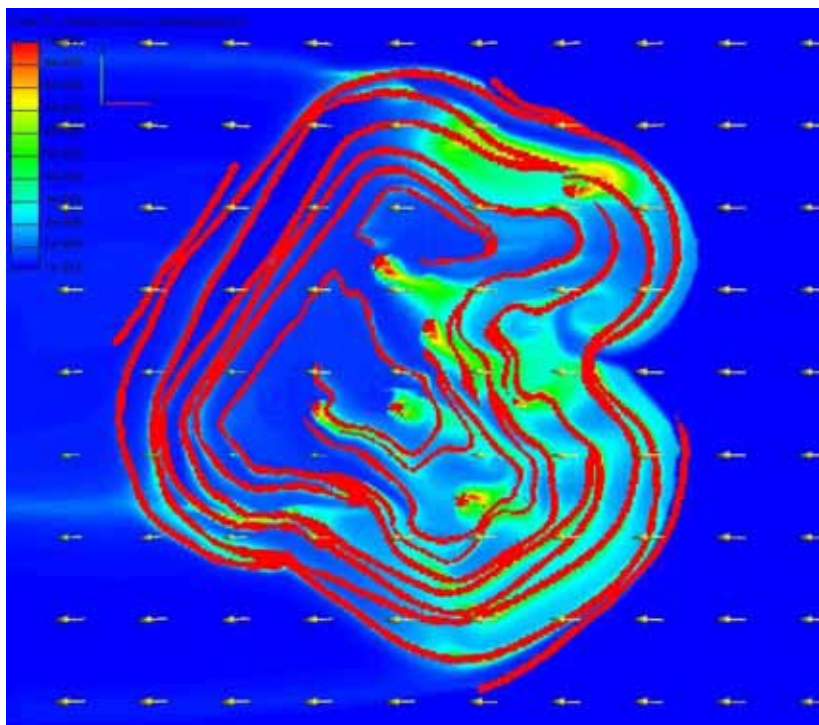


Figure 6.46: Pit surface and ground level Phase II volume fraction (dust concentration) for easterly winds, neutral boundary layer, $U_{10m} = 5$ m/s, $10 \mu\text{m}$ particles.

6.1.5 South Wind, $U_{10m} = 5$ m/s

Streamlines of flow for southerly winds ($U_{10m} = 5$ m/s) are presented in Figure 6.47. Although the pit is relatively symmetrical in an east-west direction and thus similar flow patterns would be expected for the north and south wind direction scenarios, this is clearly not the case. For the southerly wind direction only the upwind half of the pit, divided by the lobes on the east, is observed to have significant recirculation. Flow appears to enter the pit on the southwest corner, with some flowing diagonally down the northwest wall and into the base of the slightly lower southern section of the pit. It passes around this section of the pit, forming a vertical recirculation that rises to the main flow over the upper section of the pit.

The majority of the remainder of the flow that enters in the southwest corner passes more horizontally along the northwest wall, around and directly across the more elevated north section pit base. No recirculation is observed in the northern section of the pit. The majority of the flow is observed to exit the pit through the northeast wall and corners.

Iso-surfaces of Phase II fluid volume fractions for the southerly wind configuration are presented in Figure 6.48 and Figure 6.49, while contours of the pit surface and ground level concentrations are presented in Figure 6.50. The Phase II fluid or dust is seen to behave differently under southerly winds than it did for the northerly and easterly winds. Dust emitted from the excavation regions south of the ridge between the lobes on the eastern side of the pit is observed to travel in a southeast direction, recirculating within the southern lobe before passing back over the pit and out over the northern end of the pit. However, dust emitted from the roads along the western wall and also from the excavation regions and roads north of the ridge between the eastern lobes is not observed to recirculate. The flow takes the dust along the western wall, across the northern pit base and up the northern and eastern walls toward the northeast corner where it directly exits the pit at a lower level in more direct contact with the ground. Regions of significant ground level concentration external to the pit are observed emanating from the northeast corner of the pit in Figure 6.50 and can be directly traced back to excavation regions in the northern end of the pit, whereas the emissions from the southern end of the pit do not have as significant a ground level impact as they exit the pit.

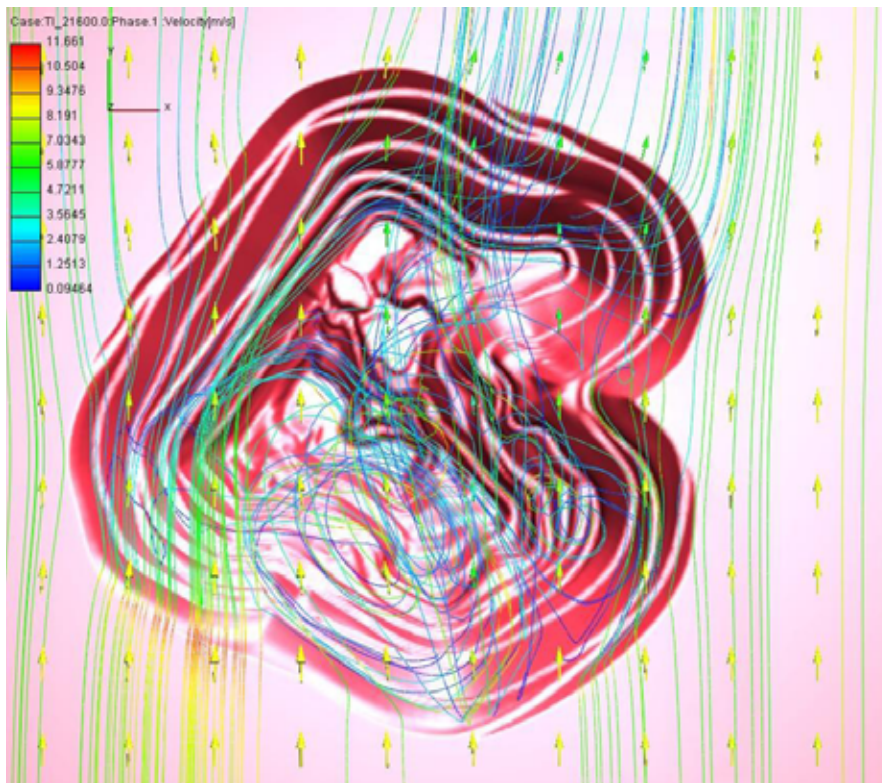


Figure 6.47: Streamlines of flow through the pit for southerly winds, neutral boundary layer, $U_{10m} = 5$ m/s.

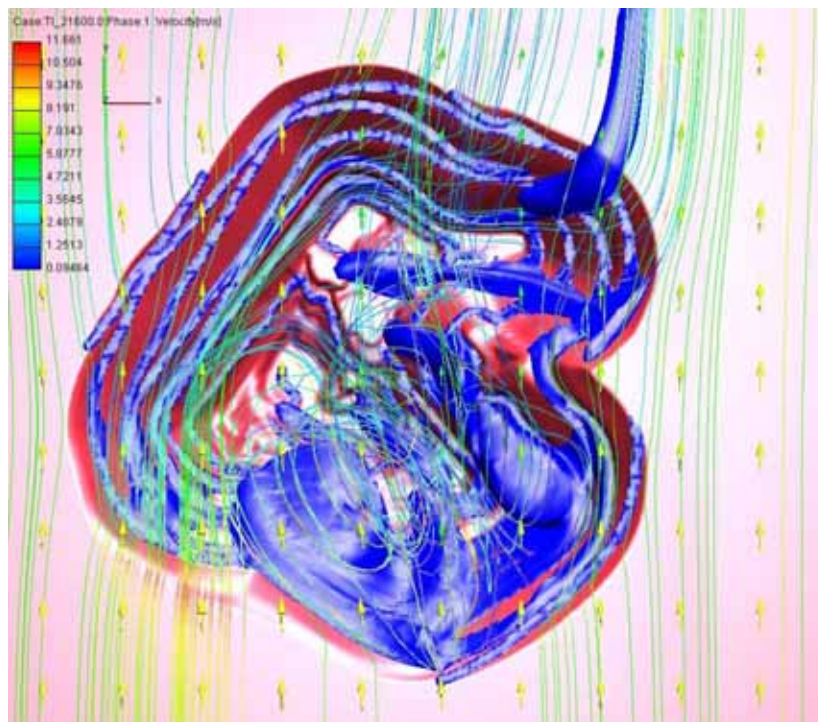


Figure 6.48: Iso-surface of Phase II volume fraction (dust concentration) ($1e-9$) and streamlines in the pit for southerly winds, neutral boundary layer, $U_{10m} = 5$ m/s, $10 \mu\text{m}$ particles.

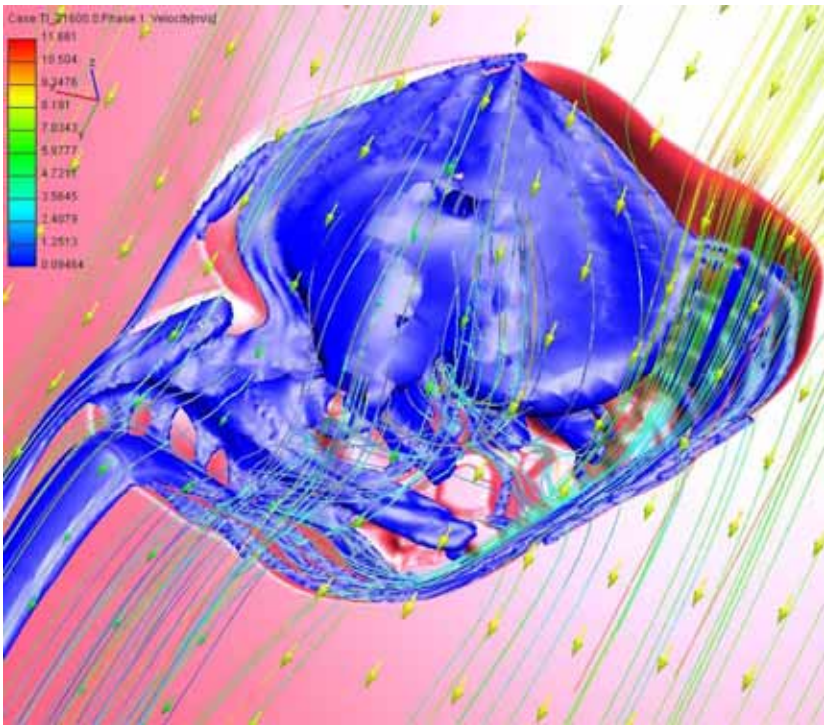


Figure 6.49: Iso-surface of Phase II volume fraction (dust concentration) ($5e-10$) and streamlines in the pit for southerly winds, neutral boundary layer, $U_{10m} = 5$ m/s, $10 \mu\text{m}$ particles.

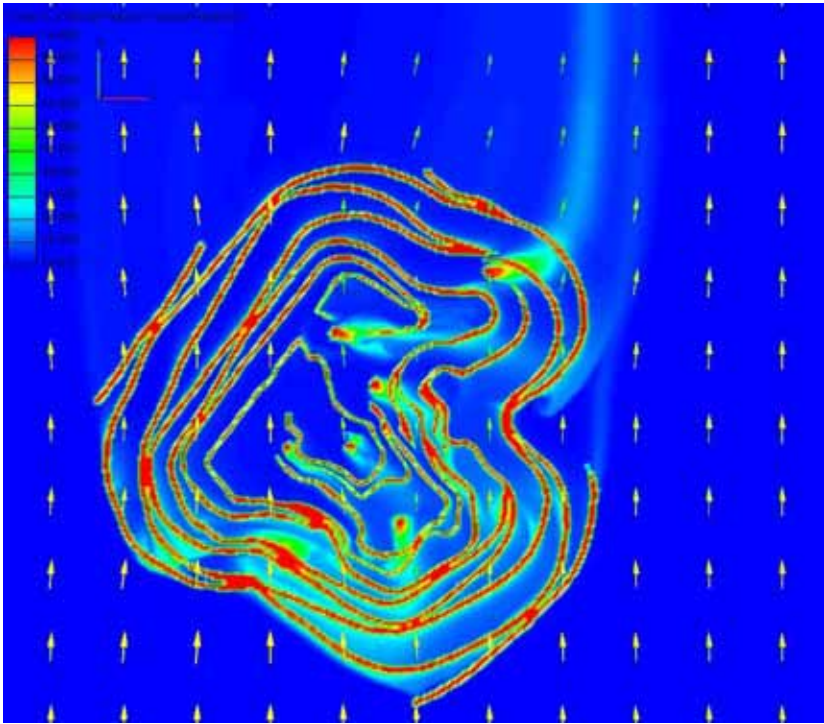


Figure 6.50: Pit surface and ground level Phase II volume fraction (dust concentration) for southerly winds, neutral boundary layer, $U_{10m} = 5$ m/s, $10 \mu\text{m}$ particles.

6.1.6 45° Wind, $U_{10m} = 5$ m/s

Streamlines of flow for northeast winds (45°) ($U_{10m} = 5$ m/s) are presented in Figure 6.51 and Figure 6.52. Two figures are presented as the simulation of flow conditions at oblique angles to the domain faces again failed to converge to a steady flow scenario for the pit. Again the flow was observed to oscillate through a range of flow conditions, driven by the influence of the pit on the flow domain in conjunction with the wall boundary conditions. As depicted in Figure 6.51 and Figure 6.52, the flow again oscillated between predominantly exiting the domain through one domain wall to the other. As the atmospheric flow oscillates, the flow structure within the pit also varies. Recirculation was not observed in the pit with the flow tending to pass down and across the pit, lateral to the flow above as evidenced in Figure 6.51 and Figure 6.52.

Iso-surfaces of Phase II fluid volume fractions for northeast wind configuration are presented in Figure 6.53 and Figure 6.54, while contours of the pit surface and ground level concentrations for the corresponding time steps are presented in Figure 6.55 and Figure 6.56. The dust plumes are seen to travel across the base of the pit, lateral to the flow above, prior to turning with the direction of the flow as they leave the pit. A recirculating flow structure in which the plume travels back over the pit is not evident.

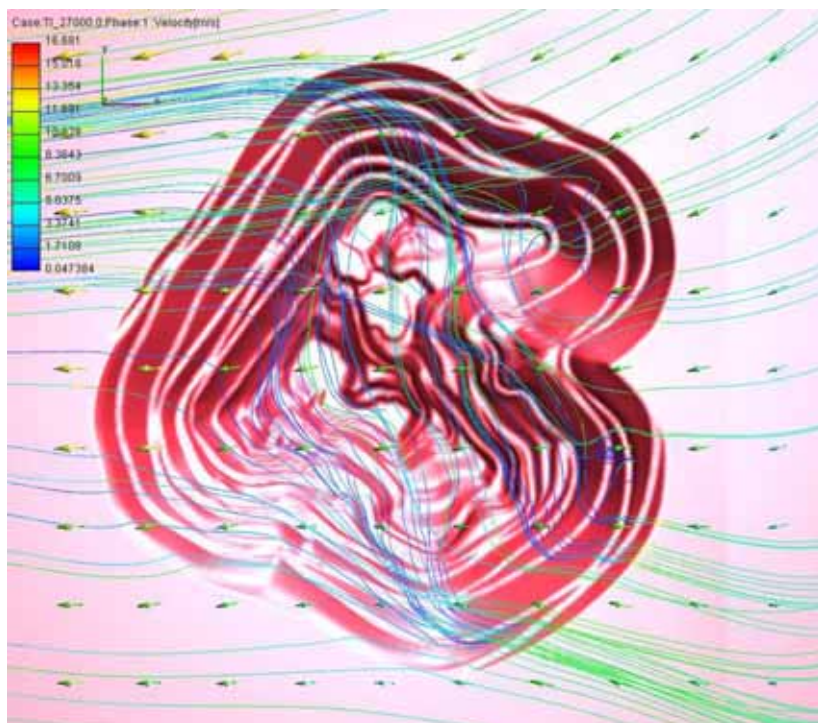


Figure 6.51: Streamlines of flow through the pit for northeast winds, neutral boundary layer, $U_{10m} = 5$ m/s.



Figure 6.52: Streamlines of flow through the pit for northeast winds, neutral boundary layer, $U_{10m} = 5$ m/s.

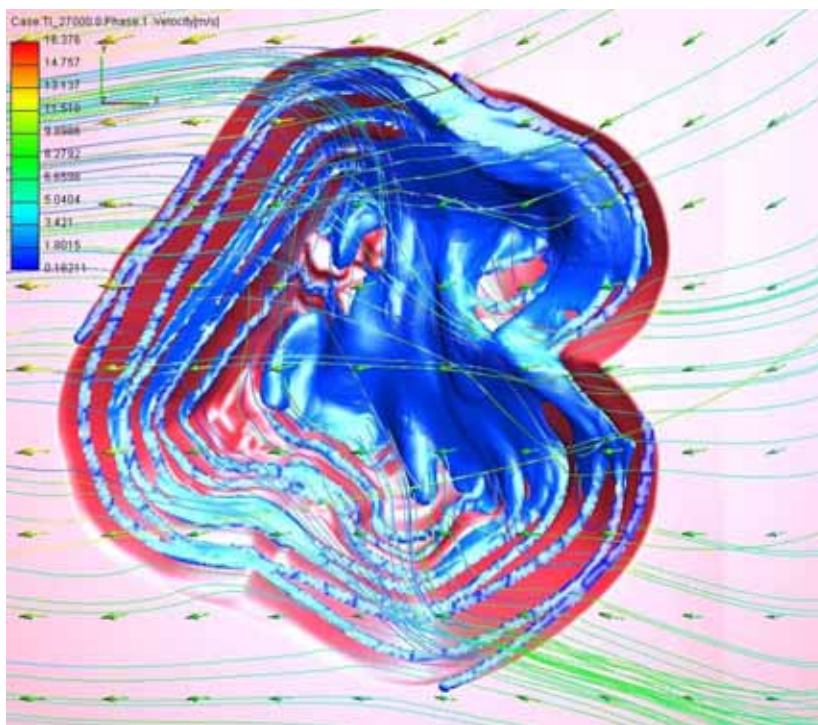


Figure 6.53: Iso-surface of Phase II volume fraction (dust concentration) ($1e-9$) and streamlines in the pit for northeast winds, neutral boundary layer, $U_{10m} = 5$ m/s, $30 \mu\text{m}$ particles.

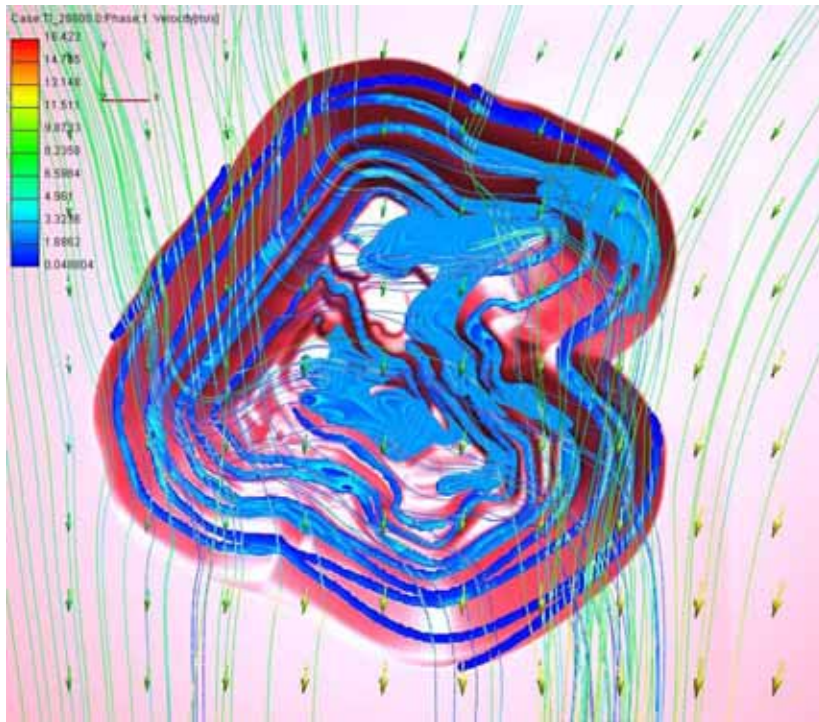


Figure 6.54: Iso-surface of Phase II volume fraction (dust concentration) ($2e-9$) and streamlines in the pit for northeast winds, neutral boundary layer, $U_{10m} = 5$ m/s, $30 \mu\text{m}$ particles.

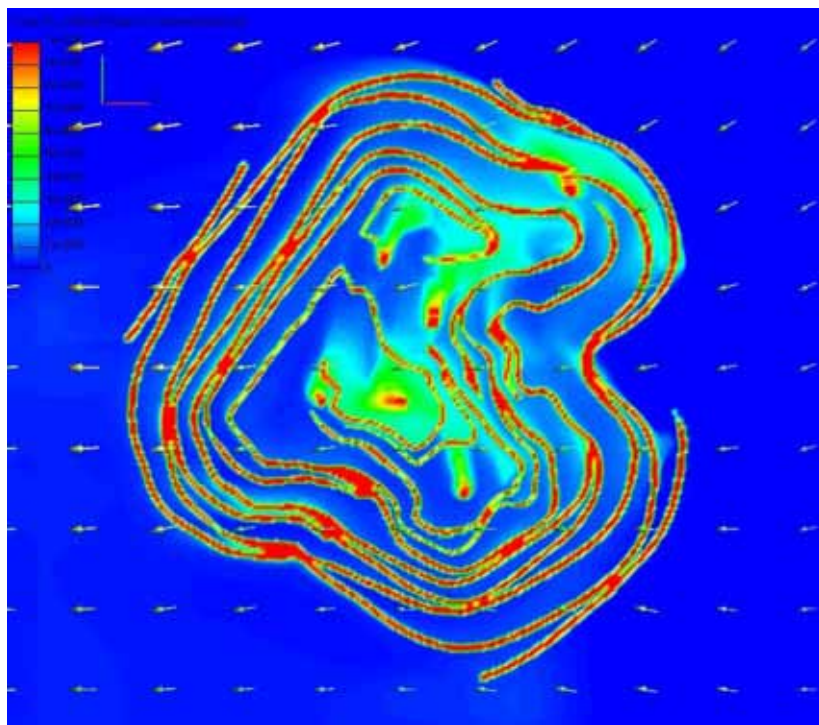


Figure 6.55: Pit surface and ground level Phase II volume fraction (dust concentration) for northeast winds, neutral boundary layer, $U_{10m} = 5$ m/s, $30 \mu\text{m}$ particles.

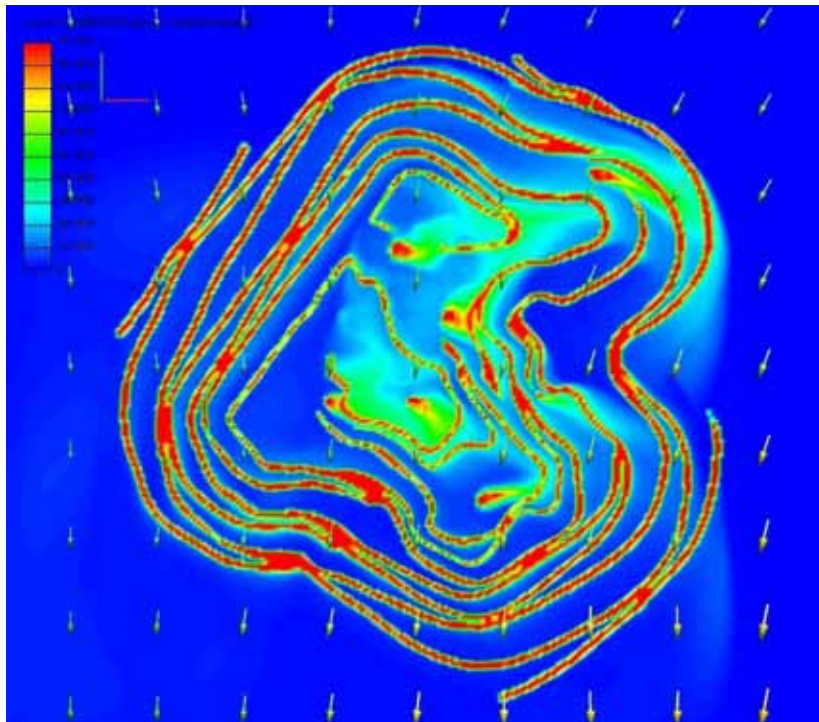


Figure 6.56: Pit surface and ground level Phase II volume fraction (dust concentration) for northeast winds, neutral boundary layer, $U_{10m} = 5$ m/s, $30 \mu\text{m}$ particles.

6.1.7 135° Wind, $U_{10m} = 5$ m/s

Streamlines of flow for southeast winds ($U_{10m} = 5$ m/s) are presented in Figure 6.57 and Figure 6.58. The southeast wind configuration displayed oscillatory behaviour similar to the northeast wind configuration. No significant recirculation zones are evident within the results presented, however this does not mean they do not occur for short periods within the cycle of the flow oscillations. Results have only been presented for discrete times. Again, there is a tendency for the flow to pass more directly through the pit, with the two instances presented showing flow entering the pit from either the northeast or southwest corners and exiting from the other. The flow in the base of the pit is perpendicular to the flow above the pit in both scenarios, with the pit effectively laterally displacing the flow that passes through it.

Iso-surfaces of Phase II fluid volume fractions for the southeast wind configuration are presented in Figure 6.59 and Figure 6.60, while contours of the pit surface and ground level concentrations for the corresponding time steps are presented in Figure 6.61 and Figure 6.62. The dust plumes are seen to travel across the base of the pit, lateral to the flow above, prior to turning with the direction of the flow as they leave the pit. Thus higher dust concentrations are observed on the eastern and southern walls respectively.

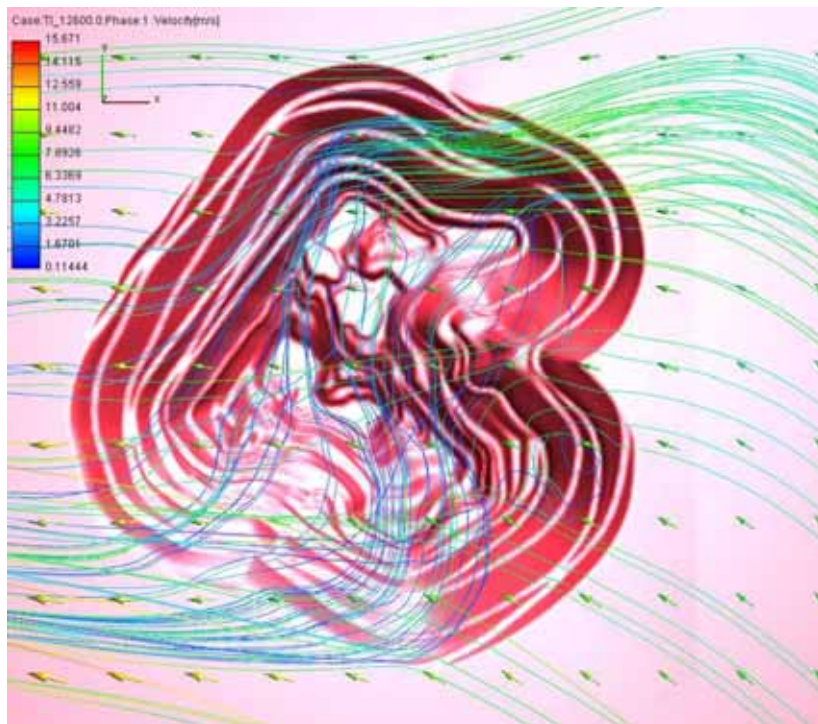


Figure 6.57: Streamlines of flow through the pit for southeast winds, neutral boundary layer, $U_{10m} = 5$ m/s.

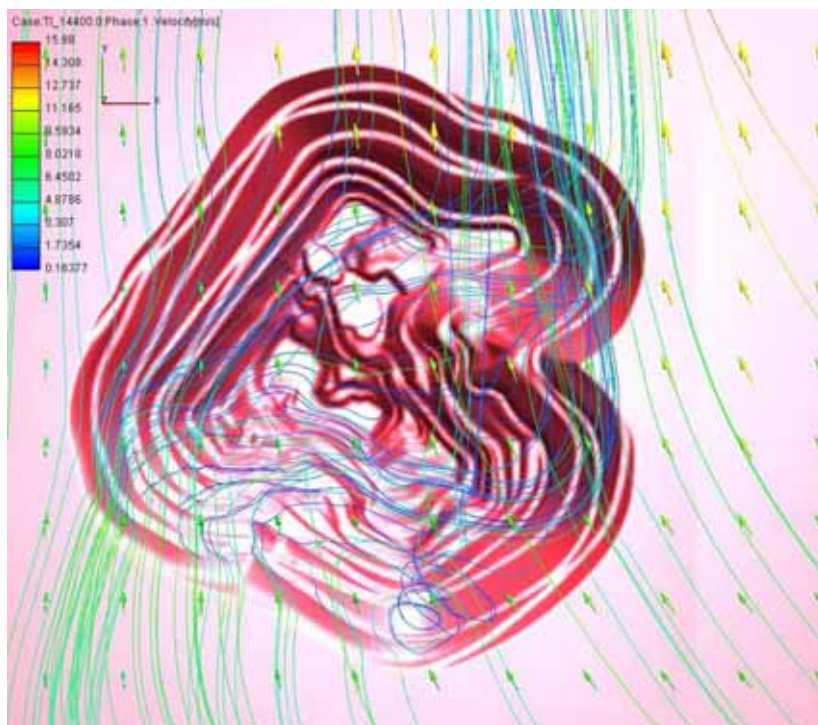


Figure 6.58: Streamlines of flow through the pit for southeast winds, neutral boundary layer, $U_{10m} = 5$ m/s.

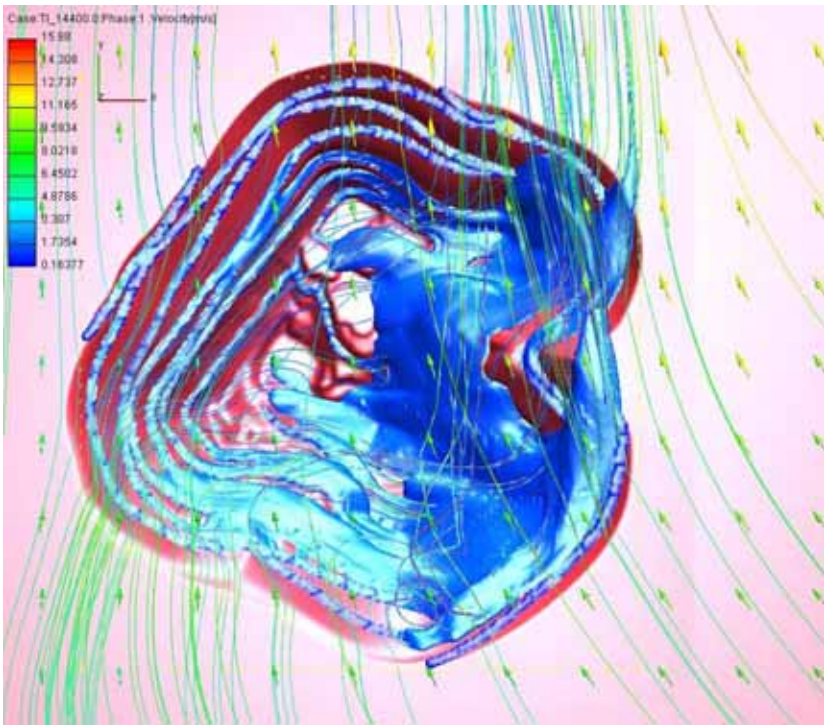


Figure 6.59: Iso-surface of Phase II volume fraction (dust concentration) ($1e-9$) and streamlines in the pit for southeast winds, neutral boundary layer, $U_{10m} = 5$ m/s, $30 \mu\text{m}$ particles.

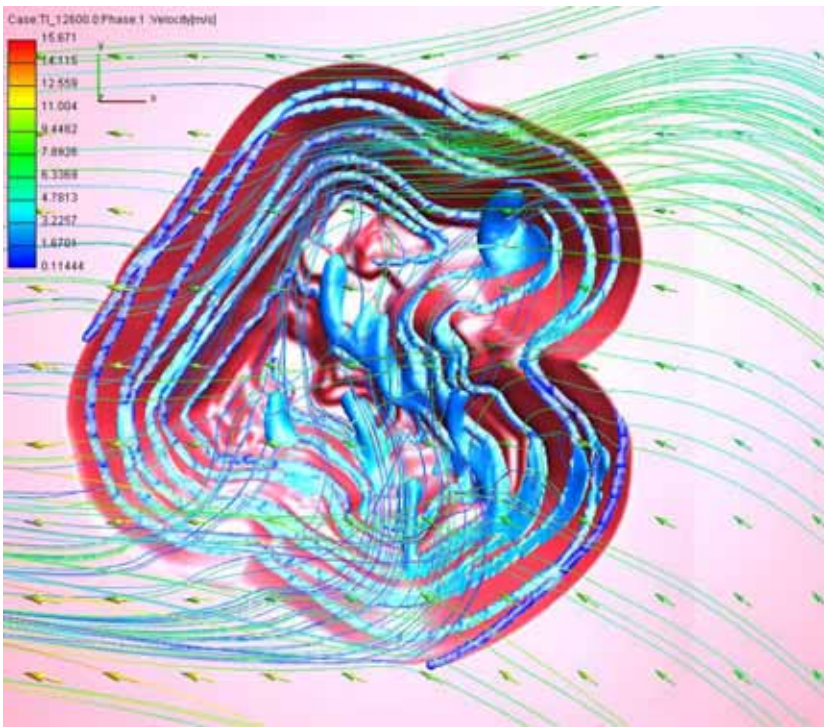


Figure 6.60: Iso-surface of Phase II volume fraction (dust concentration) ($2e-9$) and streamlines in the pit for southeast winds, neutral boundary layer, $U_{10m} = 5$ m/s, $30 \mu\text{m}$ particles.

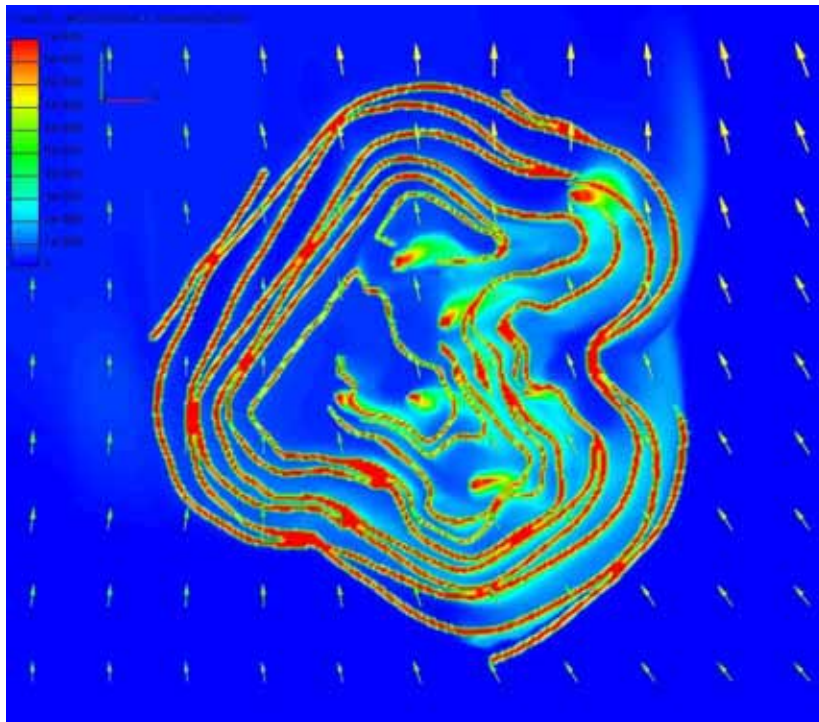


Figure 6.61: Pit surface and ground level Phase II volume fraction (dust concentration) for southeast winds, neutral boundary layer, $U_{10m} = 5$ m/s, 30 μ m particles.

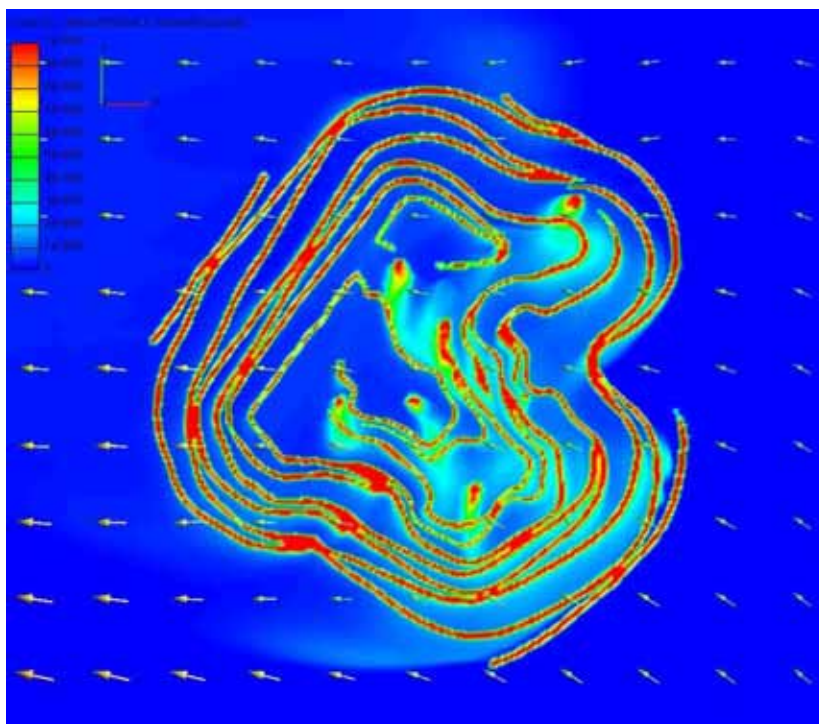


Figure 6.62: Pit surface and ground level Phase II volume fraction (dust concentration) for southeast winds, neutral boundary layer, $U_{10m} = 5$ m/s, 30 μ m particles.

7 DUST DEPOSITION AND PIT RETENTION

Dry deposition is a process of removal or depletion of dust, or more precisely particulate, as it contacts a solid surface; the walls and base of the pit in this case. The approach used to achieve the plume depletion or deposition in the simulations is outlined below.

The approach is based upon the use of a deposition velocity as typically used in air quality dispersion models (Apsley et al., 2005, Scire et al. 2000). It assumes the particle removal rate is adequately represented by a simple proportionality with the near surface concentration. It also assumes the removal process is irreversible and thereby precludes re-suspension of particles.

7.1 Dry Deposition Calculation

The dry deposition flux, F_d , can be determined assuming the rate of deposition per unit area is proportional to the near-surface concentration, $C(x,y,0)^b$, which effectively defines the dry deposition velocity, v_d as a proportionality constant.

$$F_d = v_d C(x,y,0) \text{ (kg/m}^2\text{s)} \quad \text{Equation 7-1}$$

The deposition velocity, v_d is a function of the particle characteristics, the nature of the surface and the wind speed, among other generally less significant factors.

For particles, both gravitational settling and diffusion will contribute to the overall rate of deposition. Gravitational settling of particles is the rate at which a particle will 'fall' to the ground under its own mass and is a balance between the gravitational force and the aerodynamic drag force as the particle falls, commonly referred to as the **terminal velocity** of a particle. Diffusion refers to the rate at which particles are mixed to a surface as a result of turbulence in the flow, effectively the dispersion of the particles onto the surface.

Diffusivity theory can be used to derive an expression for the overall deposition velocity, v_d :

$$v_d = v_t / (1 - \exp(-v_t/v_d')) \quad \text{Equation 7-2}$$

where

$$\begin{aligned} v_t &= \text{terminal or gravitational settling velocity, and} \\ v_d' &= \text{diffusive component of the deposition velocity} \end{aligned}$$

7.1.1 Gravitational Settling Velocity

Gravitational settling is an important part of the particle deposition process. The gravitational settling velocity, v_t is typically determined from the diameter and density on the assumption of spherical particles. This is what the multiphase component of the CFD model calculates in determining the relative behaviour of the two fluid components within the model. The gravitational settling velocity is the difference between the velocity of the Phase I fluid (air) and the velocity of the Phase II fluid or spherical dust particles.

^b A terrain-following coordinate system is assumed.

A comparison of the gravitational settling velocity calculated from the CFD model simulations over flat terrain^c with gravitational settling velocities derived from the parameterisations of the atmospheric dispersion models CALPUFF and ADMS is presented in Figure 7.1. The comparison shows good agreement for particles of 10 µm and above, particularly with the ADMS parameterisation. The output resolution (number of significant figures written to the file) in the CFD model limited the reliability of the comparison below 10 µm. Typically, gravitational settling is the significant deposition process for particles above 10 µm, while diffusive deposition is more dominant for particles smaller than 10 µm.

In typical atmospheric dispersion models it is assumed the surface is flat and that the flow is straight, thus the gravitational settling velocity refers solely to gravitational settling, resulting in an advection of the particles toward the ground at a constant rate based on the particle size. The CFD model allows for the simulation of terrain features and flow curvature. In addition to gravitational settling, inertial influences may also cause impaction on the surface as the flow curves. Under such a scenario, the deposition velocity is the velocity at which a particle travels toward the boundary faces of a cell relative to the air or primary fluid phase, i.e. the difference in velocity components normal to a boundary face. With the pit having walls and a base etc., it is possible a boundary cell within the domain may have more than one boundary face on which the particulate may deposit.

Thus, the gravitational settling velocity was determined directly from the difference in cell wall normal velocity between the two fluid phases, air and particles, derived from each in-pit boundary cell within the CFD domain.

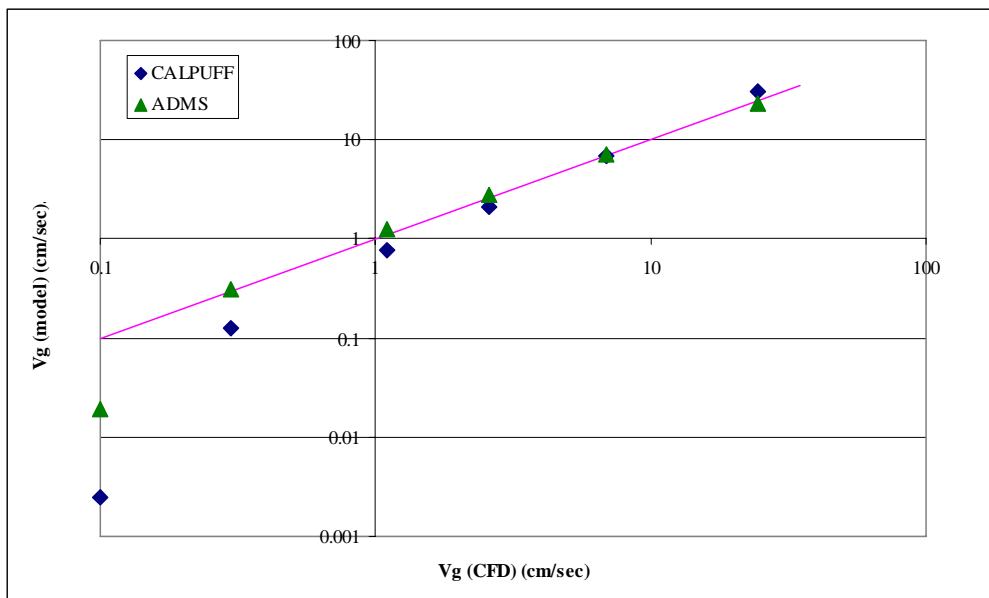


Figure 7.1: Comparison of gravitational settling velocity derived from the CFD multiphase simulation over flat terrain with the parameterisations of the atmospheric dispersion model CALPUFF and ADMS over a particle size range from 2.5 µm to 100 µm.

^c The difference in the vertical velocity component.

7.1.2 Diffusive Deposition Velocity

Deposition is a very complex variety of physical and chemical processes whereby particles, and other airborne material for that matter, are transported to and removed at the surface. The representation of deposition in terms of a single parameter, the deposition velocity, tends to obscure the real processes.

The pollutant, or particles in this case, is transported to the vicinity of the surface through turbulent dispersion. However, there are a number of possible mechanisms by which the pollutant can cross into the final sub-layer of the flow and thus become deposited. The processes are determined by the nature of the surface (smooth, rough, water, vegetation) and also the pollutant. Typically, resistance models are used to represent the resistance of the pollutant to cross into the deposition zone. The resistance, r , is the reciprocal of the deposition velocity, $1/v_d$.

For particles the diffusive deposition velocity can be expressed as^d:

$$v_d' = 1/(r_a + r_d) \quad \text{Equation 7-3}$$

Assuming neutral stability, the atmospheric resistance, r_a , can be determined from:

$$r_a = \ln(z_c/z_o)/ku_* \quad \text{Equation 7-4}$$

where;

- z_c = Cell reference height (cell centre distance normal to the face in this case)
- z_o = Surface roughness length
- k = Von Karman constant
- u_* = Friction velocity

The deposition layer resistance, r_d , can be parameterised as:

$$r_d = (Sc^{(-2/3)} + 10^{-3/St})^{-1} u_*^{-1} \quad \text{Equation 7-5}$$

where:

- Sc = Schmidt number = v/D
- St = Stokes number = $(v_t/g)(u_*^2/v)$

and;

- v = viscosity of air
- D = Brownian diffusivity

7.1.3 Deposition CFD Application

A CFD user function incorporating Equation 7-1 to Equation 7-5 was developed and applied to each in-pit wall and base surface cell at each time step of the CFD simulation. The total deposition rate for each defined surface region was calculated for each time step as the sum of the deposition for each cell face within the region

^d Assuming the surface is vegetation free.

and written to the operational run log file. The pit configuration comprised of three defined depletion surface regions.

The dust sources, being the roads and excavation areas, were not defined as depletion surfaces in either pit configuration. Their definition as inlet sources of particles and air prohibited their use as deposition surfaces. The flow is often observed to pass around the pit walls, and advect the dust along the roads. The current analysis incorporates deposition on the roads and excavation sites based on the relative surface areas.

This approach is considered to be conservative^e as deposition, particularly of the larger particles, is approximately proportional to the projected horizontal surface area, with the roads, in particular, representing a significant proportion of the horizontal surface area. Additionally, the deposition rate is a direct function of the surface concentration, with highest concentrations observed along the roads and at the excavation sites. The flow and dust behaviour observed in the pit and presented in Section 6 indicate that the use of alternative dust source methods that would enable the inclusion of the road and excavation regions as deposition surfaces should be considered as a model improvement.

7.2 Discrete Particle Size Deposition and Retention

As discussed above in Section 5.2, the two-phase fluid approach allowed the representation of one discrete particle size per simulation, with one phase representing the air and the second fluid phase the discrete spherical particles of defined density and diameter. Results of the CFD simulation predictions for the individual discrete particle size deposition rates are presented and discussed below. A base case model configuration is used to investigate the influence of particle size on the in-pit deposition rates. While the influence of variations in meteorological conditions such as wind speed, atmospheric stability and wind direction are investigated for a limited number of up to two discrete particle sizes.

As mentioned above, the total particulate deposition rate on to a number of defined in-pit surfaces was calculated and written to the operation run log file for each simulation time step. The summation of the deposition for the individual in-pit surfaces provided an estimate of the total in-pit deposition. An alternative means of determining the deposition rate is through a mass balance of the second phase fluid or particle flux across the domain. The source mass flux of particulate or dust released from the road and excavation areas was known. Integration across the domain enabled the determination of the mass flux downwind of the pit. As deposition was only allowed on in-pit surfaces, continuity of mass enabled the determination of the total in-pit deposition as the difference between the mass of particulate released into the pit and the mass passing through the domain downwind of the pit.

For simulations that provided a steady state solution to the flow (i.e. those not at an oblique angle to the domain boundaries) the two approaches converged to a similar prediction of deposition rates and thus pit retention, although this generally took several hours of simulated real time to achieve.

^e Underestimate the total deposition and thus pit retention.

Deposition within the pit was initially investigated for the base case model configuration of a north wind neutral boundary layer with $U_{10m} = 5$ m/s. The simulations were conducted for four discrete particle sizes, with an emission source area factor of 1.226 applied to the predicted deposition estimates for each individual particle size to account for the additional area of the roads and excavation areas. At each discrete particle size, the percentage pit retention was determined from the predicted deposition rate and the known in-pit dust emission rate.

The variation of the predicted pit retention with particle size under the base case neutral boundary layer is presented in Figure 7.2. The third order polynomial presented in the figure gives a good representation up to the maximum particle size simulated ($50 \mu\text{m}$). As expected the pit retention rate is seen to increase with particle size. Extrapolation above $50 \mu\text{m}$ indicates all particles above about $60 \mu\text{m}$ are deposited and thus are retained within the pit. Pit retention levels for the smallest particles ($2.5 \mu\text{m}$) are predicted to be in the order of 0.5%.

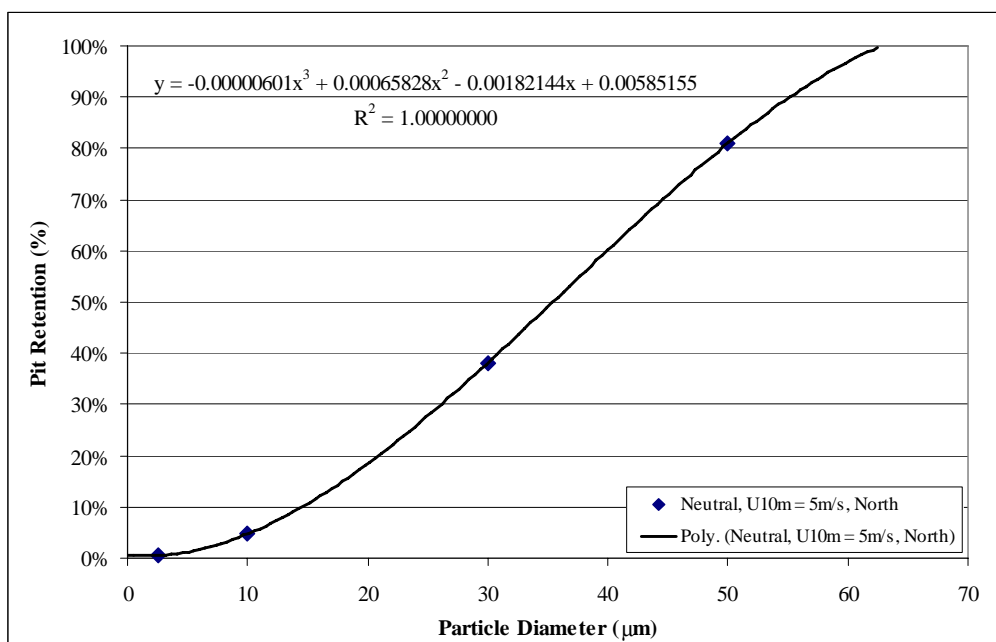


Figure 7.2: Predicted pit retention variation with discrete particle size for the pit with the base case neutral boundary layer, north winds, $U_{10m} = 5$ m/s.

Figure 7.3 summarises the influence of atmospheric stability on the pit retention. Simulations were performed with particle diameters of 10 and $30 \mu\text{m}$ for both the stable and unstable atmospheric flow cases for comparison with the base case neutral simulations. Again, the investigation was performed for northerly winds only.

Again, the results suggest that pit retention may increase very slightly in the stably stratified atmospheric conditions, most likely due to a slight decrease in the pit surface velocities. This may be due to the lower wind velocity in the lower sections

of the atmospheric flow or a reduction in dispersion from the surface due to stratification of the flow along the pit surface. However, the influence is only slight, and clearly the stratified approach flow simulated did not result in any significant change in the flow or dust behaviour within the pit. Again, findings may differ with lower ambient velocities and it maybe worthwhile attempting the simulations at wind speeds of the order 0.6 m/s. This would emulate the 2 m/s neutral flow scenario under equivalent stable conditions.

Retention is slightly increased for the unstable boundary layer simulations. Again, it should be remembered that the wind profile was of a reduced velocity and consequently the increase in pit retention may be a direct result of the lower wind speeds.

The simulations provide no conclusive evidence that atmospheric stability will significantly influence deposition rates within the pit and thus pit retention.

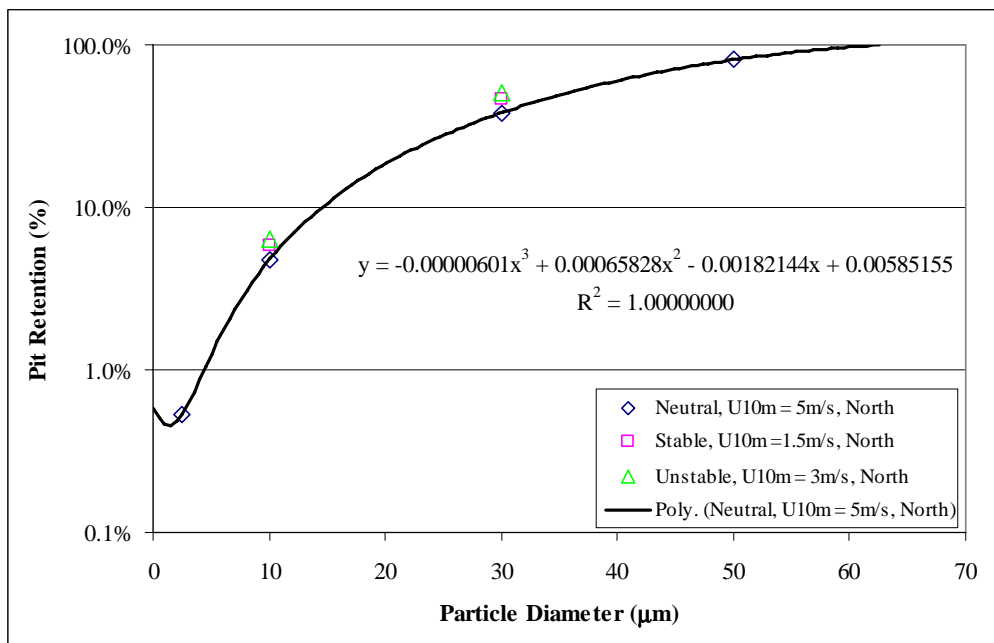


Figure 7.3: Predicted pit retention variation with atmospheric stability for the pit under northerly winds.

The influence of wind direction on the pit retention is summarised in Figure 7.4. Four additional wind directions were investigated, with simulations performed for two discrete particle sizes of 10 and 30 µm for the south and east winds and for only the larger particle size for the northeast and southeast winds. The predicted rates are compared with the full range of particle sizes simulated for the base case configuration to provide perspective on the degree of variation of pit retention due to wind direction.

It is evident in Figure 7.4, that generally speaking the wind direction does not have a significant influence on the pit retention. However, there does appear to be one exception to this, being the case of the southerly winds. Predicted pit retention is in

the order of 40% lower than for the other wind directions. Interestingly, the southerly wind direction was the scenario for which the flow structure within the pit varied most significantly from the typical. The recirculation established in only the upwind half of the pit, with the flow passing directly across the northern half of the pit. Further discussion on the flow structure is presented in Section 6.1.5, however it appears the difference in flow structure has resulted in less interaction of the dust plumes with the surface of the pit and consequently less deposition and thus pit retention.

Although the flow behaviour for the oblique angled winds (northeast and southeast) is also observed to differ from that observed for winds perpendicular to the domain boundaries, the variation in flow structure did not significantly affect pit retention. The fact that for the flow structures developed in both situations, flow is observed to pass from one side to the other along the surface of the pit is thought to have resulted in dust having virtually equivalent opportunity to deposit, apart from the case of the southerly winds.

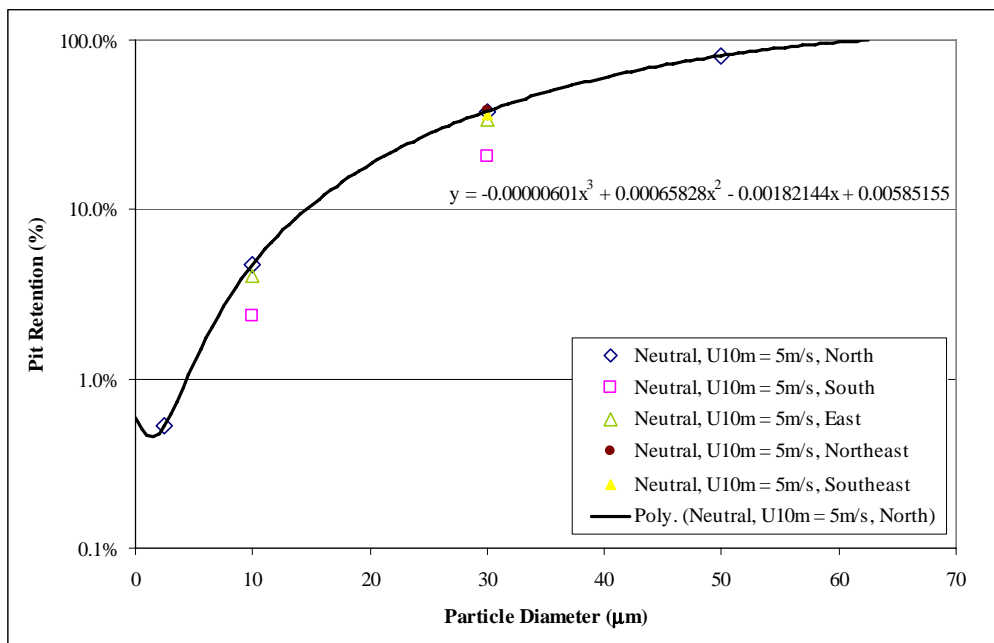


Figure 7.4: Predicted pit retention variation with wind direction with the base case neutral boundary layer, $U_{10m} = 5$ m/s.

The influence of ambient wind speed on deposition and thus pit retention was also investigated. A comparison of pit retention under neutral northerly winds for wind speeds of between $U_{10m} = 2$ and 10 m/s is presented in Figure 7.5. Again the simulations were performed for the two discrete particle sizes of 10 and 30 µm for the $U_{10m} = 2$ and 10 m/s configurations for comparison with the four discrete particle sizes simulate for the base case $U_{10m} = 5$ m/s scenario. The results demonstrate conclusively that the pit retention increases with a reduction in wind speed. The relative magnitude of the variation in pit retention with wind speed is observed to be consistent across the range of particle sizes investigated. The simulations predict all particles larger than about 40 µm will be deposited within the

pit at the lower wind speed. At the higher wind speed, a proportion of particles of up to about 70 µm aerodynamic diameter will be released from the pit.

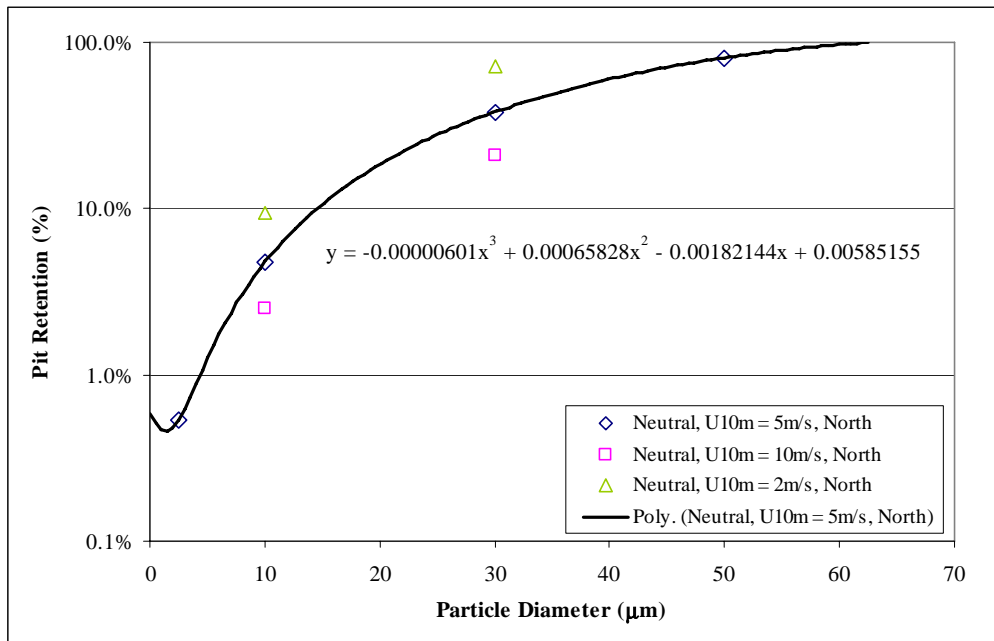


Figure 7.5: Predicted pit retention variation with wind speed under neutral boundary layer northerly winds.

7.3 Cumulative Pit Retention

Estimation of the cumulative pit retention over a defined particle size range (i.e. PM10^f) can be achieved through integration, or summation, of the pit retention across the range of particles considered. This requires knowledge of the distribution of the emitted particulate in addition to the deposition or retention characteristics across the full particle size range.

A sufficient number of discrete particle sizes were simulated for the base case scenarios (i.e. neutral north wind with $U_{10m} = 5$ m/s) to enable extrapolation of pit retention characteristics across the full particle size range as demonstrated in Table 7.1 and Figure 7.2.

The particle size distribution was estimated from the combined in-pit particulate emission rates as presented in Table 4.1. The geometric mean and standard deviation particle diameter summarised in Table 7.1.

Table 7.1: Estimated geometric mean and standard deviation for dust emissions.

Geometric Mean Diameter (µm)	Geometric Standard Deviation (µm)
20.76	4.86

^f PM10 includes particles up to 10 µm aerodynamic diameter.

Piece-wise linear, 3rd order polynomial and linear least squares representations of the pit retention rate were applied to provide a representation of the uncertainty arising from the limited range of particles sizes simulated. The estimated particle size distribution retention rates under the base case neutral winds are presented in Figure 7.6. Again, the pit retention representation methods provide relatively similar estimates of pit retention for particles above 10 μm , with considerable variability below the 10 μm particle size. No retention for particles below 1.5 μm is observed for the piece-wise linear representation and below 6 μm for the linear least squares estimate. The 3rd order polynomial provides for retention of particles smaller than 0.5 μm . Particles above about 60 μm are fully retained within the pit, virtually independent of the extrapolation method.

A summary of the estimated PM_{2.5}, PM₁₀ and TSP particle fraction pit retention factors based on the particle size distributions represented in Figure 7.6 and the 3 individual pit retention extrapolation methods is presented in

Table 7.2. The variability, and thus uncertainty, in the predicted retention rate for the smaller particle fractions, especially the PM_{2.5} fraction, is again evident, with predicted retention rates ranging from 0 to 0.48 %. The relative uncertainty is reduced for the larger particle fractions, particularly the TSP fraction covering the full particle size distribution. The 3rd order polynomial results, probably the most reliable, predict about 0.5% of PM_{2.5}, 1.5% of PM₁₀ and 38% of TSP emissions will be retained within the pit for neutral boundary layer northerly winds with $U_{10m} = 5$ m/s.

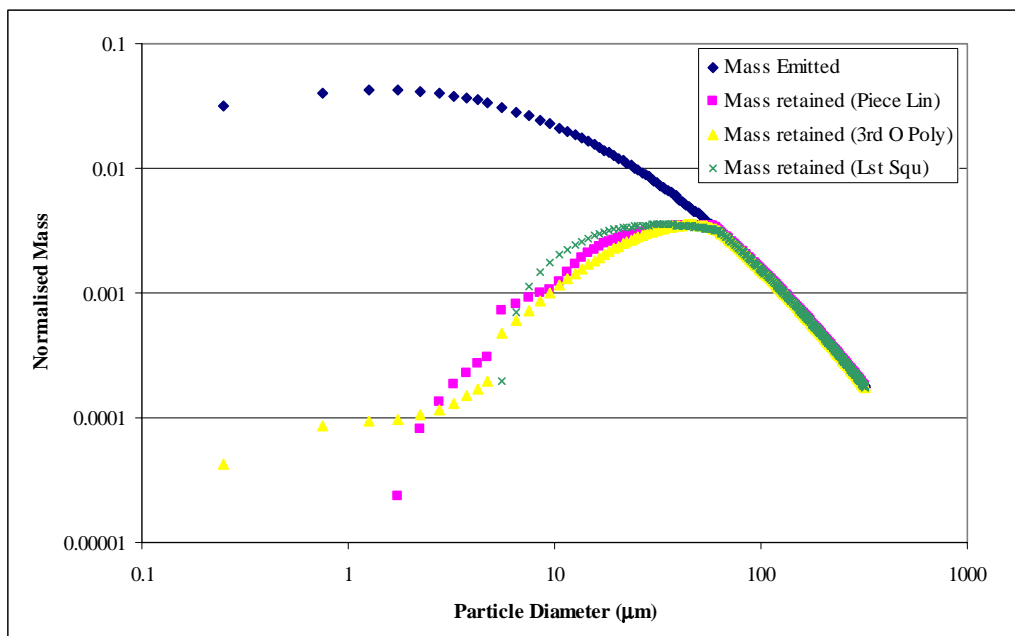


Figure 7.6: Normalised mass distribution and estimated pit retention as a function of particle size for the pit north wind, base case neutral boundary layer for $U_{10m} = 5$ m/s.

Table 7.2: Summary of estimated pit retention rates for PM2.5, PM10 and TSP particle fractions for the pit dust emissions, with base case neutral boundary layer, north wind, $U_{10m} = 5$ m/s simulated atmospheric conditions.

	Piece-wise linear	3rd order polynomial	Linear least squares
PM2.5	0.12%	0.48%	0.00%
PM10	1.8%	1.5%	1.6%
TSP	38.7%	38.0%	39.7%

Simulations of pit retention were performed at two additional wind speeds, $U_{10m} = 2$ and 10 m/s. However, insufficient discrete particle sizes were simulated to enable independent determination of size fraction pit retention rates with suitable certainty. Constant relative variation of the pit retention rate with particle size was assumed to enable estimation of the cumulative pit retention for the individual standard size fractions (PM2.5, PM10 and TSP) from the more detailed $U_{10m} = 5$ m/s simulations. The estimated variation of pit retention with particle size with $U_{10m} = 2$ and 10 m/s is presented in Figure 7.7 along with the extrapolated results of the $U_{10m} = 5$ m/s scenario. It is evident the results are derived via application of a constant factor over most of the particle distribution, however, the increase in the size of particles that may escape the pit with wind speed is evident around the region of the 40 to 100 μm particles.

Again, integration across the particle size distribution provides an estimate of pit retention factors for the standard particle size fractions of PM2.5, PM10 and TSP. Results are summarised in Table 7.3 for wind speeds of $U_{10m} = 2, 5$ and 10 m/s. As expected, pit retention rates are higher at the lower wind speed, with estimates of 0.93% for PM2.5, 2.9% for PM10 and 47.5% for TSP. The lower wind speed estimates are observed to be in better agreement with the NPI recommended rates, particularly in respect of TSP. As the wind speed increases, the deposition rate is observed to decrease, with the simulations predicting that just over $\frac{1}{4}$ of the total particulate is retained at the higher wind speed of $U_{10m} = 10$ m/s.

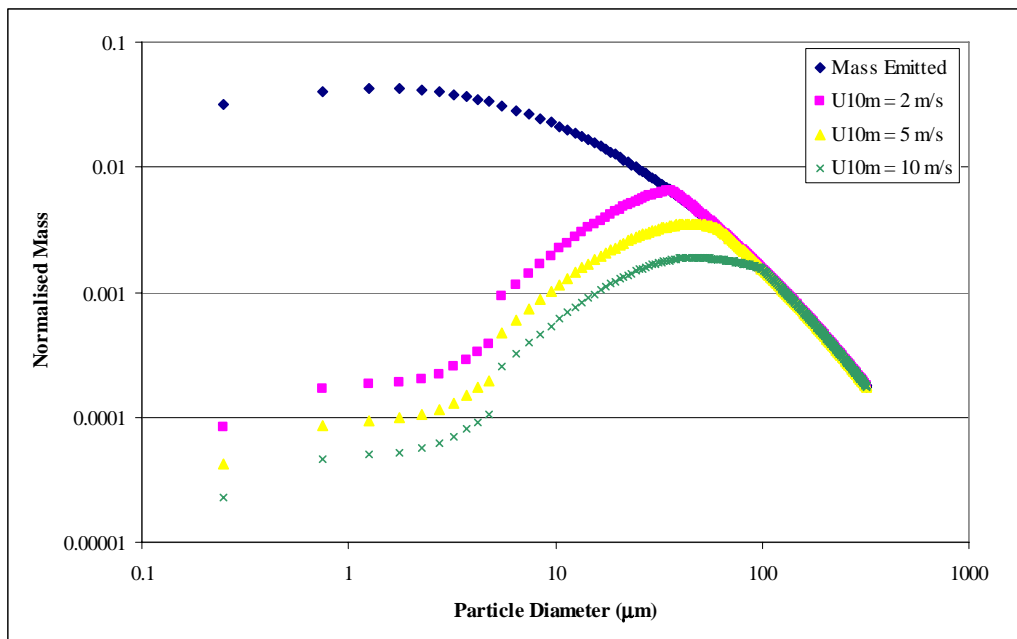


Figure 7.7: Normalised mass distribution and estimated pit retention as a function of particle size for neutral boundary layer, north wind for $U_{10m} = 2, 5$ and 10 m/s. Note: $U_{10m} = 2$ and 10 m/s results are estimated by a constant factor from the $U_{10m} = 5$ m/s retention distribution.

Table 7.3: Summary of estimated pit retention rates for PM2.5, PM10 and TSP particle fractions with neutral boundary layer, north wind, $U_{10m} = 2, 5$ and 10 m/s simulated atmospheric conditions.

	$U_{10m} = 2$ m/s	$U_{10m} = 5$ m/s	$U_{10m} = 10$ m/s
PM2.5	0.93%	0.48%	0.26%
PM10	2.9%	1.5%	0.81%
TSP	47.5%	38.0%	27.9%

7.4 Deposition and Retention Summary

The dry deposition flux within the proposed Olympic Dam open pit has been predicted using a deposition velocity approach as typically used in air quality dispersion models. The approach assumes the particle removal rate is dependent upon the rate of gravitational settling and diffusion of the particles to the surface as well as the near surface concentration. It also assumes the removal process is irreversible and thereby precludes re-suspension of particles.

The deposition algorithm was developed and incorporated into the CFD solver through the application of a user function. The deposition algorithm determined the rate of deposition on individual surface cells within the proposed open pit domains based on local velocity and turbulence characteristics. The simulations were based upon determination of deposition and thus in-pit retention for a range of discrete particle sizes with base case meteorological condition (neutral north wind $U_{10m} =$

5 m/s). Perturbations to the base case meteorological conditions were investigated for a limited range of particle sizes.

Particle size and wind speed were found to be the two primary factors that influenced the deposition and thus pit retention rate. As would be expected, higher pit retention was predicted for larger particles and lower wind speeds. The flow within the pit was responsive to winds at an elevation of 100 m or more and thus variations in atmospheric stability did not significantly influence deposition and thus pit retention rates. Wind direction was also found not to significantly influence deposition rates and thus pit retention.

The estimates of in-pit dust emissions distribution and predicted discrete particle size retention rates were used to calculate cumulative pit retention estimates for the standard particle size fractions of PM_{2.5}, PM₁₀ and TSP. Estimated particle fraction retention rates were found to be lower than those recommend in the NPI, however, for the lower wind speed the difference, particularly for TSP was small. At higher wind speeds the predicted retention rates were a factor of two or more less than the NPI recommended values.

The retention rates estimated in this study are likely to be conservative (i.e. underestimate actual rates), particularly in relation to the diffusive deposition component. Further investigation into the uncertainty and the diffusive deposition component and improvement of the parameterisation would be recommended. Investigation into the significance of deposition onto the emission sources (roads and excavation region) would also be recommended. The methodology could also be improved through better characterisation of the particle size distributions of the various in-pit dust emission sources, particularly the major sources such as the operation of trucks on the haul roads and the loading of the haul trucks.

8 CONCLUSIONS

Computational Fluid Dynamics modelling has been used to assess the flow and dust behaviour within the proposed expansion of the Olympic Dam open pit mining facility during Year 40 of the project to investigate deposition, and thus retention, of particulate released through in-pit activities.

The CFD modelling software AVL SWIFT Version 8.41 was used for the fluid flow and thermodynamic modelling undertaken in the study. Swift employs a Finite Volume discretisation method to solve the fundamental physical conservation laws in their integral form. The $k-\epsilon$ turbulence model was used to obtain a steady state solution of the conservation equations.

The Olympic Dam mine expansion was modelled with the open pit as the only infrastructure element. The pit was approximately 3 km by 3 km and over 900 m deep at Year 40. The waste rock dump - a rectangular structure of approximately 9.2 km by 4.6 km with a height of 100 m at Year 40 of the expanded operation; and the tailings retention system - a sequence of cells, each approximately 2 km by 2 km, reaching a final height of 50 m; where not represented in the simulations.

The dust, or particulate, was represented as a second phase of fluid comprising discrete 'bubbles' of defined radius and density within the continuous primary fluid phase (air). Momentum exchange occurs between the two fluid phases due to drag and turbulence dispersion forces. The approach uses volume fraction to represent the distribution of the two flow phases (air and dust) in addition to all other flow variables for each phase.

Due to time constraints, simulations concentrated on a base case meteorological condition of north wind neutral stability with $U_{10m} = 5$ m/s. Simulations for the base case meteorological condition covered a range of discrete particle sizes. Perturbations to the base case meteorological condition included simulations at four additional wind directions and variations to atmospheric stability and wind speed. Only a limited number of discrete particle sizes were simulated under perturbation meteorological conditions.

The study has investigated the in-pit flow and dispersion for a number of meteorological conditions. It has produced a large amount of data that could be further investigated and enhanced through improvements to the model. However, the primary aim was to understand the basic flow structure developed within the pit and the resulting transport, dispersion and deposition of dust within the pit. Although many other aspects of modelling could be investigated in detail, the report has aimed to present the primary structure of the flow within the pit and the consequential impacts on particulate deposition and thus pit retention. The findings of the investigation in relation to this are briefly summarised and discussed below.

The aspect ratio of the southern section of the pit is such that vortex or recirculating structures that form are in the order of the size of the pit, with the in-pit surface flow typically passing through the pit and out in one, or at most a couple of, circulations. Other flow patterns, particularly for the oblique wind angles for which the solution demonstrated oscillatory behaviour, show the flow passing directly down a pit face, across the base, typically laterally to the flow above, and up a diagonally opposite face from where it exits the pit.

As a result of the flow patterns within the pit, the dust, particularly that emitted toward the base of the pit, is generally only in contact with the wall as it travels up one side of the pit. The dust is then observed to either pass back over the pit as it rejoins the external flow, often at an elevated level, or directly out of the pit in the cases where flow passes more directly through the pit. There do not appear to be any regions of significant dust build-up, with most dust emissions from within the pit appearing to deposit or lift from the pit walls if they do remain in the pit for a period. It should be noted the investigation has not considered externally generated dust that may enter the pit within the free stream atmospheric flow, enhancing dust concentrations within the pit.

Although thermal influences within the pit and the overlying atmospheric flow were seen to affect near surface temperatures, particularly in the very base of the pit, for the simulations performed thermal influences were not observed to significantly alter the main flow structure. Under high solar insolation, surface temperatures at the base of the pit were predicted to be in the order of 20 to 30°C and possibly more, above ambient surface level temperatures.

The dry deposition flux within the proposed Olympic Dam pit has been predicted using a deposition velocity approach as typically used in air quality dispersion models. A deposition algorithm was developed and incorporated into the CFD solver through the application of a user function. The approach assumes the particle removal rate is dependent upon the rate of gravitational settling and diffusion of the particles to the surface as well as the near surface concentration. It also assumes the removal process is irreversible, thereby precluding re-suspension of particles.

Particle size and wind speed were found to be the two primary factors that influenced the deposition and thus pit retention rate. As would be expected, higher pit retention was predicted for larger particles and lower wind speeds. The flow within the pit was responsive to winds at an elevation of 100 m or more and thus variations in atmospheric stability did not significantly influence deposition and pit retention rates. Wind direction was also found not to significantly influence deposition rates and thus pit retention.

The estimated particle size distribution of the in-pit dust emissions and predicted discrete particle size retention rates were used to calculate cumulative pit retention estimates for the standard particle size fractions of PM2.5, PM10 and TSP for the base case meteorological conditions. Assuming constant relative variation of pit retention with wind speed for a discrete particle size it is possible to estimate the cumulative pit retention for wind speeds of $U_{10m} = 2$ and 10 m/s for the individual standard size fractions (PM2.5, PM10 and TSP) from the $U_{10m} = 5$ m/s predictions. Predicted standard particle size fraction retention rates across the wind speed range simulated are summarised in Table 8.1

Table 8.1 Estimates for different size fractions can be calculated.

Table 8.1: Summary of predicted pit retention rates for PM2.5, PM10 and TSP particle fractions for neutral stability, north wind with $U_{10m} = 2, 5$ and 10 m/s.

	2 m/s	5 m/s	10 m/s
YEAR	40	40	40
PM2.5	0.93%	0.48%	0.26%
PM10	2.9%	1.5%	0.81%
TSP	47.5%	38.0%	27.9%

Estimated particle fraction retention rates were found to be lower than those recommend in the NPI, however, at the lower wind speed of $U_{10m} = 2$ m/s the difference was small, particularly for the TSP fraction. At higher wind speeds the predicted retention rates were a factor of two or more less than the NPI recommended values.

The retention rates estimated in this study are likely to be conservative (i.e. underestimate actual rates), particularly in relation to the diffusive deposition component. Further investigation into the uncertainty of the diffusive deposition predictions and improvement of the parameterisation would be recommended. Investigation into the significance of deposition onto the emission sources (roads and excavation region) would also be recommended.

The methodology used to predict size fraction retention rates could also be improved through better characterisation of the particle size distributions of the various in-pit dust emission sources, particularly the major sources such as the operation of trucks on the haul roads and the loading of the haul trucks at the excavation sites.

9 REFERENCES

- Apsley D. D., Dyster S. J., McHugh C. (2005) Modelling dry deposition: ADMS Technical specification paper P17/13E/05.
- AVL (2005), Multiphase flow, SWIFT Version 8.
- Bhaskar R [1987]. Spatial and temporal behavior of dust in mines: theoretical and experimental studies [Dissertation]. University Park, PA: The Pennsylvania State University, Department of Mineral Engineering
- Bhaskar R, Ramani RV [1989]. Dust flows in mine airways: a comparison of experimental results and mathematical predictions. In: Frantz RL, Ramani RV, eds. Publications produced in the Generic Mineral Technology Center for Respirable Dust in the year 1988. Washington, DC: U.S. Department of the Interior, Bureau of Mines, Office of Mineral Institutes, pp. 31–39.
- Cole CF, Fabrick AJ [1984]. Surface mine pit retention. *J Air Pollut Control Assoc* 34(6):674–675.
- Courtney WG, Kost J, Colinet JF [1982]. Dust deposition in coal mine airways. Pittsburgh, PA: U.S. Department of the Interior, Bureau of Mines, Technical Progress Report (TPR) 116. NTIS No. PB 82–194853.
- Courtney WG, Cheng L, Divers EF [1986]. Deposition of respirable coal dust in an airway. Pittsburgh, PA: U.S. Department of the Interior, Bureau of Mines, RI 9041. NTIS No. PB 87–139424.
- D’Abreton P., Castillo E. (2006) Olympic Dam EIS Local Climate Study, Pacific Air & Environment Pty Ltd
- Grainger C., Meroney R. N. (1993) Dispersion in an open-cut coal mine in stably stratified flow. *Jrnl. of Boundary Layer Meteorology*, Vol. 63, 1993, pp. 117-140.
- Panofsky, H. A., and J. A. Dutton, 1984: *Atmospheric Turbulence*. John Wiley and Sons, 397 pp..
- Reed, W. R. (2005) Significant dust dispersion models for mining operations. Information Circular 9478, Department of Health and Human Services, National Institute for Occupational Safety and Health, Pittsburgh.
- Sato, Y., Sekoguchi K., (1975) Liquid velocity distribution in two-phase bubble flow. *Int. J. Multiphase Flow*, 2, 79.
- Schlichting, H. (1979) Boundary-layer theory. Seventh edition. McGraw-Hill , New York, New York, USA.

Scire J. S., Strimaitis D. G., Yamartino R. J. (2000) A User's guide to the CALPUFF dispersion model. Earth Tech, Inc.

Srinivasa RB, Baafi EY, Aziz NI, Singh RN [1993]. Three dimensional numerical modelling of air velocities and dust control techniques in a longwall face. In: Proceedings of the Sixth U.S. Mine Ventilation Symposium (Salt Lake City, UT, June 21–23, 1993). Littleton, CO: Society for Mining, Metallurgy, and Exploration, Inc., pp. 287–292.

Theofanus T. G., Sullivan J. P. (1982) Turbulence in Two-Phase Dispersed Flows," J. Fluid Mechanics, Vol-116, 343-362.

TRC Environmental Consultants, Inc. [1995]. Dispersion of airborne particulates in surface coal mines: data analysis. Washington, DC: U.S. Environmental Protection Agency, Office of Air and Radiation, Office of Air Quality Planning and Standards.

US EPA (2006) Basic concepts in environmental science; Module 3: Characteristics of particles; size distribution, URL:
<http://www.epa.gov/eogapti1/module3/distribu/distribu.htm>

Wala AM, Yingling JC, Zhang J, Ray R [1997]. Validation study of computational fluid dynamics as a tool for mine ventilation design. In: Ramani RV, ed. Proceedings of the Sixth International Mine Ventilation Congress (Pittsburgh, PA, May 17–22, 1997). Littleton, CO: Society for Mining, Metallurgy, and Exploration, Inc., pp. 519–525.

Xu L, Bhaskar R [1995]. A simple model for turbulent deposition of mine dust. In: Proceedings of the Seventh U.S. Mine Ventilation Symposium (Lexington, KY, June 5–7, 1995). Littleton, CO: Society for Mining, Metallurgy, and Exploration, Inc., pp. 337–343.

Yong Shi, Feng, X.S. and Wei F.S. (2000) Three-dimensional non-hydrostatic numerical simulation for the PBL of an open-pit mine, Boundary-Layer Meteorology, **94**: 197–224.